The Dissertation Committee for Divya Thakur

certifies that this is the approved version of the following dissertation:

Adaptation, Gyro-Free Stabilization, and Smooth Angular Velocity Observers for Attitude Tracking Control Applications

Committee:

Maruthi R. Akella, Supervisor

Behcet Acikmese

Srinivas Bettadpur

Sun Hur-Diaz

Glenn Lightsey

Adaptation, Gyro-Free Stabilization, and Smooth Angular Velocity Observers for Attitude Tracking Control Applications

by

Divya Thakur, B.S.As.E.; M.S.E.

Dissertation

Presented to the Faculty of the Graduate School of

The University of Texas at Austin

in Partial Fulfillment

of the Requirements

for the Degree of

Doctor of Philosophy

The University of Texas at Austin

August 2014

To Brian,

As we embark together on new adventures.

Acknowledgments

My sincerest gratitude to my advisor Dr. Akella, for giving me the support and freedom to pursue the problems of interest to me. Thank you for being there with your guidance and unending insight whenever I struggled with research, while giving me the space to discover my own ideas. I am immensely grateful for your mentorship and for helping me to develop the intellectual maturity to tackle challenging problems.

I would like to thank my committee members: Dr. Glenn Lightsey, Dr. Srinivas Bettadpur, Dr. Sun Hur-Diaz, and Dr. Behcet Acikmese for taking the time to review my dissertation and participate in the defense, and for providing valuable feedback. I appreciate all our discussions regarding my research and for all your insightful comments. I would also like to thank all the professors who have guided me in my education over the last decade. Their dedication as teachers and mentors has contributed immensely to shaping my life and career choices.

I would also like to thank Dr. Belinda Marchand, my advisor as a Master's student and during the first year of PhD. I have learned, and continue to learn so much from you about research, academic pursuits, career choices, and life in general. I am grateful for our friendship and for all your support

and encouragement over the years.

My research group has always been a tremendous source of support during my PhD. Thanks to Dr. Srikant Sukumar, Dr. Apurva Chunodkar, Dr. Travis Mercker, Sungpil Yang, Sonia Hernandez, Kelley Hutchins, and Miki Szmuk for many interesting discussions and exchange of ideas. Thanks especially to Srikant and Sonia for our research collaborations, and to Sungpil for always taking the time to discuss various problems and concepts.

I have been lucky enough to forge long lasting friendships during my time in graduate school. Thanks to Bonnie, Apurva, Ben, David, Greg, Andrew, Sara, Vivek, and Etienne for helping me to always stay positive and reminding me to have a little fun every now and then.

To my parents, Anita and Vijainder, thank you for bringing me up in a home that nurtured scientific curiosity, and for your love and support. To my sister, Su, who has never let me doubt myself: you are my rock.

Lastly, none of this would have been possible without the unwavering support and love of my best friend and husband, Brian. It has been an adventurous few years for us and I'm glad I had you through it all. Thanks for giving me the space when I needed it, especially during the last few months of dissertation writing. I love you, and feel blessed everyday to have you in my life.

Divya Thakur

The University of Texas at Austin

August 2014

Adaptation, Gyro-Free Stabilization, and Smooth Angular Velocity Observers for Attitude Tracking Control Applications

Divya Thakur, Ph.D.
The University of Texas at Austin, 2014

Supervisor: Maruthi R. Akella

This dissertation addresses the problem of rigid-body attitude tracking control under three scenarios of high relevance to many aerospace guidance and control applications: adaptive attitude-tracking control law development for a spacecraft with time-varying inertia parameters, velocity-free attitude stabilization using only vector measurements for feedback, and smooth angular velocity observer design for attitude tracking in the absence of angular velocity measurements.

Inertia matrix changes in spacecraft applications often occur due to fuel depletion or mass displacement in a flexible or deployable spacecraft. As such, an adaptive attitude control algorithm that delivers consistent performance

when faced with uncertain time-varying inertia parameters is of significant interest. This dissertation presents a novel adaptive control algorithm that directly compensates for inertia variations that occur as either pure functions of the control input, or as functions of time and/or the state.

Another important problem considered in this dissertation pertains to rigid-body attitude stabilization of a spacecraft when only a set of inertial sensor measurements are available for feedback. A novel gyro-free attitude stabilization solution is presented that directly utilizes unit vector measurements obtained from inertial sensors without relying on observers to reconstruct the spacecraft's attitude or angular velocity.

As the third major contribution of this dissertation, the problem of attitude tracking control in the absence of angular velocity measurements is investigated through angular velocity observer (estimator) design. A new angular velocity observer is presented which is smoothed and ensures asymptotic convergence of the estimation errors irrespective of the initial true states of the spacecraft. The combined implementation of a separately designed proportional-derivative type controller using estimates generated by the observer results in global asymptotic stability of the overall closed-loop tracking error dynamics. Accordingly, a separation-type property is established for the rigid-body attitude dynamics, the first such result to the author's best knowledge, using a smooth (switching-free) observer formulation.

Contents

Acknowledgments **v**

Abstract **vii**

List of Figures **xiii**

Chapter 1 Introduction **1**

1.1 Motivation 1

1.2 Literature Review 5

1.2.1 Adaptive Attitude Control for Time-Varying Parameters 5

1.2.2 Gyro-Free Attitude Stabilization 7

1.2.3 Smooth Angular Velocity Observer 10

1.3 Dissertation Outline 13

Chapter 2 Background **17**

2.1 Rigid Body Kinematics and Dynamics 17

2.1.1 Direction Cosine Matrix 18

2.1.2 Unit Quaternion Representation 20

2.1.3 Tracking Error Dynamics 21
2.2 Smooth Projection Mechanism in Adaptive Control 23
2.2.1 Persistence of Excitation 29
2.3 Mathematical Concepts 30
2.3.1 Passive Systems Theory 30
2.3.2 Barbalat's Lemma 30
2.3.3 Strict Lyapunov Functions 31
2.3.4 Linear Filters 32

Chapter 3 Adaptive Attitude-Tracking Control of Spacecraft with Uncertain Time-Varying Inertia Parameters 33

3.1 Problem Statement 35
3.1.1 Characterization of Time-Varying Inertia Matrix 36
3.2 Adaptive Attitude Tracking for Unknown Inertia with Time and State Dependencies 42
3.2.1 Smooth Parameter Projection 46
3.3 Adaptive Attitude Tracking Control for Unknown Inertia with Input Dependency 50
3.4 Numerical Simulations 58
3.4.1 Deployable Appendage 61
3.4.2 Fuel Loss Compensation 66
3.5 Concluding Remarks 73

Chapter 4 Gyro-Free Rigid Body Attitude Stabilization using

only Vector Measurements on $SO(3)$ **74**

4.1 Problem Formulation 75

4.1.1 Measurement Model and Orientation Error 76

4.2 Velocity-Free Attitude Control 78

4.2.1 Preliminary Results 78

4.2.2 Gyro-Free Attitude Stabilization Control Law 86

4.3 Numerical Simulations 93

4.3.1 Vector Measurement Only Feedback Control with Perfect Measurements 94

4.3.2 Vector Measurement Only Feedback Control with Noisy Measurements 97

4.4 Conclusion 100

Chapter 5 Partial Lyapunov Strictification: Smooth Angular Velocity Observers for Attitude Tracking Control **104**

5.1 Preliminaries 107

5.1.1 Rigid Body Dynamics 108

5.1.2 Full-State PD Attitude Control 108

5.2 Angular Velocity Observer Development 110

5.2.1 Estimation Framework 110

5.2.2 Smooth Observer 111

5.2.3 Towards a Strict Lyapunov Function 116

5.3 Separation Property of Angular Velocity Observer Based Attitude Control 126

5.4 Numerical Simulations 128
5.4.1 Quaternion Measurements Without Noise 129
5.4.2 Quaternion Measurements With Noise 133
5.4.3 Estimated Quaternion Using QUEST 139
5.4.4 Inertia Matrix Uncertainty 141
5.5 Conclusions 142

Chapter 6 Conclusions **144**
6.1 Summary 144
6.2 Statement of Contributions 148
6.3 Recommendations for Future Research 150

Appendices **153**

Appendix A List of Publications **153**
A.1 Relevant Journal Publications 153
A.2 Relevant Conference Publications 154
A.3 Other Publications 154

Bibliography **155**

Vita **168**

List of Figures

3.1 A spacecraft with mass displacement due to deploying appendages. 38

3.2 Spacecraft with a single propellant tank undergoing fuel mass-loss proportionate to the commanded control torque. 40

3.3 Baseline performance of proposed and comparison controllers, generated using constant and known $\mathbf{J}_0$ in Eq. (3.57). 60

3.4 Principal moments of inertia of time-dependent $\mathbf{J}(t)$ for a spacecraft with moving/articulating parts. 62

3.5 Adaptive attitude-tracking control simulation for spacecraft with time-dependent inertia matrix variations due to mass displacement. 63

3.6 Commanded control effort for adaptive control simulation of spacecraft with time-dependent inertia variations. 64

3.7 Parameter estimates of the unknown $\mathbf{J}_0$ and $\mathbf{J}_1$ matrices for mass displacement example. 65

3.8 Adaptive attitude-tracking control response for a spacecraft with fuel mass-loss induced inertia variations. 69

3.9 Commanded control effort for adaptive control simulation of a spacecraft with fuel loss tracking a non-PE signal. 70
3.10 Parameter estimates of unknown $\mathbf{J}_0$ and $\mathbf{J}_1$ matrices (fuel-loss example). 71
3.11 Principal moments of inertia of the control norm dependent inertia matrix simulating variations due to fuel mass-loss. . . 72

4.1 Comparison of the novel gyro-free controller with a full state feedback controller without measurement noise. 95
4.2 Commanded control effort and time evolution of the auxiliary state $\mathbf{z}(t)$ when no measurement noise is present. 96
4.3 Comparison of the novel gyro-free controller with a full state feedback controller in the presence of measurement noise. . . . 98
4.4 Control magnitude for closed-loop system when measurements are noisy. 99
4.5 Attitude and angular velocity stabilization simulation for proposed controller using 10 random initial conditions subject to measurement noise. 102
4.6 Control history for proposed controller simulation using 10 random initial conditions and noisy measurements. 103

5.1 Comparison of observer-based PD control with full-state feedback control without measurement noise. 131

5.2 Angular velocity estimation error and commanded control effort for attitude tracking control simulation in the absence of measurement noise. 132
5.3 Attitude tracking control simulation comparing performance of observer-based and full-state feedback control laws when noise is present in attitude measurements. 134
5.4 Estimation error evolution and commanded control effort for attitude tracking in the presence of measurement noise. 135
5.5 Attitude tracking control simulation for proposed observer-controller scheme using 10 random initial conditions with noisy attitude measurements. 137
5.6 Estimation error evolution and commanded control effort for simulation conducted with the combined observer-controller implementation using 10 random initial conditions. 138
5.7 Attitude tracking control simulation for observer and controller driven by estimates of $\mathbf{q}$ generated by QUEST algorithm (no sensor noise). System response is identical to that in Figs. 5.1-5.2 where the quaternion is assumed to be directly available. . 140
5.8 Convergence properties of state estimation errors from the observer when inertia matrix parameters are uncertain. 142

Chapter 1

Introduction

1.1 Motivation

Attitude control is one of the most widely studied topics in nonlinear controls literature, with many technically rich results addressing a wide array of constraints and physical limitations dictated by the underlying application. In the field of aerospace engineering, the attitude control system is a critical component of spacecraft mission design, with the success of a mission often directly relying on the spacecraft's ability to accurately track a desired orientation. Recent advances in sensor and actuator hardware technology have enabled the design of spacecraft missions of far greater complexity than in previous decades. To meet the demands of newer and more challenging control objectives and increased precision requirements, attitude control synthesis continues to be investigated under various practical considerations. While new problems continue to be posed, theoretical advances in the controls literature have per-

mitted opportunities for revisiting certain analytically challenging classical problems and elegant results to be put forth.

Among existing attitude control solutions, a significant amount of work is geared towards addressing the problem of unknown or uncertain system parameters using adaptive control techniques [1, 7, 16, 26, 55, 77]. In the context of spacecraft attitude tracking, adaptive control theory has been applied extensively to account for mass properties that cannot be exactly determined during pre-flight testing. The majority of available adaptive attitude-tracking control literature is focused, however, on rigid spacecraft with uncertain parameters that are constant and don't display any time-variation. While this assumption may be adequate for some spacecraft with very slowly varying system parameters, a growing number of missions anticipate having to incorporate spacecraft with rapidly deployable appendages coupled with fast propulsive maneuvers which may result in appreciable variations in the inertia parameters. For example, in a deployable spacecraft, an expanding solar array or sensor boom causes mass displacement. Similarly, a spacecraft undergoing demanding rotational or translational maneuvers rapidly loses a significant amount of mass due to fuel depletion. In both cases, the result is a system with a time-varying inertia profile, which must be taken into consideration for precise attitude tracking requirements. This dissertation addresses the problem of rapidly varying inertia matrix parameters through the design of a novel adaptive attitude tracking control law that directly compensates for inertia variations occurring as a result of fuel mass-loss or mass-displacement due to

deploying spacecraft appendages.

Attitude control laws are typically configured using the quaternion vector or an equivalent attitude representation such as Modified Rodriguez Parameters or Gibb's vectors [58]. In practice though, no physical sensor is able to directly measure the attitude of a vehicle. Rather, the attitude is reconstructed with an observer (estimation) scheme that relies on inertial sensor measurements and rate gyro information. However, in several practical implementations, reliable angular velocity information may not always be available, and gyro failures or noise effects could lead to a severely compromised attitude control system. Thus, in the setting of complete absence of rate measurements, a stabilizing attitude controller that utilizes vector measurements directly for feedback, without relying on intermediate estimates of some attitude parameterization or angular velocity feedback, is crucial for the success of the spacecraft's mission.

In this dissertation, a novel attitude stabilization control law is presented which relies on the direct feedback of vector measurements obtained from inertial sensors. The control law neither requires angular velocity measurements, nor does it rely on any observer or estimation schemes to reconstruct either the angular velocity or the attitude of the spacecraft. Further, since the proposed controller is configured directly using vector measurements, it does not suffer from the undesirable *unwinding* phenomenon typically observed with quaternion-based feedback controllers, where the spacecraft may start at rest arbitrarily close to the desired attitude and unnecessarily rotate

through large angles before stabilizing to the desired attitude [10].

Along parallel lines of inquiry, this dissertation examines the implementation of proportional-derivative (PD) feedback controllers using a combined observer-controller architecture. The majority of the PD control designs require angular velocity measurements to be directly available for feedback. However, as noted earlier, this requirement may not always be accurately satisfied, and gyro failures may result in a detrimental loss of pointing and tracking accuracy. Designing an observer for the nonlinear and time-varying rigid body dynamics is complicated by the fact that, in general, no separation property exists for nonlinear systems. Therefore, the closed-loop stable implementation of a full-state feedback attitude control law using angular velocity estimates is a problem of great theoretical and practical importance.

A very recent result [15] proposed a switched angular velocity observer that established for the first time a separation property for rigid body attitude tracking control. However, the observer design relies on a switching logic that can introduce hardware fatigue. The lack of a smooth angular velocity observer in current literature motivates the third area of research in this dissertation, which focuses on the construction of a novel smooth angular velocity observer that, when combined with a standard PD-type controller, renders the resulting closed-loop system (almost) globally asymptotically stable. An important separation property is established for the rigid-body attitude tracking problem using the proposed smooth angular velocity formulation, the first such result to the best of the author's knowledge. The separation property

is realized through the use of a novel Lyapunov "strictification" [33, 34, 37] strategy, a process by which a non-strict Lyapunov function is transformed into a partially strict Lyapunov function whose derivative contains additional desirable non-positive terms. Within the context of the smooth observer, the introduction of additional non-positive terms of the estimation error signals in the Lyapunov function derivative helps dominate undesirable terms arising due to the observer implementation, and is critical in proving the separation property result.

1.2 Literature Review

In this section, a detailed survey of existing literature is provided for the three main problems treated in this dissertation. The first review addresses relevant results within the context of adaptive control for time-varying parameters, while the second and third examine existing work related respectively to gyro-free control using vector measurements only and smooth angular velocity observer construction for rigid body attitude tracking applications.

1.2.1 Adaptive Attitude Control for Time-Varying Parameters

Classical literature in the area of adaptive control has addressed the problem of time-varying plant parameters but for linear dynamic systems. The methodology in [5] considers linear systems with time-varying parameters in

a compact set, while [41, 83] address linear systems with unknown but slowly time-varying parametric uncertainties. More recent results provide extensions to limited classes of nonlinear time-varying plants that are not readily extendable to the rigid body problem; the formulation of [81] accounts for unknown periodic time-varying uncertainties that may be rapidly time-varying but with known periodicity, whereas algorithms for uncertain time-varying parameters with known bounds are reported in [20]. The result presented in this dissertation extends the problem of adaptive control for the highly nonlinear rigid body dynamics to account for time-varying system (inertia matrix) parameters with both multiplicative and additive uncertainty.

The problem formulation and corresponding solution approach presented here are both motivated by the underlying assumption that inertia matrix variations often occur as a result of a known and well-modeled dynamic phenomena. While this assumption may appear restrictive, in fact, it readily serves many practical applications. For example, in the case of mass-loss due to fuel consumption, the rate of change of the spacecraft mass is a function of the applied control and is easily characterized for the onboard actuator components. Inertia parameter variations arising due to mass displacement caused by deploying appendages, as well as any other time or state dependent inertia parameters could also be treated within the framework of the proposed control strategy. Reference [76] addresses a similar problem wherein the inertia matrix description is provided as an unknown constant component as well as a time-varying component of known variation profile but unknown bound.

However, the formulation in [76] only considers variations in the inertia matrix of a purely time-dependent nature. In this dissertation, the salient and distinguishing feature of the novel control method is its ability to handle not only time-dependent, but also a combination of time and state or purely input dependent variations of the inertia matrix.

1.2.2 Gyro-Free Attitude Stabilization

The orientation of a rigid body is described using a rotation matrix, a 3×3 orthogonal matrix with determinant equal to 1. Rotation matrices, also known as direction cosine matrices, constitute the special orthogonal group of rigid rotations in $\mathbb{R}^3$, which is denoted by $SO(3)$. While attitude stabilization control laws that use rotation matrices directly have been recently investigated [11, 19, 46, 50], the majority of previous results use either a three-parameter (modified Rodrigues parameters) or quaternion representation of the attitude [31, 47, 74, 77, 79]. Stabilization control laws are typically formulated using attitude and angular velocity measurements. It is a well-established fact that stabilization can be achieved even in the absence of angular velocity feedback owing to the fact that the rigid body dynamics satisfy a passivity property: the map from torque as input and angular velocity as output is passive [31, 47, 61, 74]. However, regardless of the specific attitude parameterization utilized, most control methods assume that the attitude measurement is readily available for feedback. In practice, though, no sensor is able to directly measure the attitude of a vehicle. Rather, the spacecraft's attitude

is obtained through an observer or estimation algorithm typically driven by measurements from rate gyros, sun sensors, star sensors, and/or a wide array of other such sensors.

Batch-type attitude estimators such as QUEST, ESOQ, ESOQ-2, and their variants are based on the classical Wahba problem [35, 36, 42, 59, 75]. These numerical algorithms treat attitude determination as a static optimization problem by solving for the quaternion using unit vector measurements obtained from inertial sensors at a single point in time. However, due to this memoryless approach, these algorithms are known to suffer from robustness issues and are sensitive to measurement noise. Extensions to these algorithms have been formulated using a filter approach to handle sequential measurements over a range of time [9, 17, 57]. However, where efficiency and robustness are concerned, sequential estimation techniques based on the extended Kalman filter (EKF) are the real workhorse for aerospace applications [30]. Linear filtering algorithms are able to handle measurement noise and provide more efficiency by employing rate gyro information along with vector measurements in a complementary manner [17]. Several rich results that address the development of nonlinear attitude observers with rigorous convergence proofs are also available in this regard [2, 32, 73]. However, like their linear filter counterparts, nonlinear observer algorithms also typically either rely on perfect knowledge of the angular velocity or, more recently, with the availability of the angular velocity subject to unknown constant bias [40]. Hence, when angular velocity is unavailable, the use of estimation/observer algorithms which

are driven by angular velocity measurements is obviously infeasible.

In the setting of complete absence of rate measurements, the development of a stabilizing controller that utilizes vector measurements directly for feedback, without relying on the estimated attitude vector or angular velocity feedback, remains a significant open problem. A recent result in [62] addresses the same problem of velocity-free attitude stabilization control scheme relying solely on body vector measurements. The underlying solution approach in Reference [62] uses a quaternion-based attitude observer-like signal, referred to as the 'dynamic auxiliary system', for control synthesis. While the auxiliary system does not exhibit the classical separation property (rather it is dependent on a specific control law), its dynamical construction is similar to that of an attitude observer scheme. The asymptotic stabilization of the rigid body's attitude and angular velocity depends on the asymptotic convergence of the quaternion observer-like signal.

In contrast to the results in [62], the control design in this dissertation is rooted in the classical passive systems framework. In essence, the inherent passivity properties of the rigid body dynamics are exploited to develop a control scheme that does not rely on angular velocity and uses unit vector measurements directly for stabilization. The work herein draws from the classical results of References [31, 47, 74] where the authors derive passivity-based velocity-free attitude controllers using either quaternions, Rodrigues, or Modified Rodrigues parameters for kinematic representation. The distinguishing feature of this work is that no attitude parameterization is used and instead

the proposed control directly employs vector measurements of unit length. Further, unlike [62], the control law does not rely on an attitude observer-like signal. Instead, the attitude and angular velocity convergence is obtained directly from feedback of vector measurements. To the best knowledge of the author, the problem of stabilizing a spacecraft in the passivity framework, wherein vector measurements are used directly for feedback and no observers are implemented, has not been previously solved.

The work presented in this dissertation shares slight similarities with a rather recent result in [19] where a stabilizing attitude controller is formulated that uses all unit vector measurements directly, rather than determining or parameterizing the rigid body's rotation matrix first. However, the most significant distinction is that unlike the formulation herein, the results in Reference [19] require the availability of perfect angular velocity measurements. Thus, the development of a set point regulation control law using passivity approach with only unit vector measurements as feedback is one of the novel contributions of this dissertation.

1.2.3 Smooth Angular Velocity Observer

Several proportional-derivative (PD) type attitude tracking control laws are available in existing literature for rigid spacecraft implementations [25, 29, 77, 79, 80]. Due to the well known fact that the configuration space of the attitude motion $SO(3)$ is not a contractible space, it is impossible for any continuous state-feedback control law to render global asymptotic stability

[10, 77]. Therefore, the standard notion of "almost" global asymptotic stability is adopted for this problem to imply stability over an open and dense set in $SO(3)$. The majority of the PD control designs expect perfectly measured angular velocity information for controller feedback, an assumption that is not always satisfied in practical applications.

As noted earlier, the passivity property of the rigid body dynamics can be exploited to satisfy attitude tracking through a proportional-only feedback controller even in the complete absence of angular velocity measurements, using only attitude feedback. For the implementation of full PD-type control laws, the unavailability of angular velocity measurements has been dealt with through a combined observer-controller architecture.

The observer approach was first considered by Salcudean [49] who proposed a nonlinear observer based on extensions of the classic Luenberger observer for a second-order system. While closed-loop system stability was not proven in this case, Reference [49] conjectured the existence of a separation property in which the observer and controller can be designed separately with the desired stability properties and thereafter combined to retain closed-loop system properties. In Nicosia and Tomei [44], an angular velocity observer is presented, which, when combined with any state feedback controller, is stable within an estimated region of attraction under mild assumptions on the controller. In Caccavale and Villani [12], two alternative strategies are proposed, the first of which employs a second-order model-based observer, which when tuned with the proposed control law, achieves a locally stable closed-loop

system. The second strategy is based on a lead filter for estimating angular velocity error. Schlanbusch et. al [54] use a quaternion-based hybrid output feedback controller for attitude tracking control in the absence of angular velocity. A switching observer is used to reconstruct the angular velocity. Closed-loop system stability is guaranteed for all initial conditions inside a compact set which may be made arbitrarily large by increasing the control gains.

More recently, the work by Chunodkar and Akella [15] established for the first time an almost globally stable result on a separation property with an angular velocity observer when combined with a proportional-derivative type control structure. The observer in [15] employs a switching logic, similar in spirit to the hybrid-logic of [54], by instantaneously resetting the attitude estimation to zero. However, the observer in [15] is formulated in a different framework that employs a novel definition for angular velocity estimation error to satisfy $\mathcal{C}^0$ continuity, and, in contrast to [54], ensures global asymptotic stability of estimation error states independently of the control torque. Thus, while the result in [15] is a significant advancement in the area of designing angular-velocity estimators, the observer's reliance on a switching scheme may potentially expose the control system to undesirable high-frequency switching, especially when attitude measurements are known to be noisy. Although the total number of switches is guaranteed to be finite and a finite dwell time exists between successive switches in [15], high-rate chatter due to rapid switching could still potentially lead to hardware fatigue. To this end, the design of a

smooth (non-switching) angular velocity observer is of significant interest for attitude tracking applications.

In this dissertation, a novel smooth angular velocity observer is presented that, when combined with an independently designed PD-type controller, renders the closed-loop rigid body dynamics (almost) globally asymptotically stable. The problem framework and proposed solution bear some superficial similarities to Reference [15]. However, the fundamental contribution of the proposed observer construction is that, unlike Reference [15], the design here does not rely on any switching logic to guarantee asymptotic convergence of the angular velocity state estimation error. Thus, the observer ensures $\mathcal{C}^{\infty}$ continuity of estimation states. The main feature of this extremely important technical result stems from the use of a partial Lyapunov "strictification" process [34] that enables the closed-loop stability and convergence analysis to proceed along novel lines in a spiral logic fashion.

1.3 Dissertation Outline

The remainder of the dissertation is organized as follows:

In Chapter 2, a discussion of mathematical concepts relevant to this dissertation has been provided. A detailed derivation of the rigid body attitude dynamics is provided along with a discussion on different attitude parameterizations. In addition, a brief review of certainty-equivalence based adaptive control is presented along with pertinent definitions to allow the reader to better follow the theoretical development in the dissertation.

In Chapter 3, an adaptive control law for attitude tracking applications is developed for the case when the spacecraft inertia matrix experiences fast variations either due to fuel depletion (mass loss) or deploying parts (mass displacement). A detailed derivation of the adaptive control law is provided along with a rigorous stability analysis. The fuel loss case is modeled assuming uniform mass loss from a single propellant tank whose principal axes are collocated with the body-fixed axes of the main spacecraft. A smooth projection scheme is utilized to bound the inertia parameter estimates to within a convex set. This helps in guaranteeing that the control remains bounded for all time for the particular case when the inertia matrix is dependent on the control input. In particular, the coupling that occurs in the dynamical equations as a result of this input dependency leads to a control law with regions of singularity. These regions are easily avoided if the inertia parameter estimates are bounded away from zero, which is accomplished through the projection mechanism [27, 82]. In the numerical simulations studies, the adaptive control law is applied to two cases: a spacecraft undergoing fuel depletion, and a spacecraft experiencing mass displacement due to expanding and contracting appendages. In both cases, it is shown that the overall closed-loop performance is greatly increased when the adaptive control takes explicit account of inertia variations as opposed to an existing adaptive control law in literature that does not account for inertia variations.

In Chapter 4, an attitude stabilization control law is developed without angular velocity and using vector measurements directly for feedback. With a

total of $N \geq 2$ independent unit vector measurements available, the orientation error is expressed as the difference between the body vector measurement and the desired vector measurement. The control is formulated with feedback of a cross product term between the body and desired unit vector measurements as well as feedback of an auxiliary signal, which is the output of a linear time-invariant system. Through Lyapunov-based stability analysis, it is shown that the attitude stabilization control objective is satisfied with asymptotic convergence as long as the initial conditions satisfy a mild constraint. Some additional discussion and analysis are provided to highlight the primary obstacles that prevent the extension of this stabilization control law to the full attitude tracking problem. Following the control law development, numerical simulations are shown to corroborate the theoretical findings. Simulation studies also indicate that the control law is robust to measurement noise.

Chapter 5 presents the development of a smooth nonlinear angular velocity observer for attitude tracking control applications. Unlike existing approaches, the proposed observer does not rely on a switching strategy to ensure convergence to the true states. The smooth observer design ensures asymptotic convergence of estimation errors irrespective of the control design or the initial true state of the spacecraft. A Lyapunov function "strictification" process is carried out in order to obtain a partially strict Lyapunov function comprised of negative terms in all estimation states. This step is crucial in enabling a separation property to be established, whereby an independently designed PD control law driven by angular velocity estimates generated by the smooth ob-

server results in global asymptotic stability of the overall closed-loop tracking error dynamics. All pertinent details related to the observer development as well as the separation property result are shown along with rigorous proofs. The theoretical findings are validated in simulations, which also show that a PD control law integrated with the proposed observer are robust to noisy measurements. The convergence performance of the observer is also investigated through numerical simulations when inertia matrix parameters are unknown or uncertain.

Finally, Chapter 6 concludes with a summary of the theoretical development in preceding chapters. The original theoretical contributions resulting from this research are highlighted along with their practical applications. In addition, important avenues for future research directions are discussed.

Chapter 2

Background

In this chapter, the dynamical model for the spacecraft attitude tracking problem is developed. Rigid body kinematics are derived using quaternions to express the orientation of the spacecraft, while rigid body dynamics are expressed in terms of Euler's rotational equations of motion. A brief introduction to adaptive control is provided along with an overview of a $\mathcal{C}^1$ parameter projection mechanism. In addition, an overview of relevant mathematical concepts is provided in order to allow the reader to follow the development of controller and observer designs in subsequent chapters.

2.1 Rigid Body Kinematics and Dynamics

The configuration space of rigid body attitude motion is the set of all rotation matrices $SO(3)$ which comprise the special orthogonal group of rigid rotations in $\mathcal{R}^3$. The nine parameter rotation matrix, also known as the direction

cosine matrix, represents all attitudes uniquely. While a few recent control designs have been performed directly on $SO(3)$ [19, 46, 50], attitude control is typically studied using various minimal three or non-minimal four attitude parameterizations [58]. Every minimal parameter representation such as Euler angles or Modified Rodrigues parameters suffers from either kinematic or geometric singularities that prevent global definitions for continuous control laws. Therefore, these representations are limited to local attitude maneuvers [14]. On the other hand, non-minimal parameters such as unit quaternions and axis-angle representations are globally defined but cannot represent all attitudes uniquely. For a given attitude, the unit quaternions $+\mathbf{q}$ and $-\mathbf{q}$ both represent the same physical origination of the body. Thus, the notion of almost global stability is used in the context of attitude control because the unit quaternion does not allow for globally continuous stabilizing control laws [10, 77].

A quick review of attitude kinematics derived using both direction cosine matrices and quaternions is provided here. In addition, a thorough review of spacecraft rotation dynamics is provided in the proceeding sections.

2.1.1 Direction Cosine Matrix

A complete kinematic and dynamic description for rigid body rotational motion is provided using direction cosine matrix and Euler's rotational equations. For the sake of notational simplicity, the time argument t is left out except for emphasis in certain places. The orientation of a rigid body can be expressed in

terms of the direction cosine matrix, also known as a rotation matrix, $\mathbf{C}$ evolving on the special orthogonal group $SO(3) = \left\{\mathbf{C} \in \mathbb{R}^{3\times 3} | \mathbf{C}^{\mathrm{T}}\mathbf{C} = \mathbf{I}, \det[\mathbf{C}] = 1\right\}$, where $\mathbf{I}$ is the 3×3 identity matrix. The rotational kinematics of the rigid body expressed in terms of $\mathbf{C}$ takes the form

$$\dot{\mathbf{C}} = -S(\boldsymbol{\omega})\mathbf{C}, \tag{2.1}$$

where $\mathbf{C}$ denotes the orientation of the body-fixed frame $\mathcal{B}$ with respect to the inertial frame $\mathcal{I}$, and the angular velocity $\boldsymbol{\omega} \in \mathbb{R}^3$ is expressed in the body-fixed frame. In Eq. (2.1), $S(\cdot) : \mathbb{R}^3 \to \mathfrak{so}(3)$ where $\mathfrak{so}(3) = \left\{\mathbf{S} \in \mathbb{R}^{3\times 3} | \mathbf{S}^{\mathrm{T}} = -\mathbf{S}\right\}$ is the set of skew-symmetric matrices such that

$$S(\mathbf{v}) = \begin{bmatrix} 0 & -v_3 & v_2 \\ v_3 & 0 & -v_1 \\ -v_2 & v_1 & 0 \end{bmatrix},$$

with $\mathbf{v} = [v_1, v_2, v_3]^{\mathrm{T}} \in \mathbb{R}^3$. The vector cross-product operation between two vectors $\mathbf{v}, \mathbf{w} \in \mathbb{R}^3$ can be expressed as $S(\mathbf{v})\mathbf{w} = \mathbf{v} \times \mathbf{w}$.

The dynamics of the rigid body are governed by Euler's rotational equations of motion and are given by

$$\mathbf{J}\dot{\boldsymbol{\omega}} = -S(\boldsymbol{\omega})\mathbf{J}\boldsymbol{\omega} + \mathbf{u}, \tag{2.2}$$

where $\mathbf{J} \in \mathbb{R}^{3\times 3}$, $\mathbf{J}^{\mathrm{T}} = \mathbf{J} > 0$ is the constant inertia matrix and $\mathbf{u} \in \mathbb{R}^3$ is the external control torque applied to the system.

2.1.2 Unit Quaternion Representation

In order to globally represent the attitude coordinates of the spacecraft without singularities, the minimal four parameter unit quaternion (or the Euler parameter) representation is sought. The four-dimensional unit quaternion represents the orientation of the body frame $\mathcal{B}$ with respect to the inertial frame $\mathcal{N}$, and is comprised of scalar and vector components denoted as $q_0 \in \mathbb{R}$ and $\mathbf{q_v} \in \mathbb{R}^3$, respectively. Thus, $\mathbf{q} = \left[q_0,\ \mathbf{q_v}^{\mathrm{T}}\right]^{\mathrm{T}}$ and satisfies the unit-norm constraint ${q_0}^2 + {\mathbf{q_v}}^{\mathrm{T}}\mathbf{q_v} = 1$. The kinematic differential equation of the attitude motion of a rigid spacecraft is expressed in terms of $\mathbf{q}$ as [53]

$$\dot{\mathbf{q}} = \frac{1}{2}\mathbf{E}(\mathbf{q})\boldsymbol{\omega}, \tag{2.3}$$

where the 4×3 matrix $\mathbf{E}(\mathbf{q})$ is defined as

$$\mathbf{E}(\mathbf{q}) = \begin{bmatrix} -\mathbf{q}_v^{\mathrm{T}} \\ q_0\mathbf{I}_{3\times 3} + S\left(\mathbf{q}_v\right) \end{bmatrix}, \tag{2.4}$$

where $\mathbf{I}_{3\times 3}$ is the 3×3 identity matrix. Note that Eq. (2.3) is the analogous kinematic differential equation to that governing the direction cosine matrix in Eq. (2.1). The matrix $\mathbf{E}(\mathbf{q})$ satisfies the following important properties:

$$\mathbf{E}^{\mathrm{T}}(\mathbf{q})\mathbf{E}(\mathbf{q}) = \mathbf{I}_{3\times 3}; \quad \mathbf{E}^{\mathrm{T}}(\mathbf{q})\mathbf{q} = 0. \tag{2.5}$$

Consequently, from Eqs. (2.3) and (2.5), the angular velocity $\boldsymbol{\omega}$ may be expressed in terms of $\dot{\mathbf{q}}$ as follows:

$$\boldsymbol{\omega} = 2\mathbf{E}^{\mathrm{T}}(\mathbf{q})\dot{\mathbf{q}}. \tag{2.6}$$

2.1.3 Tracking Error Dynamics

A development of the quaternion and angular velocity tracking error dynamics is shown next. The reference attitude trajectory is denoted by $\mathbf{q}_r$ and evolves according to the following dynamical equation

$$\dot{\mathbf{q}}_r = \frac{1}{2}\mathbf{E}(\mathbf{q}_r)\boldsymbol{\omega}_r, \tag{2.7}$$

where $\boldsymbol{\omega}_r$ is the bounded and smooth reference angular velocity defined in frame $\mathcal{R}$. Let $\hat{\boldsymbol{b}}$, $\hat{\boldsymbol{r}}$, and $\hat{\boldsymbol{n}}$ represent the unit vector triads in the body frame $\mathcal{B}$, reference frame $\mathcal{R}$, and inertial frame $\mathcal{N}$, respectively. The mapping from unit quaternion space to the proper orthogonal matrix space $SO(3)$ is given in terms of the direction cosine matrix. In particular, the following transformations are sought

$$\begin{aligned}
\mathcal{N} \xrightarrow{\mathbf{q}} \mathcal{B} &\Rightarrow \{\hat{\boldsymbol{b}}\} = \mathbf{C}(\mathbf{q})\{\hat{\boldsymbol{n}}\},\\
\mathcal{N} \xrightarrow{\mathbf{q}_r} \mathcal{R} &\Rightarrow \{\hat{\boldsymbol{r}}\} = \mathbf{C}(\mathbf{q}_r)\{\hat{\boldsymbol{n}}\},\\
\mathcal{R} \xrightarrow{\mathbf{q}_e} \mathcal{B} &\Rightarrow \{\hat{\boldsymbol{b}}\} = \mathbf{C}(\mathbf{q}_e)\{\hat{\boldsymbol{r}}\}.
\end{aligned}$$

where $\mathbf{C}(\mathbf{q})$ is parametrized in terms of the quaternion $\mathbf{q}$ as follows [53, 58]

$$\mathbf{C}(\mathbf{q}) = ({q_0}^2 - {\mathbf{q}_\mathbf{v}}^T\mathbf{q}_\mathbf{v})\mathbf{I} + 2\mathbf{q}_\mathbf{v}{\mathbf{q}_\mathbf{v}}^T - 2q_0 S\left(\mathbf{q}_v\right). \tag{2.8}$$

The direction cosine matrix, $\mathbf{C}(\mathbf{q}_r)$ rotates the inertial frame $\mathcal{N}$ to $\mathcal{R}$ and can be defined similarly in terms of $\mathbf{q}_r$ by replacing the argument $\mathbf{q}$ in Eq. (2.8) with $\mathbf{q}_r$. The composite rotation from $\mathcal{R}$ to $\mathcal{B}$ frame can be represented in terms of $\mathbf{C}(\mathbf{q}_e)$ defined as

$$\mathbf{C}(\mathbf{q}_e) = \mathbf{C}(\mathbf{q})\mathbf{C}^{\mathrm{T}}(\mathbf{q}_r) \tag{2.9}$$

which leads to the definition of the multiplicative quaternion attitude tracking error $\mathbf{q}_e$. The angular velocity tracking error $\boldsymbol{\omega}_e$ is defined as

$$\begin{aligned} \boldsymbol{\omega}_e &= \boldsymbol{\omega} - \mathbf{C}(\mathbf{q}_e)\boldsymbol{\omega}_r \\ &= \boldsymbol{\omega} - \boldsymbol{\omega}_r^B, \end{aligned} \tag{2.10}$$

where $\boldsymbol{\omega}_r^B = \mathbf{C}(\mathbf{q}_e)\boldsymbol{\omega}_r$.

To derive the governing dynamics for the attitude error $\mathbf{C}(\mathbf{q}_e)$, the time-derivative of Eq. (2.9) is taken along with the following steps:

$$\begin{aligned} \dot{\mathbf{C}}(\mathbf{q}_e) &= -S(\boldsymbol{\omega})\mathbf{C}(\mathbf{q})\mathbf{C}^{\mathrm{T}}(\mathbf{q}_r) - \mathbf{C}(\mathbf{q})\left(S(\boldsymbol{\omega}_r)\mathbf{C}(\mathbf{q}_r)\right)^{\mathrm{T}} \\ &= -S(\boldsymbol{\omega})\mathbf{C}(\mathbf{q})\mathbf{C}^{\mathrm{T}}(\mathbf{q}_r) + \mathbf{C}(\mathbf{q})\mathbf{C}^{\mathrm{T}}(\mathbf{q}_r)S(\boldsymbol{\omega}_r) \\ &= -S(\boldsymbol{\omega})\mathbf{C}(\mathbf{q}_e) + \mathbf{C}(\mathbf{q}_e)S(\boldsymbol{\omega}_r) \\ &= -S(\boldsymbol{\omega})\mathbf{C}(\mathbf{q}_e) + S\left(\mathbf{C}(\mathbf{q}_e)\boldsymbol{\omega}_r\right)\mathbf{C}(\mathbf{q}_e) \\ &= -S(\boldsymbol{\omega}_e)\mathbf{C}(\mathbf{q}_e), \end{aligned} \tag{2.11}$$

where the following identity has been used:

$$\mathbf{C}(\mathbf{q}_e)S(\boldsymbol{\omega}_r) = S\left(\mathbf{C}(\mathbf{q}_e)\boldsymbol{\omega}_r\right)\mathbf{C}(\mathbf{q}_e),$$

which is a direct result of the fact that $\mathbf{C}(\mathbf{q}_e)S(\boldsymbol{\omega}_r)$ consists of a cross product operation under a three dimensional rigid body rotation. As such, for any vector $\mathbf{a} \in \mathcal{R}^3$, we may express the vector cross product as follows:

$$\begin{aligned}\mathbf{C}(\mathbf{q}_e)S(\boldsymbol{\omega}_r)\mathbf{a} = \mathbf{C}(\mathbf{q}_e)\left(\boldsymbol{\omega}_r \times \mathbf{a}\right) &= \mathbf{C}(\mathbf{q}_e)\boldsymbol{\omega}_r \times \mathbf{C}(\mathbf{q}_e)\mathbf{a} \\ &= S\left(\mathbf{C}(\mathbf{q}_e)\boldsymbol{\omega}_r\right)\mathbf{C}(\mathbf{q}_e)\mathbf{a}\end{aligned}$$

Differentiating Eq. (2.10) and using Eq. (2.2) along with Eq. (2.11) leads to the angular velocity error dynamics. The corresponding attitude kinematics in terms of $\mathbf{q}_e$ are obtained from Eq. (2.11). Thus, the overall attitude tracking error dynamics and kinematics are as follows [53]

$$\dot{\mathbf{q}}_e = \frac{1}{2}E(\mathbf{q}_e)\boldsymbol{\omega}_e \tag{2.12}$$

$$\mathbf{J}\dot{\boldsymbol{\omega}}_e = -S(\boldsymbol{\omega})\mathbf{J}\boldsymbol{\omega} + \mathbf{u} + \mathbf{J}\left[S(\boldsymbol{\omega}_e)\boldsymbol{\omega}_r^B - C(\mathbf{q}_e)\dot{\boldsymbol{\omega}}_r\right]. \tag{2.13}$$

2.2 Smooth Projection Mechanism in Adaptive Control

This section briefly reviews certainty-equivalence based adaptive control and smooth projection mechanism. Adaptive control adjusts to unknown system parameters by updating its controller parameters online using measured signals, and does so while maintaining stability and consistent performance of the system. A vast majority of existing adaptive attitude-control formulations for stabilizing spacecraft attitude tracking dynamics are constructed in

the certainty-equivalence (CE) framework [23, 24]. Essentially, the structure of the control when parameters are known is used to construct an equivalent adaptive controller when parameters are unknown by using their estimated values. This is known as the certainty equivalence principle.

In aerospace applications, it is often the case that some a priori knowledge exists pertaining to the structure of uncertain plant parameters. A particular and frequently occurring example of this is when the upper and lower bounds of a spacecraft's inertia matrix parameters are known during pre-flight testing. In such a case, designing a parameter update law that takes account of this information is highly advantageous as it restricts the search space (parameter estimate values) to within a feasible region of values that are taken on by the true parameters. An immediate consequence of confining parameters to a compact set is that the closed-loop system demonstrates better convergence performance and overall robustness [43]. A few parameter projection schemes are available in this regard. The technique of [8] and [21] incorporates a priori knowledge of bounds on the parameters. However, these projection mechanisms lead to a discontinuous control law which may potentially cause undesirable system performance related to high-frequency control chattering leading to excitation of unmodeled dynamics. To avoid control discontinuities, a convenient alternative is the smooth projection scheme originally suggested by Pomet et al. [45] and used in [13, 27, 82] which results in $\mathcal{C}^1$ continuous adaptive control laws. The more recent work by Akella and Subbarao [3] proposes a smooth projection scheme that results in a $\mathcal{C}^\infty$ smooth adaptive

controller.

A brief review of the projection scheme proposed in [27] (based on [45]) is summarized below. This projection scheme is implemented in the adaptive control result presented in Chapter 3. Consider the nth-order nonlinear single input system with the following structure

$$\begin{aligned} \dot{x}_i &= x_{i+1}, \quad i = 1, 2, \ldots, n-1 \\ \dot{x}_n &= \sum_{i=1}^{p} \theta_i f_i(\mathbf{x}) + u, \end{aligned} \tag{2.14}$$

with the state $\mathbf{x} = [x_1, \ldots, x_n]^T \in \mathcal{R}^n$ and input $u \in \mathcal{R}$. The constant parameters θ_1 to θ_p are unknown, but the vector $\boldsymbol{\theta} = [\theta_1, \ldots, \theta_p]^{\mathrm{T}}$ belongs to Ω, a known compact convex subset of $\mathcal{R}^p$. The functions f_i are known smooth and regular nonlinear functions. The control objective is to design a smooth adaptive controller that uses prior knowledge of the set Ω and guarantees global asymptotic stability and tracking for $x(t)$ along any bounded reference signal $x_r(t)$ with bounded derivatives up to nth order. To facilitate the adaptive control law formulation, define the tracking error $e(t) = x - x_r$. From Eq. (2.14), the following dynamics are obtained

$$\begin{aligned} \dot{e}_1 &= e_2 \\ \dot{e}_2 &= e_3 \\ &\vdots \\ \dot{e}_n &= \sum_{i=1}^{p} \theta_i f_i(\mathbf{x}) + u - \dot{x}_r^{(n)} \end{aligned} \tag{2.15}$$

where (n) denote the nth derivative. The equation above can be rewritten as

$$\dot{\mathbf{e}} = \mathbf{A}\mathbf{e} + \mathbf{b}\left(\boldsymbol{\theta}^{\mathrm{T}}\mathbf{f} + u - x_r^{(n)}\right), \tag{2.16}$$

where $\mathbf{e} = [e_1, e_2, \ldots, e_n]^{\mathrm{T}}$, $\mathbf{f} = [f_1, f_2, \ldots, f_n]^{\mathrm{T}}$, and $(\mathbf{A}, \mathbf{b})$ are controllable canonical pairs

$$\mathbf{A} = \begin{bmatrix} 0 & 1 & 0 & \ldots & 0 \\ 0 & 0 & 1 & \ldots & 0 \\ \vdots & & & & \\ 0 & 0 & \ldots & 1 & 0 \\ 0 & 0 & \ldots & 0 & 1 \\ 0 & 0 & \ldots & 0 & 0 \end{bmatrix}, \quad \mathbf{b} = \begin{bmatrix} 0 \\ 0 \\ \vdots \\ 0 \\ 0 \\ 1 \end{bmatrix}.$$

Using the standard certainty equivalence approach, the adaptive control law is prescribed as

$$u = -\hat{\boldsymbol{\theta}}^{\mathrm{T}}\mathbf{f} + x_r^{(n)} - \mathbf{K}\mathbf{e}, \tag{2.17}$$

where $\mathbf{K}$ is such that $\mathbf{A}_m = \mathbf{A} - \mathbf{b}\mathbf{K}$ is a Hurwitz matrix and $\hat{\boldsymbol{\theta}}$ is an estimate of $\boldsymbol{\theta}$ that is to be determined by the parameter update laws. The closed-loop equation is

$$\dot{\mathbf{e}} = \mathbf{A}_m\mathbf{e} - \mathbf{b}\tilde{\boldsymbol{\theta}}^{\mathrm{T}}\mathbf{f}. \tag{2.18}$$

Now consider the standard Lyapunov function candidate [27]

$$V = \mathbf{e}^{\mathrm{T}}\mathbf{P}\mathbf{e} + \frac{1}{\gamma}\tilde{\boldsymbol{\theta}}^{\mathrm{T}}\tilde{\boldsymbol{\theta}}, \tag{2.19}$$

where $\mathbf{P} = \mathbf{P}^{\mathrm{T}} > 0$ is the solution of the Lyapunov equation $\mathbf{P}\mathbf{A}_m + \mathbf{A}_m^{\mathrm{T}}\mathbf{P} = -\mathbf{Q}$ with $\mathbf{Q} = \mathbf{Q}^{\mathrm{T}} > 0$, γ is any positive scalar constant, and $\tilde{\boldsymbol{\theta}} = \hat{\boldsymbol{\theta}} - \boldsymbol{\theta}$ is the parameter estimation error. The time-derivative of V along the trajectories of the system is given by

$$\dot{V} = -\mathbf{e}^{\mathrm{T}}\mathbf{Q}\mathbf{e} + \frac{1}{\gamma}\tilde{\boldsymbol{\theta}}^{\mathrm{T}}\left(\dot{\hat{\boldsymbol{\theta}}} - 2\mathbf{f}\mathbf{e}^{\mathrm{T}}\mathbf{P}\mathbf{b}\right). \tag{2.20}$$

Let $\boldsymbol{\phi}$ be defined such that

$$\boldsymbol{\phi} = 2\mathbf{f}\mathbf{e}^{\mathrm{T}}\mathbf{P}\mathbf{b}. \tag{2.21}$$

The parameter adaptation rule is to be chosen in such a manner that yields

$$\tilde{\boldsymbol{\theta}}^{\mathrm{T}}\left[\dot{\hat{\boldsymbol{\theta}}} - \frac{1}{\gamma}\boldsymbol{\phi}\right] \leq 0$$

while ensuring $\hat{\boldsymbol{\theta}}(t) \in \Omega$ for all $t \geq 0$. Suppose Ω is the convex set $\Omega = \left\{\boldsymbol{\theta} \mid \boldsymbol{\theta}^{\mathrm{T}}\boldsymbol{\theta} \leq \beta\right\}$ and let $\hat{\Omega} = \left\{\hat{\boldsymbol{\theta}} \mid \hat{\boldsymbol{\theta}}^{\mathrm{T}}\hat{\boldsymbol{\theta}} \leq \beta + \delta\right\}$, where $\beta > 0$ and $\delta > 0$ are known. Let the adaptation rule be given by

$$\dot{\hat{\boldsymbol{\theta}}} = \mathrm{Proj}(\hat{\boldsymbol{\theta}}, \boldsymbol{\phi}) \tag{2.22}$$

where $\mathrm{Proj}(\hat{\boldsymbol{\theta}}, \boldsymbol{\phi})$ is defined as

$$\mathrm{Proj}(\hat{\boldsymbol{\theta}}, \boldsymbol{\phi}) = \begin{cases} \frac{1}{\gamma}\boldsymbol{\phi}, & \text{if (i) } \|\hat{\boldsymbol{\theta}}\|^2 < \beta, \\ & \text{or (ii) } \|\hat{\boldsymbol{\theta}}\|^2 \geq \beta \text{ and } \boldsymbol{\phi}^{\mathrm{T}}\hat{\boldsymbol{\theta}} < 0, \\ \frac{1}{\gamma}\tilde{\boldsymbol{\phi}}, & \text{otherwise,} \end{cases} \tag{2.23}$$

with $\boldsymbol{\phi}$ given by Eq. (4.3) and

$$\tilde{\boldsymbol{\phi}} = \boldsymbol{\phi} - \frac{\left(\hat{\boldsymbol{\theta}}^{\mathrm{T}}\hat{\boldsymbol{\theta}} - \beta\right)\hat{\boldsymbol{\theta}}^{\mathrm{T}}\boldsymbol{\phi}}{\delta\hat{\boldsymbol{\theta}}^{\mathrm{T}}\hat{\boldsymbol{\theta}}}\hat{\boldsymbol{\theta}}. \tag{2.24}$$

Observe that $\mathrm{Proj}(\hat{\boldsymbol{\theta}}, \boldsymbol{\phi})$ is locally Lipschitz in $(\hat{\boldsymbol{\theta}}, \boldsymbol{\phi})$ and satisfies

$$\hat{\boldsymbol{\theta}}(0) \in \Omega \implies \hat{\boldsymbol{\theta}}(t) \in \hat{\boldsymbol{\theta}}, \quad \forall t \geq 0. \tag{2.25}$$

To verify this, observe that Eq. (2.25) is trivially satisfied for case (i) in Eq. (2.23). For case (ii), $\tilde{\boldsymbol{\theta}}^{\mathrm{T}}[\dot{\hat{\boldsymbol{\theta}}} - (1/\gamma)\boldsymbol{\phi}] = 0$ and $\hat{\boldsymbol{\theta}}^{\mathrm{T}}\dot{\hat{\boldsymbol{\theta}}} = (1/\gamma)\hat{\boldsymbol{\theta}}^{\mathrm{T}}\boldsymbol{\phi} \leq 0$ so $\hat{\boldsymbol{\theta}}$ is decreasing towards the origin. Finally, for case (iii), Eq. (2.23) leads to

$$\hat{\boldsymbol{\theta}}^{\mathrm{T}}\dot{\hat{\boldsymbol{\theta}}} = \begin{cases} = 0 & \text{if } \|\hat{\boldsymbol{\theta}}\|^2 = \beta + \delta, \\ < 0 & \text{if } \|\hat{\boldsymbol{\theta}}\|^2 > \beta + \delta, \\ > 0 & \text{if } \|\hat{\boldsymbol{\theta}}\|^2 < \beta + \delta. \end{cases}$$

Thus, if the initial parameter estimates are contained in the convex set Ω then $\hat{\boldsymbol{\theta}}(t) \in \hat{\Omega}$ for all time thereafter. Further, since $\mathrm{Proj}(\hat{\boldsymbol{\theta}}, \boldsymbol{\phi})$ is locally Lipschitz in the state variables, for any initial condition, the closed-loop system has a unique solution defined on some time interval $[0, T_0)$, $T_0 > 0$. Let $[0, T)$ be the maximum interval of existence of the solution. Since $\dot{V} \leq 0$, V, $\mathbf{e}$, and $\tilde{\boldsymbol{\theta}}$ are uniformly bounded on $[0, T)$. Further, since x_r is bounded, $\mathbf{x}$ is bounded on $[0, T)$ which implies that $T = \infty$. Boundedness of $\hat{\boldsymbol{\theta}}$ follows directly from $\hat{\boldsymbol{\theta}} \in \hat{\Omega}$. Finally, since all closed-loop signals are bounded, using $\dot{V} \leq -\mathbf{e}^{\mathrm{T}}\mathbf{Q}\mathbf{e}$ together with the invariance principle theorem leads to $\mathbf{e}(t) \to 0$ as $t \to \infty$. Thus, by using the smooth projection scheme Eq. (2.23), the

parameter estimates are always guaranteed to be bounded in the convex set $\hat{\Omega}$ while ensuring $\mathcal{C}^1$ continuity for the adaptive control law.

2.2.1 Persistence of Excitation

The features of a reference signal play an important role in parameter convergence. For the system described by Eq. (2.18), the estimated signals $\hat{\boldsymbol{\theta}}$ will converge to their true values provided that the underlying reference signal $u(t)$ is complex enough to produce rich excitation in the system for high quality estimation data. The reference signal that is able to uniquely identify the parameters of a system is said to be persistently exciting. Specifically, $u(t)$ is said to be persistently exciting if there exist positive constants α, and T such that

$$\int_t^{t+T} u^2(\tau)\, d\tau \geq \alpha, \qquad \forall\ t \geq 0. \tag{2.26}$$

The definition of persistence of excitation given in Equation (2.26) can be generalized for a vector signal $\mathbf{u}$ as [60]

$$\int_t^{t+T} \mathbf{u}(\tau)\mathbf{u}^T(\tau)\, d\tau \geq \alpha\mathbf{I}, \qquad \forall\ t \geq 0, \tag{2.27}$$

where $\mathbf{I}$ is the 3×3 identity matrix.

2.3 Mathematical Concepts

The following definitions and important mathematical results are used in the dissertation.

2.3.1 Passive Systems Theory

A function $\mathbf{u} \in \mathcal{L}_2$ if [28]

$$\|\mathbf{u}\|_2 = \sqrt{\int_0^\infty \mathbf{u}(t)^{\mathrm{T}}\mathbf{u}(t)\ \mathrm{d}t} < \infty \tag{2.28}$$

and $\mathbf{u} \in \mathcal{L}_{2e}$ if

$$\|\mathbf{u}\|_{2T} = \sqrt{\int_0^T \mathbf{u}(t)^{\mathrm{T}}\mathbf{u}(t)\ \mathrm{d}t} < \infty, \quad \forall\ T \in \mathbb{R}^+ \tag{2.29}$$

Definition 2.3.1. *Passivity [18]:* A system $\mathcal{H} : \mathcal{L}_{2e} \to \mathcal{L}_{2e}$ with inputs $\mathbf{u} \in \mathcal{L}_{2e}$ and outputs $\mathbf{y} \in \mathcal{L}_{2e}$ is passive if there exists some constant β such that

$$\int_0^T \mathbf{y}^{\mathrm{T}}\mathbf{u}\ \mathrm{d}t \geq \beta, \quad \forall\ \mathbf{u} \in \mathcal{L}_{2e},\ \forall\ T \in \mathbb{R}^+. \tag{2.30}$$

2.3.2 Barbalat's Lemma

The following lemma is used frequently throughout the dissertation for stability analysis:

Lemma 2.3.1. (Barbalat's Lemma)[51, 60] *Let $f(t)$ be a uniformly continuous function, such that $\lim_{t\to\infty} \int_0^t f(\tau)\, d\tau$ exists and is finite. Then, $\lim_{t\to\infty} f(t) = 0$.*

An immediate and practical corollary to Barbalat's lemma stated above is given as follows:

Corollary 2.3.2. [51] *If $f \in \mathcal{L}_\infty \cap \mathcal{L}_p$ for some integer $p \in [1, \infty)$, and $\dot{f} \in \mathcal{L}_\infty$ (bounded), then* $\lim_{t\to\infty} f(t) = 0$.

2.3.3 Strict Lyapunov Functions

The definition of *strict* Lyapunov function is formally stated here [37].

Definition 2.3.2. A real valued function $k(\cdot)$ is said to belong to class $\mathcal{K}_\infty$ if it is continuous, zero at zero, strictly increasing and $k(r) \to +\infty$ as $r \to +\infty$.

Definition 2.3.3. A function $V(t, \mathbf{x})$ is a Lyapunov function if it is continuously differentiable and there exist two functions $\alpha_1(\cdot)$ and $\alpha_2(\cdot)$ of class $\mathcal{K}_\infty$ such that

$$\alpha_1 (\|\mathbf{x}\|) \leq V (t, \mathbf{x}) \leq \alpha_2 (\|\mathbf{x}\|) .$$

Definition 2.3.4. Consider a non-autonomous system

$$\dot{\mathbf{x}} = \mathbf{f} (t, \mathbf{x}) . \tag{2.31}$$

A continuously differentiable function $V(t, \mathbf{x})$ is a *strict* Lyapunov function for system Eq. (2.31) if it is a Lyapunov function and there exists a positive definite function $\alpha_3(\cdot)$ such that

$$\frac{\partial V}{\partial t}(t, \mathbf{x}) + \frac{\partial V}{\partial \mathbf{x}}(t, \mathbf{x})\mathbf{f}(t, \mathbf{x}) \leq -\alpha_3 (\|\mathbf{x}\|) .$$

2.3.4 Linear Filters

The result stated below for a stable linear filter-type construction is used to ascertain stability properties in Chapter 5:

Lemma 2.3.3. *Consider the linear system*

$$\dot{\mathbf{x}}_f = \mathbf{A}_m \mathbf{x}_f + \boldsymbol{\omega} \tag{2.32}$$

with any Hurwitz $\mathbf{A}_m$ *and a uniformly bounded input* $\boldsymbol{\omega}$*. Then* $\mathbf{x}_f(t) \to 0$ *as* $t \to \infty \Leftrightarrow \boldsymbol{\omega}(t) \to 0$ *as* $t \to \infty$*.*

Chapter 3

Adaptive Attitude-Tracking Control of Spacecraft with Uncertain Time-Varying Inertia Parameters

While adaptive control schemes for spacecraft attitude tracking are abundant in controls literature, very few are designed to guarantee consistent performance for a spacecraft with both rigid and non-rigid (time-varying) inertia components. Since inertia matrix changes are a common occurrence due to phenomena like fuel depletion or mass displacement in a deployable spacecraft, an adaptive control algorithm that takes explicit account of such information is of significant interest. In this chapter, a novel adaptive attitude control scheme

is presented for the case when the spacecraft inertia matrix parameters have unknown rigid components and partially known variable components. The proposed controller directly compensates for inertia variations that are either pure functions of the control input, or functions of time and/or the state.

The adaptive attitude-tracking control strategy proposed in this study is based on the classical certainty-equivalence (CE) principle [24, 52]. The attitude measurements, given in terms of the unit quaternion, and the corresponding body angular rates are assumed to be perfectly measured and available for feedback. Thus, assuming an uncertain time-varying inertia matrix, the proposed control method delivers (almost) globally stabilizing closed-loop performance with asymptotic tracking of any bounded and smooth reference trajectory for most initial conditions. When dealing with an input-dependent inertia matrix, mild restrictions on the initial conditions are necessary to guarantee a bounded control input. In addition, a smooth projection scheme is implemented to bound the parameter estimates within a well-defined convex set, so as to avoid any singularity issues in the proposed controller.

In the development that follows, the attitude and angular velocity tracking-error dynamics for a spacecraft with time-varying inertia matrix are derived in Sec. 3.1. The main results of the chapter along with stability analysis are presented in Secs. 3.2-3.3: in Sec. 3.2, an adaptive attitude control law is presented for time and state dependent inertia matrices, while in Sec. 3.3, the control method is extended to handle an input-dependent inertia matrix. In Sec. 3.4, numerical simulations are provided for spacecraft appendage de-

ployment and fuel-loss scenarios. Finally, in Sec. 3.5, concluding remarks summarize presented results.

3.1 Problem Statement

A non-rigid body is characterized by a time-varying inertia matrix. As a result, the angular velocity error dynamics of Eq. (2.13) are not valid, and must be re-derived for a non-constant inertia matrix. The attitude dynamics of the non-rigid body are governed by the following rotational equations of motion:

$$\mathbf{J}\dot{\boldsymbol{\omega}} = -\dot{\mathbf{J}}\boldsymbol{\omega} - S\left(\boldsymbol{\omega}\right)\mathbf{J}\boldsymbol{\omega} + \mathbf{u}, \tag{3.1}$$

where $\mathbf{J} = \mathbf{J}(t) \in \mathbb{R}^{3\times3}$ is now a time-varying, symmetric positive-definite mass-moment of inertia matrix of the spacecraft. Using Eq. (3.1) and following through with same procedure used to obtain Eq. (2.13) for a rigid-body, the non-rigid angular velocity error dynamics are derived as

$$\dot{\boldsymbol{\omega}}_e = \mathbf{J}^{-1}\left(-\dot{\mathbf{J}}\boldsymbol{\omega} - S\left(\boldsymbol{\omega}\right)\mathbf{J}\boldsymbol{\omega} + \mathbf{u}\right) + S\left(\boldsymbol{\omega}_e\right)\mathbf{C}(\mathbf{q}_e)\boldsymbol{\omega}_r - \mathbf{C}(\mathbf{q}_e)\dot{\boldsymbol{\omega}}_r. \tag{3.2}$$

The attitude error kinematics given in Eq. (2.12) remain unchanged, and are restated below for the reader's convenience:

$$\dot{\mathbf{q}}_e = \frac{1}{2}\mathbf{E}(\mathbf{q}_e)\boldsymbol{\omega}_e. \tag{2.12}$$

3.1.1 Characterization of Time-Varying Inertia Matrix

The particular time-varying inertia matrix model treated in the upcoming adaptive control law development is expressed according to

$$\mathbf{J}(t) = \mathbf{J}_0 - \mathbf{J}_1\mathbf{\Psi}(t), \tag{3.3}$$

where $\mathbf{J}_0 \in \mathbb{R}^{3\times3}$, $\mathbf{J}_0 = \mathbf{J}_0^{\mathrm{T}} > 0$ is an unknown, constant matrix which represents the rigid portion of the spacecraft, while $\mathbf{J}_1\mathbf{\Psi}$ is the non-rigid component of the spacecraft that satisfies

$$\mathbf{J}_1\mathbf{\Psi} \in \mathbb{R}^{3\times3}, \quad \mathbf{J}_1\mathbf{\Psi} = \mathbf{\Psi}^{\mathrm{T}}\mathbf{J}_1^{\mathrm{T}}. \tag{3.4}$$

In particular, $\mathbf{J}_1 \in \mathbb{R}^{3\times n}$ is unknown and constant, while $\mathbf{\Psi}(t) \in \mathbb{R}^{n\times3}$ is known and time-dependent for any $n > 0$. In Eq. (3.3), observe that $\mathbf{J}$ is the difference of two symmetric matrices, which ensures $\mathbf{J} = \mathbf{J}^{\mathrm{T}}$ for all $t \geq 0$. Moreover, while $\mathbf{J}_1\mathbf{\Psi}$ itself may be sign-indefinite, it must ensure that $\mathbf{J} = \mathbf{J}_0 - \mathbf{J}_1\mathbf{\Psi} > 0$ for all time. In addition, to guarantee a physically possible distribution of mass, careful consideration should be given during the mathematical modeling process to ensure that the inertia matrix satisfies the following triangle inequalities for all time [78]

$$\tilde{J}_1 + \tilde{J}_2 \geq \tilde{J}_3, \quad \tilde{J}_2 + \tilde{J}_3 \geq \tilde{J}_1, \quad \tilde{J}_3 + \tilde{J}_1 \geq \tilde{J}_2, \tag{3.5}$$

where $\tilde{J}_1, \tilde{J}_2, \tilde{J}_3$ are the principal moments of inertia of the spacecraft.

We now examine specific details regarding the structure of $\mathbf{J}_1$ and $\mathbf{\Psi}$. In particular, mathematical characterizations are provided for a time and/or

state dependent inertia matrix for mass displacement due to phenomena such as deploying appendages, as well as an input, $\mathbf{u}$, dependent inertia matrix that models mass-loss due to fuel expenditure. Pertinent details related to the structure of $\mathbf{J}_1\boldsymbol{\Psi}$ are provided along with illustrative examples.

Time and/or State Dependent Inertia Matrix

When variations in $\mathbf{J}$ have explicit dependence on time or the spacecraft state $\mathbf{x} = [\mathbf{q}_{e_v}^{\mathrm{T}}, \boldsymbol{\omega}^{\mathrm{T}}]^{\mathrm{T}}$, the time-derivative of Eq. (3.3) is given by

$$\dot{\mathbf{J}}(t) = -\mathbf{J}_1\dot{\boldsymbol{\Psi}}(t, \mathbf{x}(t)) \tag{3.6}$$

where $\dot{\boldsymbol{\Psi}}(t, \mathbf{x}(t))$ is known and well characterized. If the inertia matrix in Eq. (3.6) is purely dependent on time, as is the case for a deploying appendage, the argument $\mathbf{x}$ would be dropped so that $\dot{\boldsymbol{\Psi}} = \dot{\boldsymbol{\Psi}}(t)$.

To illustrate the efficacy of Eq. (3.3) and Eq. (3.6) for moving mass problems, consider the example of a spacecraft shown in Fig. 3.1 with deploying parts. Let $\tilde{\mathbf{J}}_0$ represent the spacecraft's main body's inertia matrix relative to O, the spacecraft's center of mass, determined in the body-fixed frame $\mathcal{B}$ with basis $\boldsymbol{b} = \left\{\hat{\boldsymbol{b}}_1, \hat{\boldsymbol{b}}_2, \hat{\boldsymbol{b}}_3\right\}$. The center of mass of a moving object with unknown constant mass m_1 is located at a position $\boldsymbol{\rho}_1(t) = \rho_{1_1}(t)\hat{\boldsymbol{b}}_1 + \rho_{1_2}(t)\hat{\boldsymbol{b}}_2 + \rho_{1_3}(t)\hat{\boldsymbol{b}}_3$ relative to O. This object has an unknown moment of inertia $\mathbf{J}'_{m_1}$ relative to a set of parallel axes located at $\boldsymbol{\rho}_1$. Another moving object with unknown mass m_2 is located at a different position $\boldsymbol{\rho}_2(t)$ (relative to O), and is characterized by an unknown inertia matrix $\mathbf{J}'_{m_2}$ relative to a parallel set of axes at its own

center of mass. Observe that both position vectors $\boldsymbol{\rho}_1(t)$ and $\boldsymbol{\rho}_2(t)$ are known functions of time that are each bounded and smooth.

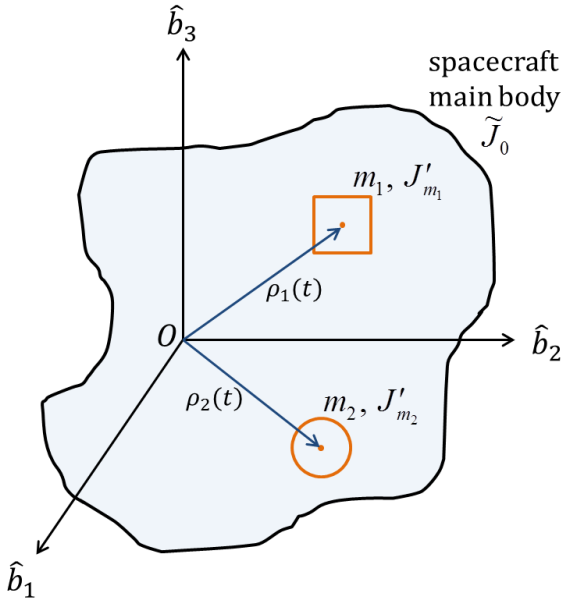

Figure 3.1: A spacecraft with mass displacement due to deploying appendages.

Through an application of the parallel-axis theorem, and assuming that the spacecraft center of mass is unaffected by mass movement, the overall inertia matrix of the spacecraft is given by

$$\mathbf{J} = \tilde{\mathbf{J}}_0 + \mathbf{J}'_{m_1} + m_1 \left[\boldsymbol{\rho}_1^{\mathrm{T}}\boldsymbol{\rho}_1\mathbf{I} - \boldsymbol{\rho}_1\boldsymbol{\rho}_1^{\mathrm{T}}\right] + \mathbf{J}'_{m_2} + m_2 \left[\boldsymbol{\rho}_2^{\mathrm{T}}\boldsymbol{\rho}_2\mathbf{I} - \boldsymbol{\rho}_2\boldsymbol{\rho}_2^{\mathrm{T}}\right] \tag{3.7}$$

which is easily written in the form of Eq. (3.3) with $\mathbf{J}_0$ given by

$$\mathbf{J}_0 = \tilde{\mathbf{J}}_0 + \mathbf{J}'_{m_1} + \mathbf{J}'_{m_2} \tag{3.8}$$

and $\mathbf{J}_1\boldsymbol{\Psi}$ expressed as

$$\mathbf{J}_1\boldsymbol{\Psi} = -\begin{bmatrix} m_1\mathbf{I} & m_2\mathbf{I} \end{bmatrix}\begin{bmatrix} \boldsymbol{\rho}_1^{\mathrm{T}}(t)\boldsymbol{\rho}_1(t)\mathbf{I} - \boldsymbol{\rho}_1(t)\boldsymbol{\rho}_1^{\mathrm{T}}(t) \\ \boldsymbol{\rho}_2^{\mathrm{T}}(t)\boldsymbol{\rho}_2(t)\mathbf{I} - \boldsymbol{\rho}_2(t)\boldsymbol{\rho}_2^{\mathrm{T}}(t) \end{bmatrix} \tag{3.9}$$

where $\mathbf{I}$ is the 3×3 identity matrix, $\mathbf{J}_1 \in \mathbb{R}^{3\times 6}$ is unknown and constant, while $\boldsymbol{\Psi} \in \mathbb{R}^{6\times 3}$ is known and time-dependent and can be easily differentiated to obtain $\dot{\boldsymbol{\Psi}}(t)$.

Input Dependent Inertia Matrix

For the specific case of spacecraft undergoing fuel loss, the matrix $\dot{\boldsymbol{\Psi}}$ depends explicitly on the control vector components $\mathbf{u}$, such that

$$\dot{\mathbf{J}}(t) = -\mathbf{J}_1\dot{\boldsymbol{\Psi}}(\mathbf{u}(t)). \tag{3.10}$$

Observe that $\boldsymbol{\Psi} = \int_0^t \dot{\boldsymbol{\Psi}}(\mathbf{u}(\tau))\,\mathrm{d}\tau$ can be numerically computed for feedback. It is important to note that no general mass depletion model exists in this regard, and that the structure of $\dot{\boldsymbol{\Psi}}$ is a factor of the propulsion system, and more specifically, the propellant reservoir/tank configuration within the spacecraft.

One particular model for fuel-loss is discussed next, wherein a single propellant tank is assumed to undergo uniform mass-loss as a result of control torque action. The center of mass, P, of the tank is located at at $\boldsymbol{\rho} = \rho_1\hat{\boldsymbol{b}}_1 + \rho_2\hat{\boldsymbol{b}}_2 + \rho_3\hat{\boldsymbol{b}}_3$ relative to the known spacecraft mass center O. It is reasonable to assume that the fuel tank's principal axes are parallel with the body-fixed axes. The configuration, as illustrated in Fig. 3.2, is applicable to many existing

spacecraft, especially for spacecraft of smaller scale such as micro-satellites.

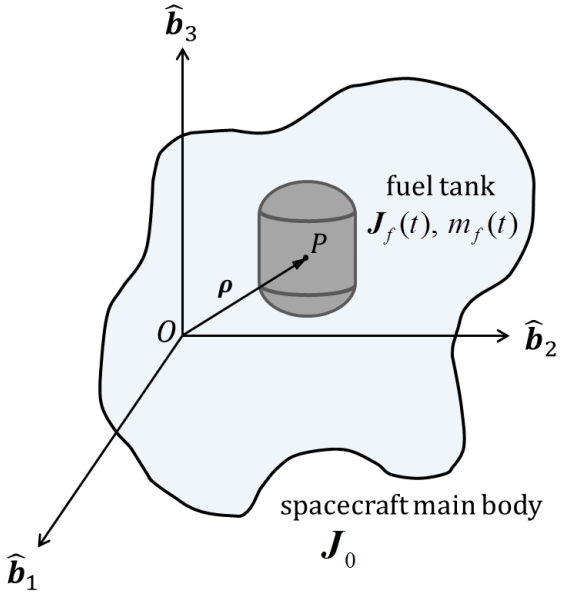

Figure 3.2: Spacecraft with a single propellant tank undergoing fuel mass-loss proportionate to the commanded control torque.

The inertia matrix of the spacecraft's main body, relative to its center of mass O, is denoted by $\mathbf{J}_0$. The principal moment of inertia matrix of the fuel tank relative to P is denoted as $\mathbf{J}_f(t)$ and derived as follows. Using the mass relation

$$\dot{m}_f(t) = -c\|\mathbf{u}\|; \quad m_f(0) = m_{f_0} \tag{3.11}$$

where $m_f(t)$ is the time-varying mass of the propellant tank, $m_{f_0} > 0$ is its fuel mass at time $t = 0$ and the constant $c > 0$, which relates the control torque $\mathbf{u}$ to mass loss, is imprecisely determined, and ignoring slosh effects, it can be

shown that $\mathbf{J}_f$ evolves according to the dynamical equation

$$\dot{\mathbf{J}}_f = -\text{diag}\left\{\alpha_1,\ \alpha_2,\ \alpha_3\right\}\|\mathbf{u}\|, \tag{3.12}$$

where $\alpha_i = d_i c > 0$ for all $i = 1, 2, 3$ is an unknown constant given as the product of the torque-to-mass relational constant c and the constant $d_i > 0$ which depends on the dimension and shape of the fuel tank. For example, if the fuel tank is a sphere of radius r, then $d_i = (2/5)r^2$. The expression in Eq. (3.12) can be readily integrated to obtain $\mathbf{J}_f$ relative to P. Next, applying the parallel-axis theorem to determine $\mathbf{J}_f$ relative to O leads to the expression $-\mathbf{J}_1\boldsymbol{\Psi} = \mathbf{J}_f + m_f(t)\left[\boldsymbol{\rho}^{\mathrm{T}}\boldsymbol{\rho}\mathbf{I} - \boldsymbol{\rho}\boldsymbol{\rho}^{\mathrm{T}}\right]$, where $\mathbf{J}_1\boldsymbol{\Psi}$ represents the variable component of the overall spacecraft inertia matrix $\mathbf{J}$. Differentiating this expression and using the mass change relation in Eq. (3.11) together with Eq. (3.12), yields the following dynamical equation governing the evolution of the matrix $\mathbf{J}_1\boldsymbol{\Psi}$

$$-\mathbf{J}_1\dot{\boldsymbol{\Psi}}(\mathbf{u}) = -\underbrace{\left(\text{diag}\left\{\alpha_1,\ \alpha_2,\ \alpha_3\right\} + c\left[\boldsymbol{\rho}^{\mathrm{T}}\boldsymbol{\rho}\mathbf{I} - \boldsymbol{\rho}\boldsymbol{\rho}^{\mathrm{T}}\right]\right)}_{\mathbf{J}_1}\underbrace{\|\mathbf{u}\|\mathbf{I}}_{\dot{\boldsymbol{\Psi}}(u)}, \tag{3.13}$$

where $\mathbf{J}_1$ is symmetric, positive definite, and unknown, while $\dot{\boldsymbol{\Psi}}(\mathbf{u}) = \|\mathbf{u}\|\mathbf{I}$.

Finally, with the dynamical model and inertia matrix characterizations in place, the control objective is now stated. The adaptive control objective is to track any prescribed reference trajectory, $[\mathbf{q}_r(t), \boldsymbol{\omega}_r(t)]$, with bounded and smooth $\boldsymbol{\omega}_r(t)$, for all initial conditions, $[\mathbf{q}(0), \boldsymbol{\omega}(0)]$, assuming full-state feedback and arbitrarily large uncertainty in the $\mathbf{J}_0$ and $\mathbf{J}_1$ matrix components. That is, a control torque, $\mathbf{u}$, needs to be designed such that the tracking error

signals converge, $\lim_{t\to\infty}\left[\mathbf{q}_{e_v}(t),\ \boldsymbol{\omega}_e(t)\right] = 0$, while ensuring that all closed-loop signals remain bounded at all times. Subsequent control development will specifically treat inertia matrices described by Eqs. (3.6) and (3.13).

3.2 Adaptive Attitude Tracking for Unknown Inertia with Time and State Dependencies

In this section, a novel adaptive control law is presented for the attitude and angular-velocity tracking problem described by Eqs. (2.12) and (3.2) for an unknown time-varying inertia matrix comprised of only state and time dependent terms and that evolves according to Eq. (3.6). First, in order to facilitate the adaptive controller development, some pertinent definitions and algebraic manipulations are introduced. To begin with, the dynamics of Eq. (3.2) are rearranged into a parameter-affine form through the judicious addition and subtraction of the terms

$$-\frac{1}{2}\left[q_{e0}\mathbf{I} + S\left(\mathbf{q}_{e_v}\right)\right]\boldsymbol{\omega}_e - \mathbf{J}^{-1}\beta\mathbf{q}_{e_v} - \mathbf{J}^{-1}k_v\boldsymbol{\omega}_e - \frac{1}{2}\mathbf{J}^{-1}\dot{\mathbf{J}}\left[\boldsymbol{\omega}_e + \mathbf{q}_{e_v}\right]$$

where $\beta, k_v > 0$. Thus,

$$\begin{aligned}\dot{\boldsymbol{\omega}}_e = &-\frac{1}{2}\left[q_{e0}\mathbf{I} + S\left(\mathbf{q}_{e_v}\right)\right]\boldsymbol{\omega}_e - \mathbf{J}^{-1}\beta\mathbf{q}_{e_v} - \mathbf{J}^{-1}k_v\boldsymbol{\omega}_e - \frac{1}{2}\mathbf{J}^{-1}\dot{\mathbf{J}}\left[\boldsymbol{\omega}_e + \mathbf{q}_{e_v}\right] \\ &+ \mathbf{J}^{-1}\left(\mathbf{u} + \frac{1}{2}\mathbf{J}\left[q_{e_0}\mathbf{I} + S\left(\mathbf{q}_{e_v}\right)\right]\boldsymbol{\omega}_e + \beta\mathbf{q}_{e_v} + k_v\boldsymbol{\omega}_e\right. \\ &\left. + \frac{1}{2}\dot{\mathbf{J}}\left[\boldsymbol{\omega}_e + \mathbf{q}_{e_v}\right] - S\left(\boldsymbol{\omega}\right)\mathbf{J}\boldsymbol{\omega} - \dot{\mathbf{J}}\boldsymbol{\omega} + \mathbf{J}\boldsymbol{\phi}\right) \quad (3.14)\end{aligned}$$

where $\boldsymbol{\phi} = S(\boldsymbol{\omega}_e)\mathbf{C}(\mathbf{q}_e)\boldsymbol{\omega}_r - \mathbf{C}(\mathbf{q}_e)\dot{\boldsymbol{\omega}}_r$. Recalling that $\mathbf{J} = \mathbf{J}_0 - \mathbf{J}_1\boldsymbol{\Psi}$ and $\dot{\mathbf{J}} = -\mathbf{J}_1\dot{\boldsymbol{\Psi}}$ and following through with some minor algebraic manipulations, it is straightforward to obtain

$$\begin{aligned}\dot{\boldsymbol{\omega}}_e = &-\frac{1}{2}\left[q_{e0}\mathbf{I} + S\left(\mathbf{q}_{e_v}\right)\right]\boldsymbol{\omega}_e - \mathbf{J}^{-1}\beta\mathbf{q}_{e_v} - \mathbf{J}^{-1}k_v\boldsymbol{\omega}_e + \frac{1}{2}\mathbf{J}^{-1}\mathbf{J}_1\dot{\boldsymbol{\Psi}}\left[\boldsymbol{\omega}_e + \mathbf{q}_{e_v}\right] \\ &+ \mathbf{J}^{-1}\Bigg(\mathbf{u} + \beta\mathbf{q}_{e_v} + k_v\boldsymbol{\omega}_e + \mathbf{J}_0\left(\frac{1}{2}\left[q_{e_0}\mathbf{I} + S\left(\mathbf{q}_{e_v}\right)\right]\boldsymbol{\omega}_e + \boldsymbol{\phi}\right) \\ &- S(\boldsymbol{\omega})\mathbf{J}_0\boldsymbol{\omega} - \mathbf{J}_1\boldsymbol{\Psi}\left(\frac{1}{2}\left[q_{e_0}\mathbf{I} + S\left(\mathbf{q}_{e_v}\right)\right]\boldsymbol{\omega}_e + \boldsymbol{\phi}\right) \\ &+ S(\boldsymbol{\omega})\mathbf{J}_1\boldsymbol{\Psi}\boldsymbol{\omega} + \mathbf{J}_1\dot{\boldsymbol{\Psi}}\left\{\omega - \frac{1}{2}\left[\boldsymbol{\omega}_e + \mathbf{q}_{e_v}\right]\right\}\Bigg) \quad (3.15)\end{aligned}$$

In Eq. (3.15), notice that $\mathbf{J}_0$ multiplies terms in a linear fashion, thus allowing the regressor matrix $\mathbf{W}_1$ to be constructed in the following manner

$$\mathbf{W}_1\boldsymbol{\theta}^* = \mathbf{J}_0\left(\frac{1}{2}\left[q_{e_0}\mathbf{I} + S\left(\mathbf{q}_{e_v}\right)\right]\boldsymbol{\omega}_e + \boldsymbol{\phi}\right) - S(\boldsymbol{\omega})\mathbf{J}_0\boldsymbol{\omega}, \quad (3.16)$$

where $\boldsymbol{\theta}^* = [J_{0_{11}}, J_{0_{12}}, J_{0_{13}}, J_{0_{22}}, J_{0_{23}}, J_{0_{33}}]^{\mathrm{T}}$ contains the six unique parameters of $\mathbf{J}_0$. Similarly, $\mathbf{J}_1$ also multiplies terms linearly in Eq. (3.15), which allows the regressor matrix definitions for $\mathbf{W}_2$ and $\mathbf{W}_3$ to be given by

$$\mathbf{W}_2\boldsymbol{\sigma}^* = -\mathbf{J}_1\boldsymbol{\Psi}\left(\frac{1}{2}\left[q_{e_0}\mathbf{I} + S\left(\mathbf{q}_{e_v}\right)\right]\boldsymbol{\omega}_e + \boldsymbol{\phi}\right) + S(\boldsymbol{\omega})\mathbf{J}_1\boldsymbol{\Psi}\boldsymbol{\omega}, \quad (3.17)$$

$$\mathbf{W}_3\boldsymbol{\sigma}^* = \mathbf{J}_1\dot{\boldsymbol{\Psi}}\left\{\boldsymbol{\omega} - \frac{1}{2}\left[\boldsymbol{\omega}_e + \mathbf{q}_{e_v}\right]\right\} \quad (3.18)$$

where $\boldsymbol{\sigma}^* \in \mathbb{R}^{3n}$ comprises the $3n$ parameters of the $\mathbf{J}_1$ matrix. Note that the regressor matrix $\mathbf{W}_2$ does not contain any $\dot{\boldsymbol{\Psi}}$ terms. By substituting Eqs. (3.16)-(3.18) into Eq. (3.15), the angular velocity error dynamics are

reduced to

$$\dot{\boldsymbol{\omega}}_e = -\frac{1}{2}\left[q_{e_0}\mathbf{I} + S\left(\mathbf{q}_{e_v}\right)\right]\boldsymbol{\omega}_e - \mathbf{J}^{-1}\beta\mathbf{q}_{e_v} - \mathbf{J}^{-1}k_v\boldsymbol{\omega}_e + \frac{1}{2}\mathbf{J}^{-1}\mathbf{J}_1\dot{\boldsymbol{\Psi}}\left[\boldsymbol{\omega}_e + \mathbf{q}_{e_v}\right] + \mathbf{J}^{-1}\left(\mathbf{u} + \beta\mathbf{q}_{e_v} + k_v\boldsymbol{\omega}_e + \mathbf{W}_1\boldsymbol{\theta}^* + \left(\mathbf{W}_2 + \mathbf{W}_3\right)\boldsymbol{\sigma}^*\right). \quad (3.19)$$

Since terms involving $\boldsymbol{\theta}^*$ and $\boldsymbol{\sigma}^*$ are unknown, and cannot be directly canceled by $\mathbf{u}$, the control is designed using parameter estimates, $\hat{\boldsymbol{\theta}}$ and $\hat{\boldsymbol{\sigma}}$. That is,

$$\mathbf{u} = -\beta\mathbf{q}_{e_v} - k_v\boldsymbol{\omega}_e - \mathbf{W}_1\hat{\boldsymbol{\theta}} - \left[\mathbf{W}_2 + \mathbf{W}_3\right]\hat{\boldsymbol{\sigma}} \quad (3.20)$$

with parameter estimation update laws

$$\dot{\hat{\boldsymbol{\theta}}} = \gamma_1\mathbf{W}_1^{\mathrm{T}}\left[\boldsymbol{\omega}_e + \mathbf{q}_{e_v}\right], \quad (3.21)$$

$$\dot{\hat{\boldsymbol{\sigma}}} = \gamma_2\left[\mathbf{W}_2 + \mathbf{W}_3\right]^{\mathrm{T}}\left[\boldsymbol{\omega}_e + \mathbf{q}_{e_v}\right], \quad (3.22)$$

where $k_v, \beta, \gamma_1, \gamma_2 > 0$ are any scalar constants. Finally, by substituting Eq. (3.20) into Eq. (3.19), the following closed-loop tracking-error dynamics are obtained:

$$\dot{\boldsymbol{\omega}}_e = -\frac{1}{2}\left[q_{e_0}\mathbf{I} + S\left(\mathbf{q}_{e_v}\right)\right]\boldsymbol{\omega}_e - \mathbf{J}^{-1}\beta\mathbf{q}_{e_v} - \mathbf{J}^{-1}k_v\boldsymbol{\omega}_e + \frac{1}{2}\mathbf{J}^{-1}\mathbf{J}_1\dot{\boldsymbol{\Psi}}\left[\boldsymbol{\omega}_e + \mathbf{q}_{e_v}\right] + \mathbf{J}^{-1}\big(-\mathbf{W}_1\tilde{\boldsymbol{\theta}} - \left(\mathbf{W}_2 + \mathbf{W}_3\right)\tilde{\boldsymbol{\sigma}}\big), \quad (3.23)$$

where $\tilde{\boldsymbol{\theta}} = \hat{\boldsymbol{\theta}} - \boldsymbol{\theta}^*$ and $\tilde{\boldsymbol{\sigma}} = \hat{\boldsymbol{\sigma}} - \boldsymbol{\sigma}^*$ are the estimation error quantities. The main result is now stated in the theorem that follows.

Theorem 3.2.1. *Consider the attitude tracking error system of Eqs.* (2.12) *and* (3.2) *with a time and/or state dependent inertia matrix* $\mathbf{J}$ *given by Eq.* (3.3)

with derivative Eq. (3.6)*. Suppose further that* $\mathbf{J}_1$ *and* $\mathbf{J}_0$ *are unknown. Then the adaptive control law Eq.* (3.20)*, along with the parameter estimation update laws Eqs.* (3.21)-(3.22) *guarantee asymptotic convergence of the tracking error signals* $\lim_{t\to\infty}\left[\mathbf{q}_{e_v}(t),\ \boldsymbol{\omega}_e(t)\right] = 0$ *for any initial condition* $[\mathbf{q}(0), \boldsymbol{\omega}(0)]$ *and all reference trajectories* $[\mathbf{q}_r(t), \boldsymbol{\omega}_r(t)]$*, with smooth and bounded* $\boldsymbol{\omega}_r(t)$*, while ensuring boundedness for all closed-loop signals.*

Proof. Consider the following positive semi-definite Lyapunov-like function

$$V = \frac{1}{2}\left(\boldsymbol{\omega}_e + \mathbf{q}_{e_v}\right)^{\mathrm{T}} \mathbf{J}\left(\boldsymbol{\omega}_e + \mathbf{q}_{e_v}\right) + (\beta + k_v)\left(\mathbf{q}_{e_v}^{\mathrm{T}}\mathbf{q}_{e_v} + (q_{e_0} - 1)^2\right) + \frac{1}{2\gamma_1}\tilde{\boldsymbol{\theta}}^{\mathrm{T}}\tilde{\boldsymbol{\theta}} + \frac{1}{2\gamma_2}\tilde{\boldsymbol{\sigma}}^{\mathrm{T}}\tilde{\boldsymbol{\sigma}}. \quad (3.24)$$

Taking the derivative of V and using the closed-loop system dynamics in Eqs. (2.12) and (3.23) along with the identity $\left(\boldsymbol{\omega}_e + \mathbf{q}_{e_v}\right)^{\mathrm{T}}\left(\mathbf{q}_{e_v} \times \boldsymbol{\omega}_e\right) = 0$ and making appropriate cancellations leads to

$$\begin{aligned}
\dot{V} &= \left(\boldsymbol{\omega}_e + \mathbf{q}_{e_v}\right)^{\mathrm{T}}\left(-\frac{1}{2}\mathbf{J}_1\dot{\boldsymbol{\Psi}}\left[\boldsymbol{\omega}_e + \mathbf{q}_{e_v}\right] + \mathbf{J}\left(\dot{\boldsymbol{\omega}}_e + \dot{\mathbf{q}}_{e_v}\right)\right) - 2(\beta + k_v)\,\dot{q}_{e_0} \\
&\quad + \frac{1}{\gamma_1}\tilde{\boldsymbol{\theta}}^{\mathrm{T}}\dot{\hat{\boldsymbol{\theta}}} + \frac{1}{\gamma_2}\tilde{\boldsymbol{\sigma}}^{\mathrm{T}}\dot{\hat{\boldsymbol{\sigma}}} \\
&= \left(\boldsymbol{\omega}_e + \mathbf{q}_{e_v}\right)^{\mathrm{T}}\left(-\beta\mathbf{q}_{e_v} - k_v\boldsymbol{\omega}_e - \mathbf{W}_1\tilde{\boldsymbol{\theta}} - (\mathbf{W}_2 + \mathbf{W}_3)\,\tilde{\boldsymbol{\sigma}}\right) + (\beta + k_v)\,\mathbf{q}_{e_v}^{\mathrm{T}}\boldsymbol{\omega}_e \\
&\quad + \frac{1}{\gamma_1}\tilde{\boldsymbol{\theta}}^{\mathrm{T}}\dot{\hat{\boldsymbol{\theta}}} + \frac{1}{\gamma_2}\tilde{\boldsymbol{\sigma}}^{\mathrm{T}}\dot{\hat{\boldsymbol{\sigma}}} \\
&= -k_v\|\boldsymbol{\omega}_e\|^2 - \beta\|\mathbf{q}_{e_v}\|^2 + \tilde{\boldsymbol{\theta}}^{\mathrm{T}}\left(\frac{1}{\gamma_1}\dot{\hat{\boldsymbol{\theta}}} - \mathbf{W}_1^{\mathrm{T}}\left(\boldsymbol{\omega}_e + \mathbf{q}_{e_v}\right)\right) \\
&\quad + \tilde{\boldsymbol{\sigma}}^{\mathrm{T}}\left(\frac{1}{\gamma_2}\dot{\hat{\boldsymbol{\sigma}}} - (\mathbf{W}_2 + \mathbf{W}_3)^{\mathrm{T}}\left(\boldsymbol{\omega}_e + \mathbf{q}_{e_v}\right)\right)
\end{aligned}$$

By selecting $\dot{\hat{\boldsymbol{\theta}}}$ and $\dot{\hat{\boldsymbol{\sigma}}}$ according to Eqs. (3.21) and (3.22), one obtains

$$\dot{V} = -k_v \|\boldsymbol{\omega}_e\|^2 - \beta \|\mathbf{q}_{e_v}\|^2$$

which is negative semi-definite. Since $V \geq 0$ and $\dot{V} \leq 0$, V is a monotonic function indicating that $V(t) \leq V(0)$. Consequently, all closed loop signals are bounded. Furthermore, $\int_0^t \dot{V}(t)\,\mathrm{d}t$ exists and is finite which implies that $\mathbf{q}_{e_v}, \boldsymbol{\omega}_e, \in \mathcal{L}_2 \cap \mathcal{L}_\infty$ and, consequently, from Eqs. (2.12) and (3.23) it follows that $\dot{\mathbf{q}}_{e_v}, \dot{\boldsymbol{\omega}}_e, \in \mathcal{L}_\infty$. Invoking Barbalat's Lemma leads to $\lim_{t\to\infty} \left[\mathbf{q}_{e_v}(t), \boldsymbol{\omega}_e(t)\right] = 0$. □

3.2.1 Smooth Parameter Projection

The parameter update laws in Eqs. (3.21) and (3.22) suffer from the drawback that the parameters $\hat{\boldsymbol{\theta}}$ and $\hat{\boldsymbol{\sigma}}$ can drift arbitrarily away from their respective true values. However, if the true parameters are bounded by a known scalar constant, then the estimates can also be constrained to evolve within a bounded convex set with known bound. This can be accomplished by modifying the parameter update laws by using a smooth projection algorithm [13, 82].

A suitable modification for the update law for $\hat{\boldsymbol{\theta}}$ is discussed next. To this end, define two convex sets

$$\boldsymbol{\Omega}_{\boldsymbol{\theta}^*} \triangleq \left\{\boldsymbol{\theta}^* \in \mathbb{R}^6 \mid \|\boldsymbol{\theta}^*\|^2 < \epsilon_1\right\}, \quad \boldsymbol{\Omega}_{\hat{\boldsymbol{\theta}}} \triangleq \left\{\hat{\boldsymbol{\theta}} \in \mathbb{R}^6 \mid \|\hat{\boldsymbol{\theta}}\|^2 < \epsilon_1 + \delta_1\right\} \quad (3.25)$$

for known $\epsilon_1 > 0$ and $\delta_1 > 0$. Consider the following smooth projection scheme

for $\hat{\boldsymbol{\theta}}$

$$\dot{\hat{\boldsymbol{\theta}}} = \text{Proj}\left(\hat{\boldsymbol{\theta}}, \boldsymbol{\Phi}\right); \quad \boldsymbol{\Phi} \triangleq \mathbf{W}_1^{\mathrm{T}}\left[\boldsymbol{\omega}_e + \mathbf{q}_{e_v}\right], \tag{3.26}$$

where

$$\text{Proj}\left(\hat{\boldsymbol{\theta}}, \boldsymbol{\Phi}\right) \triangleq \begin{cases} \gamma_1 \boldsymbol{\Phi} & \text{if (1) } \|\hat{\boldsymbol{\theta}}\|^2 < \epsilon_1 \text{ or} \\ & \text{if (2) } \|\hat{\boldsymbol{\theta}}\|^2 \geq \epsilon_1 \text{ and } \boldsymbol{\Phi}^{\mathrm{T}}\hat{\boldsymbol{\theta}} \leq 0 \\ \gamma_1 \left(\boldsymbol{\Phi} - \frac{\left(\|\hat{\boldsymbol{\theta}}\|^2 - \epsilon_1\right)\boldsymbol{\Phi}^{\mathrm{T}}\hat{\boldsymbol{\theta}}}{\delta_1 \|\hat{\boldsymbol{\theta}}\|^2}\hat{\boldsymbol{\theta}}\right) & \text{if (3) } \|\hat{\boldsymbol{\theta}}\|^2 \geq \epsilon_1 \text{ and } \boldsymbol{\Phi}^{\mathrm{T}}\hat{\boldsymbol{\theta}} > 0 \end{cases} \tag{3.27}$$

The projection operator $\text{Proj}\left(\hat{\boldsymbol{\theta}}, \boldsymbol{\Phi}\right)$ is locally Lipschitz [82] in $\left(\hat{\boldsymbol{\theta}}, \boldsymbol{\Phi}\right)$ and switches smoothly between cases (1), (2), and (3). Note that this update law is exactly equal to Eq. (3.21) in cases (1) and (2). Furthermore, it is straightforward to show that $\text{Proj}\left(\hat{\boldsymbol{\theta}}, \boldsymbol{\Phi}\right)$ satisfies

$$\hat{\boldsymbol{\theta}}(0) \in \boldsymbol{\Omega}_{\hat{\boldsymbol{\theta}}} \Rightarrow \hat{\boldsymbol{\theta}}(t) \in \boldsymbol{\Omega}_{\hat{\boldsymbol{\theta}}} \tag{3.28}$$

for all $t \geq 0$. In case (1), Eq. (3.28) readily holds since $\hat{\boldsymbol{\theta}} \in \boldsymbol{\Omega}_{\boldsymbol{\theta}^*}$ and $\boldsymbol{\Omega}_{\boldsymbol{\theta}^*} \subset \boldsymbol{\Omega}_{\hat{\boldsymbol{\theta}}}$. In case (2), $\|\hat{\boldsymbol{\theta}}\|^2$ evolves according to

$$\frac{\mathrm{d}}{\mathrm{dt}}\|\hat{\boldsymbol{\theta}}\|^2 = 2\hat{\boldsymbol{\theta}}^{\mathrm{T}}\dot{\hat{\boldsymbol{\theta}}} = 2\gamma_1 \hat{\boldsymbol{\theta}}^{\mathrm{T}}\boldsymbol{\Phi},$$

which is trivially negative semi-definite by the conditions stated in case (2). Consequently, the estimates approach the origin. Finally, for case (3),

$$\frac{\mathrm{d}}{\mathrm{dt}}\|\hat{\boldsymbol{\theta}}\|^2 = 2\hat{\boldsymbol{\theta}}^{\mathrm{T}}\dot{\hat{\boldsymbol{\theta}}} = 2\frac{\gamma_1}{\delta}\hat{\boldsymbol{\theta}}^{\mathrm{T}}\boldsymbol{\Phi}\left(\delta_1 + \epsilon_1 - \|\hat{\boldsymbol{\theta}}\|^2\right),$$

which decreases when $\|\hat{\boldsymbol{\theta}}\|^2 > \epsilon_1 + \delta_1$, increases if $\|\hat{\boldsymbol{\theta}}\|^2 < \epsilon_1 + \delta_1$, and is exactly

zero when $\|\hat{\boldsymbol{\theta}}\|^2 = \epsilon_1 + \delta_1$. Thus, the adaptation law in Eq. (3.26) ensures that $\hat{\boldsymbol{\theta}}(t)$ remains in the set $\boldsymbol{\Omega}_{\hat{\boldsymbol{\sigma}}}$.

A smooth projection parameter update law for $\hat{\boldsymbol{\sigma}}$ is synthesized in a fashion identical to $\hat{\boldsymbol{\theta}}$. Assuming that $\|\boldsymbol{\sigma}^*(t)\|$ is bounded by an a priori available constant value, define two convex sets

$$\boldsymbol{\Omega}_{\boldsymbol{\sigma}^*} \triangleq \left\{ \boldsymbol{\sigma}^* \in \mathbb{R}^{3m} \mid \|\boldsymbol{\sigma}^*\|^2 < \epsilon_2 \right\}, \quad \boldsymbol{\Omega}_{\hat{\boldsymbol{\sigma}}} \triangleq \left\{ \hat{\boldsymbol{\sigma}} \in \mathbb{R}^{3m} \mid \|\hat{\boldsymbol{\sigma}}\|^2 < \epsilon_2 + \delta_2 \right\} \tag{3.29}$$

for known $\epsilon_2 > 0$ and $\delta_2 > 0$. The smooth projection scheme for $\hat{\boldsymbol{\sigma}}$ is then given by

$$\dot{\hat{\boldsymbol{\sigma}}} = \mathrm{Proj}\left(\hat{\boldsymbol{\sigma}}, \boldsymbol{\Gamma}\right); \quad \boldsymbol{\Gamma} \triangleq \left[\mathbf{W}_2 + \mathbf{W}_3\right]^{\mathrm{T}} \left[\boldsymbol{\omega}_e + \mathbf{q}_{e_v}\right], \tag{3.30}$$

where

$$\mathrm{Proj}\left(\hat{\boldsymbol{\sigma}}, \boldsymbol{\Gamma}\right) \triangleq \begin{cases} \gamma_2 \boldsymbol{\Gamma} & \text{if (1) } \|\hat{\boldsymbol{\sigma}}\|^2 < \epsilon_2 \text{ or} \\ & \text{if (2) } \|\hat{\boldsymbol{\sigma}}\|^2 \geq \epsilon_2 \text{ and } \boldsymbol{\Gamma}^{\mathrm{T}} \hat{\boldsymbol{\sigma}} \leq 0 \\ \gamma_2 \left(\boldsymbol{\Gamma} - \frac{\left(\|\hat{\boldsymbol{\sigma}}\|^2 - \epsilon_2\right) \boldsymbol{\Gamma}^{\mathrm{T}} \hat{\boldsymbol{\sigma}}}{\delta_2 \|\hat{\boldsymbol{\sigma}}\|^2} \hat{\boldsymbol{\sigma}} \right) & \text{if (3) } \|\hat{\boldsymbol{\sigma}}\|^2 \geq \epsilon_2 \text{ and } \boldsymbol{\Gamma}^{\mathrm{T}} \hat{\boldsymbol{\sigma}} > 0 \end{cases} \tag{3.31}$$

which is similarly locally Lipschitz and satisfies $\hat{\boldsymbol{\sigma}}(0) \in \boldsymbol{\Omega}_{\hat{\boldsymbol{\sigma}}} \Rightarrow \hat{\boldsymbol{\sigma}}(t) \in \boldsymbol{\Omega}_{\hat{\boldsymbol{\sigma}}}$.

Theorem 3.2.2. *Suppose that $\boldsymbol{\theta}^* \in \boldsymbol{\Omega}_{\boldsymbol{\theta}^*}$, $\boldsymbol{\sigma}^* \in \boldsymbol{\Omega}_{\boldsymbol{\sigma}^*}$, and inertia matrix $\mathbf{J}$ in Eq.* (3.3) *is time and/or state dependent with dynamics given by Eq.* (3.6) *and unknown $\mathbf{J}_0$ and $\mathbf{J}_1$. Then, the adaptive control law Eq.* (3.20) *together with smooth-projection update laws Eqs.* (3.26) *and* (3.30) *and initial conditions $\hat{\boldsymbol{\theta}}(0) \in \boldsymbol{\Omega}_{\hat{\boldsymbol{\theta}}}$ and $\hat{\boldsymbol{\sigma}}(0) \in \boldsymbol{\Omega}_{\hat{\boldsymbol{\sigma}}}$, stabilizes the system of Eqs.* (2.12) *and* (3.2)

while ensuring boundedness for all closed-loop signals and asymptotic convergence of the tracking error $\lim_{t\to\infty}\left[\mathbf{q}_{e_v}(t),\ \boldsymbol{\omega}_e(t)\right] = 0$ *for all initial conditions* $[\mathbf{q}(0), \boldsymbol{\omega}(0)]$ *and any reference trajectory* $[\mathbf{q}_r(t), \boldsymbol{\omega}_r(t)]$ *with* $\boldsymbol{\omega}_r$ *smooth and bounded.*

Proof. Consider again the Lyapunov-function V defined previously in Eq. (4.28). Evaluating $\dot{V}$ along the closed-loop system trajectories yields

$$\begin{aligned}\dot{V} &= -k_v\|\boldsymbol{\omega}_e\|^2 - \beta\|\mathbf{q}_{e_v}\|^2 + \frac{1}{\gamma_1}\tilde{\boldsymbol{\theta}}^{\mathrm{T}}\left(\dot{\hat{\boldsymbol{\theta}}} - \gamma_1\boldsymbol{\Phi}\right) + \frac{1}{\gamma_2}\tilde{\boldsymbol{\sigma}}^{\mathrm{T}}\left(\dot{\hat{\boldsymbol{\sigma}}} - \gamma_2\boldsymbol{\Gamma}\right)\\ &= -k_v\|\boldsymbol{\omega}_e\|^2 - \beta\|\mathbf{q}_{e_v}\|^2 + \dot{V}_2 + \dot{V}_3\end{aligned}$$

which is negative-semi definite if

$$\dot{V}_2 = \tilde{\boldsymbol{\theta}}^{\mathrm{T}}\left(\dot{\hat{\boldsymbol{\theta}}} - \gamma_1\boldsymbol{\Phi}\right) \leq 0, \qquad \dot{V}_3 = \tilde{\boldsymbol{\sigma}}^{\mathrm{T}}\left(\dot{\hat{\boldsymbol{\sigma}}} - \gamma_2\boldsymbol{\Gamma}\right) \leq 0.$$

If $\dot{\hat{\boldsymbol{\theta}}}$ is prescribed according to the adaptation law Eq. (3.26), $\dot{V}_2 \leq 0$ is trivially satisfied for cases (1) and (2). For case (3),

$$\begin{aligned}\tilde{\boldsymbol{\theta}}^{\mathrm{T}}\left(\dot{\hat{\boldsymbol{\theta}}} - \gamma_1\boldsymbol{\Phi}\right) &= \tilde{\boldsymbol{\theta}}^{\mathrm{T}}\left(\gamma_1\left(\boldsymbol{\Phi} - \frac{\left(\|\hat{\boldsymbol{\theta}}\|^2 - \epsilon_1\right)\boldsymbol{\Phi}^{\mathrm{T}}\hat{\boldsymbol{\theta}}}{\delta_1\|\hat{\boldsymbol{\theta}}\|^2}\hat{\boldsymbol{\theta}}\right) - \gamma_1\boldsymbol{\Phi}\right)\\ &= -\gamma_1\left(\frac{\left(\|\hat{\boldsymbol{\theta}}\|^2 - \epsilon_1\right)\boldsymbol{\Phi}^{\mathrm{T}}\hat{\boldsymbol{\theta}}}{\delta_1\|\hat{\boldsymbol{\theta}}\|^2}\tilde{\boldsymbol{\theta}}^{\mathrm{T}}\hat{\boldsymbol{\theta}}\right) \leq 0\end{aligned}$$

which is true because $\tilde{\boldsymbol{\theta}}^{\mathrm{T}}\hat{\boldsymbol{\theta}} = \|\hat{\boldsymbol{\theta}}\|^2 - \boldsymbol{\theta}^{*\mathrm{T}}\hat{\boldsymbol{\theta}} \geq 0$ when $\|\hat{\boldsymbol{\theta}}\|^2 \geq \epsilon_1$. Therefore,

$$\dot{V}_2 = \begin{cases} 0 & \text{in case (1) and case (2)} \\ -\gamma_1\left(\frac{\left(\|\hat{\boldsymbol{\theta}}\|^2-\epsilon_1\right)\boldsymbol{\Phi}^{\mathrm{T}}\hat{\boldsymbol{\theta}}}{\delta_1\|\hat{\boldsymbol{\theta}}\|^2}\tilde{\boldsymbol{\theta}}^{\mathrm{T}}\hat{\boldsymbol{\theta}}\right) \leq 0 & \text{in case (3)} \end{cases} \tag{3.32}$$

from which it follows that $\dot{V}_2 \leq 0$. Similarly, it can be shown that $\dot{V}_3 \leq 0$, from which it follows that $\dot{V} \leq 0$. As shown previously in the proof for Theorem 3.2.1, $\mathbf{q}_{e_v}, \boldsymbol{\omega}_e, \in \mathcal{L}_2 \cap \mathcal{L}_\infty$ and $\dot{\mathbf{q}}_{e_v}, \dot{\boldsymbol{\omega}}_e, \in \mathcal{L}_\infty$ can be readily asserted. Furthermore, $\dot{V}$ is uniformly continuous since $\dot{V}_2$ and $\dot{V}_3$ are Lipschitz continuous at the boundaries between their respective cases (1), (2), and (3). Thus, from an application of Barbalat's lemma, it follows then that $\lim_{t\to\infty} \left[\mathbf{q}_{e_v}(t), \boldsymbol{\omega}_e(t)\right] = 0$. □

3.3 Adaptive Attitude Tracking Control for Unknown Inertia with Input Dependency

In this section, the adaptive controller is extended to handle fuel loss compensation, wherein the spacecraft inertia matrix has an explicit control input dependency. After careful examination and judicious rearrangement of terms, the control law given by Eq. (3.20) can be expressed in terms of the control-dependent inertia matrix in Eq. (3.13) in the following manner

$$\mathbf{u} = \boldsymbol{\tau} - \|\mathbf{u}\|\hat{\mathbf{J}}_1\boldsymbol{\Omega} \tag{3.33}$$

where $\hat{\mathbf{J}}_1$ is the estimate of matrix $\mathbf{J}_1$ and,

$$\boldsymbol{\tau} = -\beta\mathbf{q}_{e_v} - k_v\boldsymbol{\omega}_e - \mathbf{W}_1\hat{\boldsymbol{\theta}} - \mathbf{W}_2\hat{\boldsymbol{\sigma}}, \tag{3.34}$$

$$\boldsymbol{\Omega} = \boldsymbol{\omega} - \frac{1}{2}\left[\boldsymbol{\omega}_e + \mathbf{q}_{e_v}\right]. \tag{3.35}$$

The second term in Eq. (3.33) is obtained by recognizing that $\mathbf{W}_3\boldsymbol{\sigma}^* = \mathbf{J}_1\dot{\boldsymbol{\Psi}}\boldsymbol{\Omega}$ and using Eq. (3.13) to express $\mathbf{W}_3\hat{\boldsymbol{\sigma}} = \|\mathbf{u}\|\hat{\mathbf{J}}_1\boldsymbol{\Omega}$. Note that, $\boldsymbol{\Omega}$ can be equivalently stated as

$$\boldsymbol{\Omega} = \frac{1}{2}\boldsymbol{\omega}_e + \boldsymbol{\omega}_{rB} - \frac{1}{2}\mathbf{q}_{e_v}, \tag{3.36}$$

where $\boldsymbol{\omega}_{rB} = \mathbf{C}(\mathbf{q}_r)\boldsymbol{\omega}_r$. In order to obtain an implementable expression for $\mathbf{u}$, Eq. (3.33) is examined further. From Eq. (3.33), the following expression is readily obtained for $\|\mathbf{u}\|^2$

$$\|\mathbf{u}\|^2 = \|\boldsymbol{\tau}\|^2 - 2\|\mathbf{u}\|\boldsymbol{\tau}^{\mathrm{T}}\hat{\mathbf{J}}_1\boldsymbol{\Omega} + \|\mathbf{u}\|^2\|\hat{\mathbf{J}}_1\boldsymbol{\Omega}\|^2, \tag{3.37}$$

which can be rearranged to obtain

$$\|\mathbf{u}\|^2\left(1 - \|\hat{\mathbf{J}}_1\boldsymbol{\Omega}\|^2\right) + 2\|\mathbf{u}\|\boldsymbol{\tau}^{\mathrm{T}}\hat{\mathbf{J}}_1\boldsymbol{\Omega} - \|\boldsymbol{\tau}\|^2 = 0. \tag{3.38}$$

Observe that Eq. (3.38) is a simple quadratic equation in $\|\mathbf{u}\|$. Suppose it is ensured that

$$\|\hat{\mathbf{J}}_1\boldsymbol{\Omega}\| < 1, \tag{3.39}$$

then $\left(1 - \|\hat{\mathbf{J}}_1\boldsymbol{\Omega}\|^2\right) > 0$ for all $t \geq 0$ and Eq. (3.38) has only the following non-negative solution for $\|\mathbf{u}\|$:

$$\|\mathbf{u}\| = \frac{-2\boldsymbol{\tau}^{\mathrm{T}}\hat{\mathbf{J}}_1\boldsymbol{\Omega} + \sqrt{4\left(\boldsymbol{\tau}^{\mathrm{T}}\hat{\mathbf{J}}_1\boldsymbol{\Omega}\right)^2 + 4\left(1 - \|\hat{\mathbf{J}}_1\boldsymbol{\Omega}\|^2\right)\|\boldsymbol{\tau}\|^2}}{2\left(1 - \|\hat{\mathbf{J}}_1\boldsymbol{\Omega}\|^2\right)} \tag{3.40}$$

which is non-negative and bounded if Eq. (3.39) holds for all $t \geq 0$. Hence, the control input expression in Eq. (3.33) together with Eq. (3.40) is bounded and implementable for $t \geq 0$ as long as the inequality in Eq. (3.39) is satisfied. Next, in order to ensure that Eq. (3.39) is satisfied for all time, observe that

$$\begin{aligned}
\|\hat{\mathbf{J}}_1 \boldsymbol{\Omega}\| &\leq \|\hat{\mathbf{J}}_1\| \|\boldsymbol{\Omega}\| \\
&\leq \|\hat{\mathbf{J}}_1\| \ \left\| \frac{\boldsymbol{\omega}_e}{2} + \boldsymbol{\omega}_{rB} - \frac{\mathbf{q}_{e_v}}{2} \right\| \\
&\leq \|\hat{\mathbf{J}}_1\| \ \left(\frac{\|\boldsymbol{\omega}_e\|}{2} + \omega_B + \frac{1}{2} \right)
\end{aligned} \tag{3.41}$$

where the bounds $\omega_B = \sup_{t \geq 0} \|\boldsymbol{\omega}_{rB}\|$ and $\|\mathbf{q}_{e_v}\| \leq 1$ have been employed to obtain Eq. (3.41). Using the 2-norm bound $\|\hat{\mathbf{J}}_1\| \leq 3 \sup_{t \geq 0} \left(\max_{i,j} |\hat{J}_{1_{ij}}(t)| \right)$, where $\hat{J}_{1_{ij}}$ is the i,jth entry of matrix $\hat{\mathbf{J}}_1$, and invoking the constraint $\|\hat{\sigma}_i\| \leq \|\hat{\boldsymbol{\sigma}}\| \leq \sqrt{\epsilon_2 + \delta_2} \ \forall \ i = 1, 2, 3$ as long as $\hat{\boldsymbol{\sigma}}$ is updated according to the smooth projection algorithm of Eq. (3.30), Eq. (3.41) can be expressed as

$$\|\hat{\mathbf{J}}_1 \boldsymbol{\Omega}\| \leq 3\sqrt{\epsilon_2 + \delta_2} \ \left(\frac{\|\boldsymbol{\omega}_e\|}{2} + \omega_B + \frac{1}{2} \right). \tag{3.42}$$

Upper bounding the right-hand side of Eq. (3.42) by unity leads to the following conservative upper bound on the norm of $\boldsymbol{\omega}_e$:

$$\|\boldsymbol{\omega}_e(t)\| < \zeta^*; \quad \zeta^* = 2 \left(\frac{1}{3\sqrt{\epsilon_2 + \delta_2}} - \omega_B - \frac{1}{2} \right), \tag{3.43}$$

where ϵ_2 and δ_2 are such that $\zeta^* > 0$ for all $t \geq 0$. Thus, if $\boldsymbol{\omega}_e$ is upper bounded according to Eq. (3.43), then $\|\hat{\mathbf{J}}_1 \boldsymbol{\Omega}\| < 1$ and the control input in Eq. (3.33) along with Eq. (3.40) is non-negative and bounded for all $t \geq 0$.

Theorem 3.3.1. *Consider the attitude tracking error system of Eqs.* (2.12)

and (2.13) *with an input dependent inertia matrix* $\mathbf{J}$ *that evolves according to Eq.* (3.13) *and components* $\mathbf{J}_1$ *and* $\mathbf{J}_0$ *being unknown. Suppose the true parameter values* $\boldsymbol{\theta}^*$ *and* $\boldsymbol{\sigma}^*$ *are such that*

$$\boldsymbol{\theta}^* \in \boldsymbol{\Omega}_{\boldsymbol{\theta}^*}; \quad \boldsymbol{\sigma}^* \in \boldsymbol{\Omega}_{\boldsymbol{\sigma}^*}, \tag{3.44}$$

and the inertia matrix $\mathbf{J}$ *is described by known values* $\lambda_{\min}$ *and* $\lambda_{\max}$*, such that*

$$\lambda_{\min} = \inf_{\substack{i=1,2,3 \\ t\geq 0}} \lambda_i(t); \quad \lambda_{\max} = \sup_{\substack{i=1,2,3 \\ t\geq 0}} \lambda_i(t) \tag{3.45}$$

where $\lambda_i(t)$ *denotes the* i^{th} *(potentially) time-varying eigenvalue of* $\mathbf{J}$ *point wise with time. Furthermore, suppose the initial conditions satisfy*

$$\left(\|\boldsymbol{\omega}_e(0)\| + 1\right)^2 < \frac{2}{\lambda_{\max}} \left[\frac{\lambda_{\min}}{2} \left(\zeta^* - 1\right)^2 - \frac{\lambda_{\min}}{2} - 4\left(\beta + k_v\right) - \frac{\tilde{\theta}_{max}}{2\gamma_1} - \frac{\tilde{\sigma}_{max}}{2\gamma_2} \right] \tag{3.46}$$

where ζ^* *is given by Eq.* (3.43) *and selected such that* $\zeta^* > 1$ *and*

$$\tilde{\theta}_{max} = \left(\sqrt{\epsilon_1 + \delta_1} + \sqrt{\epsilon_1} \right)^2, \quad \tilde{\sigma}_{max} = \left(\sqrt{\epsilon_2 + \delta_2} + \sqrt{\epsilon_2} \right)^2.$$

In addition, the right-hand side of the inequality above satisfies:

$$\left[\frac{\lambda_{\min}}{2} \left(\zeta^* - 1\right)^2 - \frac{\lambda_{\min}}{2} - 4\left(\beta + k_v\right) - \frac{\tilde{\theta}_{max}}{2\gamma_1} - \frac{\tilde{\sigma}_{max}}{2\gamma_2} \right] > 0. \tag{3.47}$$

Then, the adaptive control law in the form of Eq. (3.33) *with Eq.* (3.40) *is non-singular for all* $t \geq 0$ *and, along with smooth-projection based parameter update laws Eqs.* (3.26)- (3.30) *and initial conditions* $\hat{\boldsymbol{\theta}}(0) \in \boldsymbol{\Omega}_{\hat{\boldsymbol{\theta}}}$ *and*

$\hat{\boldsymbol{\sigma}}(0) \in \boldsymbol{\Omega}_{\hat{\boldsymbol{\sigma}}}$, *guarantees asymptotic convergence of the tracking error signals* $\lim_{t\to\infty}\left[\mathbf{q}_{e_v}(t),\ \boldsymbol{\omega}_e(t)\right] = 0$ *for all bounded and smooth reference trajectories* $[\mathbf{q}_r(t), \boldsymbol{\omega}_r(t)]$ *while ensuring boundedness for all closed-loop signals for all* $t \geq 0$.

Proof. First and foremost, it is shown that the adaptive control input given by Eq. (3.33) and Eq. (3.40) is non-singular for all $t \geq 0$. Consider again the positive semi-definite function V in Eq. (4.28). As outlined in the proof for Theorem 3.2.1, evaluating $\dot{V}$ along the closed-loop system trajectories Eqs. (2.12) and (3.23) with parameter update laws Eqs. (3.26) and (3.30) yields $\dot{V} \leq 0$. Thus, V is a monotonic function and satisfies $V(t) \leq V(0)$. For notational convenience in the analysis that follows, V in Eq. (4.28) is written as

$$V = \frac{1}{2}\left(\boldsymbol{\omega}_e + \mathbf{q}_{e_v}\right)^{\mathrm{T}} \mathbf{J}\left(\boldsymbol{\omega}_e + \mathbf{q}_{e_v}\right) + \tilde{V},$$

where the positive semi-definite function $\tilde{V}$ is simply

$$\tilde{V} = (\beta + k_v)\left(\mathbf{q}_{e_v}^{\mathrm{T}}\mathbf{q}_{e_v} + (q_{e_0} - 1)^2\right) + \frac{1}{2\gamma_1}\|\tilde{\boldsymbol{\theta}}\|^2 + \frac{1}{2\gamma_2}\|\tilde{\boldsymbol{\sigma}}\|^2.$$

Then, using the Rayleigh-Ritz inequality coupled with the monotonicity of V, one can write

$$\frac{\lambda_{\min}}{2}\|\boldsymbol{\omega}_e + \mathbf{q}_{e_v}\|^2 + \tilde{V} \leq V(t) \leq V(0). \tag{3.48}$$

Following through with some minor algebra and rearrangement of terms in

Eq. (3.48) leads to

$$\begin{aligned}\frac{\lambda_{\min}}{2}\|\boldsymbol{\omega}_e\|^2 + \frac{\lambda_{\min}}{2}\|\mathbf{q}_{e_v}\|^2 + \tilde{V} &\leq V(0) - \lambda_{\min}\boldsymbol{\omega}_e^{\mathrm{T}}\mathbf{q}_e \\ &\leq V(0) + \lambda_{\min}\|\boldsymbol{\omega}_e\|. \end{aligned} \tag{3.49}$$

Adding the terms $-\lambda_{\min}\|\boldsymbol{\omega}_e\| + \lambda_{\min}/2$ on both sides of the inequality in Eq. (3.49) and following through with completion of squares yields

$$\frac{\lambda_{\min}}{2}\left(\|\boldsymbol{\omega}_e\| - 1\right)^2 + \frac{\lambda_{\min}}{2}\|\mathbf{q}_{e_v}\|^2 + \tilde{V} \leq V(0) + \frac{\lambda_{\min}}{2} \tag{3.50}$$

Next, using again the Rayleigh-Ritz inequality and implementing the upper bound on $\|\boldsymbol{\omega}_e(0)\|$ stated in Eq. (3.46), $V(0)$ can be upper-bounded as follows:

$$\begin{aligned} V(0) &\leq \frac{\lambda_{\max}}{2}\|\boldsymbol{\omega}_e(0) + \mathbf{q}_{e_v}(0)\|^2 + 2\left(\beta + k_v\right)\left(1 - q_{e_0}\right) + \frac{1}{2\gamma_1}\|\tilde{\boldsymbol{\theta}}\|^2 + \frac{1}{2\gamma_2}\frac{\|\tilde{\boldsymbol{\sigma}}\|^2}{} \\ &\leq \frac{\lambda_{\max}}{2}\left(\|\boldsymbol{\omega}_e(0)\| + \|\mathbf{q}_{e_v}(0)\|\right)^2 + 4\left(\beta + k_v\right) + \frac{1}{2\gamma_1}\Big(\|\hat{\boldsymbol{\theta}}\| + \|\boldsymbol{\theta}^*\|\Big)^2 \\ &\quad + \frac{1}{2\gamma_2}\Big(\|\hat{\boldsymbol{\sigma}}\| + \|\boldsymbol{\sigma}^*\|\Big)^2 \\ &\leq \frac{\lambda_{\max}}{2}\left(\|\boldsymbol{\omega}_e(0)\| + 1\right)^2 + 4\left(\beta + k_v\right) + \frac{\tilde{\theta}_{\max}}{2\gamma_1} + \frac{\tilde{\sigma}_{\max}}{2\gamma_2} \\ &< \frac{\lambda_{\min}}{2}\left(\zeta^* - 1\right)^2 - \frac{\lambda_{\min}}{2}. \end{aligned} \tag{3.51}$$

Using Eq. (3.51) as the upper bound for $V(0)$ in Eq. (3.50) gives

$$\frac{\lambda_{\min}}{2}\left(\|\boldsymbol{\omega}_e\| - 1\right)^2 + \frac{\lambda_{\min}}{2}\|\mathbf{q}_{e_v}\|^2 + \tilde{V} < \frac{\lambda_{\min}}{2}\left(\zeta^* - 1\right)^2 \tag{3.52}$$

from which it readily follows that $\left(\|\boldsymbol{\omega}_e\| - 1\right)^2 < \left(\zeta^* - 1\right)^2$ and, since $\zeta^* > 1$, $\|\boldsymbol{\omega}_e(t)\| < \zeta^*$ for all $t \geq 0$, ensuring non-singularity of the control in Eq. (3.33)

with $\|\mathbf{u}\|$ prescribed according to Eq. (3.40). The remainder of the proof showing asymptotic convergence of error signals, and boundedness of closed-loop signals follows exactly according to the proof for Theorem 2. □

A few pertinent remarks and observations are now made about Theorem 3:

Remark 3.3.1. It is important to remark that the smooth projection algorithm of Eq. (3.30) is crucial for ensuring that the adaptive control solution in Eq. (3.33) with $\|\mathbf{u}\|$ given by Eq. (3.40) is uniformly bounded when dealing with inertia variations due to control-torque induced fuel expenditure. Without this assumption, no assurance can be provided that Eq. (3.38) will yield a non-singular solution for $\|\mathbf{u}\|$.

Remark 3.3.2. For the specific case of inertia variations due to fuel loss, since $\|\mathbf{J}(t)\| \leq \|\mathbf{J}_0\|$, knowing $\lambda_{\max}$ is equivalent to to having knowledge of the maximum eigenvalue of $\mathbf{J}_0$.

Remark 3.3.3. From a practical standpoint, the minimum eigenvalue of $\mathbf{J}(t)$ at any time t is larger than the minimum eigenvalue at the completion of the mission, or when the fuel mass has been entirely expended. Thus, having knowledge of $\lambda_{\min}$ is equivalent to knowing the minimum eigenvalue of the inertia matrix associated with the dry mass of the spacecraft.

Remark 3.3.4. The practical implication of requiring $\zeta^* > 1$ to ensure control implementability needs further examination. For convenience, the expression

for ζ^* from Eq. (3.43) is restated below

$$\zeta^* = 2\left(\frac{1}{3\sqrt{\epsilon_2 + \delta_2}} - \omega_B - \frac{1}{2}\right).$$

Recall that $\sqrt{\epsilon_2 + \delta_2}$ is the upper bound on estimates of $\mathbf{J}_1$, whereas ω_B is the upper bound of the reference velocity. Thus, if ϵ_2 and δ_2 are small and if ω_B is not impractically large, then $\zeta^* > 1$ can be readily satisfied. Note, that this condition is a sufficient condition and may be potentially overly conservative. It is, of course, possible for the control law to be implementable even when this condition is not satisfied.

Remark 3.3.5. Finally, a few observations are in order regarding the initial condition requirement of Eq. (3.46) to ensure control implementability. As will be shown in the numerical simulations that follow, the initial condition requirement is practically quite lenient and permits a vast range of reference trajectories and initial conditions. Re-stated below for convenience, it is observed that the right-hand side of the inequality Eq. (3.46) is essentially a function of the spacecraft inertia matrix properties, the reference trajectory, as well as the gains $\beta, k_v, \gamma_1, \gamma_2$.

$$(\|\boldsymbol{\omega}_e(0)\| + 1)^2 < \frac{2}{\lambda_{\max}}\left[\frac{\lambda_{\min}}{2}(\zeta^* - 1)^2 - \frac{\lambda_{\min}}{2} - 4(\beta + k_v) - \frac{\tilde{\theta}_{\max}}{2\gamma_1} - \frac{\tilde{\sigma}_{\max}}{2\gamma_2}\right].$$

The last three negative-definite terms on the right-hand side of this inequality can be driven close to zero through appropriate selection of gain terms. Then, if $\lambda_{\min}\left[(\zeta^* - 1)^2 - 1\right]/2$ is large enough to overcome the offending negative terms, a large range of $\boldsymbol{\omega}_e(0)$ is easily accommodated in Eq. (3.46). Again, it

is noted that the restriction on the initial condition is a sufficient condition only, and that the control may be implementable even if Eq. (3.46) is not satisfied.

3.4 Numerical Simulations

In order to show the performance characteristics of the proposed adaptive control, numerical simulations are conducted. The error tracking capabilities are compared to a high-performance non-certainty equivalence based adaptive control [55] that does not account for inertia-variations. The control protocol in [55] is referred to as "comparison" in the subsequent simulations, and is listed as

$$\mathbf{u}_{\mathrm{c}} = -\mathbf{W}_{\mathrm{c}}\left(\hat{\boldsymbol{\theta}} + \boldsymbol{\beta}_{\mathrm{c}}\right) - \gamma \mathbf{W}_f \mathbf{W}_f^{\mathrm{T}}\left[k_p\left(\boldsymbol{\omega}_f - \mathbf{q}_{e_v}\right) - \boldsymbol{\omega}_e\right] \tag{3.53}$$

$$\dot{\hat{\boldsymbol{\theta}}}_{\mathrm{c}} = \gamma \mathbf{W}_f^{\mathrm{T}}\left[\left(\alpha + k_w\right)\boldsymbol{\omega}_f + k_p \mathbf{q}_{e_v}\right] - \gamma \mathbf{W}_{\mathrm{c}}^{\mathrm{T}} \boldsymbol{\omega}_f \tag{3.54}$$

$$\boldsymbol{\beta}_{\mathrm{c}} = \gamma \mathbf{W}_f^{\mathrm{T}} \boldsymbol{\omega}_f, \tag{3.55}$$

where $k_p, k_w, \gamma > 0$, $\alpha = k_p + k_w$, and the matrix $\mathbf{W}_{\mathrm{c}}$ is given by

$$\mathbf{W}_{\mathrm{c}}\boldsymbol{\theta}^* = -S\left(\boldsymbol{\omega}\right)\mathbf{J}\boldsymbol{\omega} + \mathbf{J}\boldsymbol{\phi} + \mathbf{J}\left(k_w \boldsymbol{\omega}_e + k_p \dot{\mathbf{q}}_{e_v} + \alpha k_p \mathbf{q}_{e_v}\right), \tag{3.56}$$

where $\mathbf{J} = \mathbf{J}_0$ is constant. Finally, the signals $\mathbf{W}_f$ and $\boldsymbol{\omega}_f$ are updated using

$$\dot{\boldsymbol{\omega}}_f = -\alpha \boldsymbol{\omega}_f + \boldsymbol{\omega}_e$$

$$\dot{\mathbf{W}}_f = -\alpha \mathbf{W}_f + \mathbf{W}_{\mathrm{c}}$$

with arbitrary initial conditions $\boldsymbol{\omega}_f(0) \in \mathbb{R}^3$ and $\mathbf{W}_f(0) \in \mathbb{R}^{3\times 6}$. The choice for this comparison controller is motivated by the fact that the non-CE adaptive control in [55] has been shown to demonstrate significantly superior tracking error convergence performance to classical CE adaptive control methods owing to its attractive manifold design in the parameter adaptation dynamics. However, as shown in subsequent simulations, despite its provable performance gains for a constant inertia matrix, the non-CE adaptive controller suffers from pointing accuracy when faced with a time-varying inertia matrix.

Two types of time-varying inertia matrices are considered. In the first example, a spacecraft undergoing sensor boom deployment is modeled. In this case, a sinusoidal mass-displacement profile is used to represent persistent mass movement of an articulated appendage. In the second example, a control input dependent inertia-matrix is simulated to highlight the benefits of the novel control methodology for fuel loss compensation. In both simulations, the true value of the inertia component $\mathbf{J}_0$ is taken as

$$\mathbf{J}_0 = \begin{bmatrix} 20 & 1.2 & 0.9 \\ 1.2 & 17 & 1.4 \\ 0.9 & 1.4 & 15 \end{bmatrix} \text{ kg-m}^2, \tag{3.57}$$

For the most fair comparison, the initial value of both $\hat{\boldsymbol{\theta}}$ and $\hat{\boldsymbol{\theta}}_c$ is taken as $\hat{\boldsymbol{\theta}}_c(0) = \hat{\boldsymbol{\theta}}(0) = [21.1, 1.9, 1.4, 17.8, 2.9, 15.5]^{\mathrm{T}}$ while $\hat{\boldsymbol{\sigma}}(0) = 0$ for the proposed adaptive control law. The true values for $\mathbf{J}_1$ parameters are presented separately in the sections that follow. The initial angular velocity of the spacecraft is $\boldsymbol{\omega}(0) = [0.001, 0.001, 0.002]^{\mathrm{T}}$, while the vector component of

the initial body quaternion is given by $\mathbf{q}_v(0) = [0.1826, 0.1826, 0.1826]^{\mathrm{T}}$ with $q_0 = \sqrt{1 - 3(0.1826)^2}$. The initial reference quaternion is $\mathbf{q}_r(0) = [1, 0, 0, 0]^{\mathrm{T}}$ which indicates that the reference and inertial frames are initially aligned. Simulations are conducted for a non-persistently exciting (non-PE) reference trajectory. Obtained from the example provided in [55], the non-PE angular velocity profile is generated according to $\boldsymbol{\omega}_r(t) = r(t)[\ 1,\ \ 1,\ \ 1\ ]^{\mathrm{T}}$ rad/s with $r(t)$ given by

$$r(t) = \left(0.3\cos(0.3t)(1 - e^{0.01t^2}) + (0.08\pi + 0.006\sin(0.3t))te^{-0.01t^2}\right). \quad (3.58)$$

In order to obtain a fair comparison between $\mathbf{u}$ and $\mathbf{u}_{\mathrm{c}}$, the parameters k_v, β, k_p, and k_w are first tuned to yield similar controller performance for the ideal case, where $\mathbf{J}$ is constant and known. By selecting $\beta = 20$, $k_v = 24.5$ for $\mathbf{u}$, and $k_w = 0.5$, $k_p = 0.5$ for $\mathbf{u}_{\mathrm{c}}$, and setting $\gamma = \gamma_1 = \gamma_2 = 0$, the baseline plots shown in Fig. 3.3 show a similar controller performance.

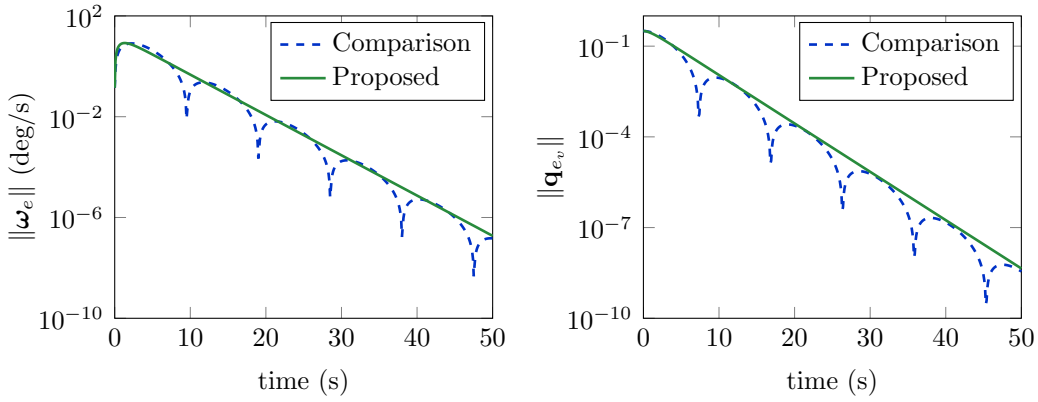

(a) Norm of angular velocity error vector

(b) Norm of quaternion error vector

Figure 3.3: Baseline performance of proposed and comparison controllers, generated using constant and known $\mathbf{J}_0$ in Eq. (3.57).

In subsequent simulations, only the parameter estimation tuning parameters $\gamma, \gamma_1, \gamma_2$ are modified to obtain the best performance for both controllers, while keeping the control gains unchanged. For both the fuel loss and simulation deployment cases, plots are provided along with a discussion to highlight important features of the controller.

3.4.1 Deployable Appendage

This section presents a simulation of the adaptive control in Eq. (3.20) along with parameter estimation update laws Eqs. (3.21)-(3.22) (without projection) for a purely time-varying inertia matrix. A spacecraft with articulating parts is modeled using Eqs. (3.7)-(3.9) with known quantities

$$\boldsymbol{\rho}_1(t) = 0.5\left[1 + \sin^2(0.1t)\right]\hat{\boldsymbol{b}}_1 \tag{3.59}$$

$$\boldsymbol{\rho}_2(t) = 0.8\left[1 + \sin^2(0.1t)\right]\hat{\boldsymbol{b}}_2, \tag{3.60}$$

along with unknown mass $m_1 = 1$ kg and $m_2 = 1.3$ kg. Thus, $\mathbf{J}_1$ is given by $\mathbf{J}_1 = -[\ 1.0 \cdot \mathbf{I},\ \ 1.3 \cdot \mathbf{I}\ ]$ where $\mathbf{I}$ is the 3×3 identity matrix. The matrix $\mathbf{J}_0$ is given by Eq. (3.57), with the assumption that the inertia contributions of the moving objects are already included in the calculation of $\mathbf{J}_0$ in accordance with Eq. (3.7), or that the moving parts are treated as point masses. Fig. 3.4 illustrates the evolution of the principal moments of inertia of this inertia matrix over a period of 400 seconds. The inertia matrix quantities remain positive definite and satisfy Eq. (3.5) throughout the simulation period.

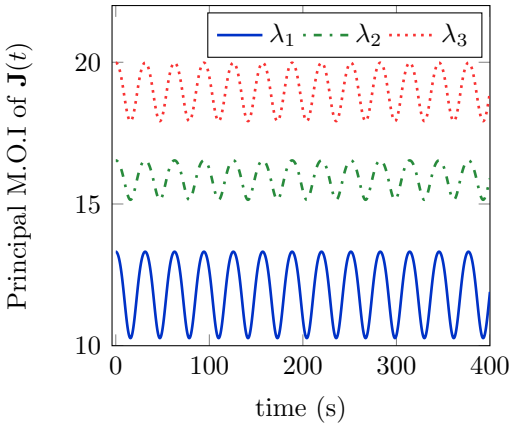

Figure 3.4: Principal moments of inertia of time-dependent $\mathbf{J}(t)$ for a spacecraft with moving/articulating parts.

The tuning parameters are selected to be $\gamma = 100$, $\gamma_1 = 60$, and $\gamma_2 = 200$ and are chosen in such a manner so as to yield a result closest to the baseline performance for each controller. Every effort was made by the authors to select the best possible tuning parameters for each control method. The results are illustrated in Figs. 3.5-3.7. While the proposed controller maintains consistent closed-loop tracking-performance, the comparison controller suffers greatly due to the persistent variations in the input dependent inertia matrix. In fact, as is evident in Figs. 3.5a-3.5b, the comparison controller shows significantly diminished asymptotic convergence compared to the proposed controller. For smaller times the comparison controller shows reduction in error norms, however the error norms saturate around 0.5 deg/s for angular velocity and near 0.001 for the quaternion error. In contrast, the proposed controller drives the angular velocity tracking error norm to below 0.001 deg/s and the quaternion error vector norm to below 1×10^{-4} within 400 seconds.

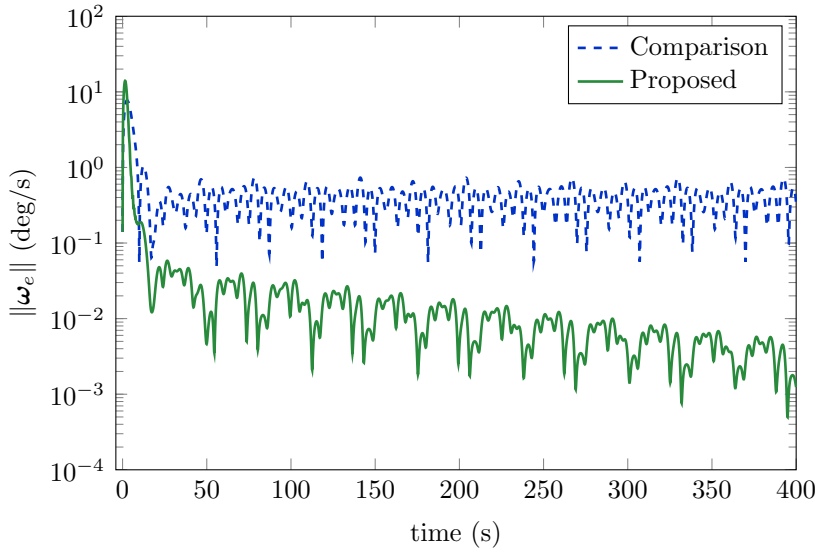

(a) Norm of angular velocity error vector

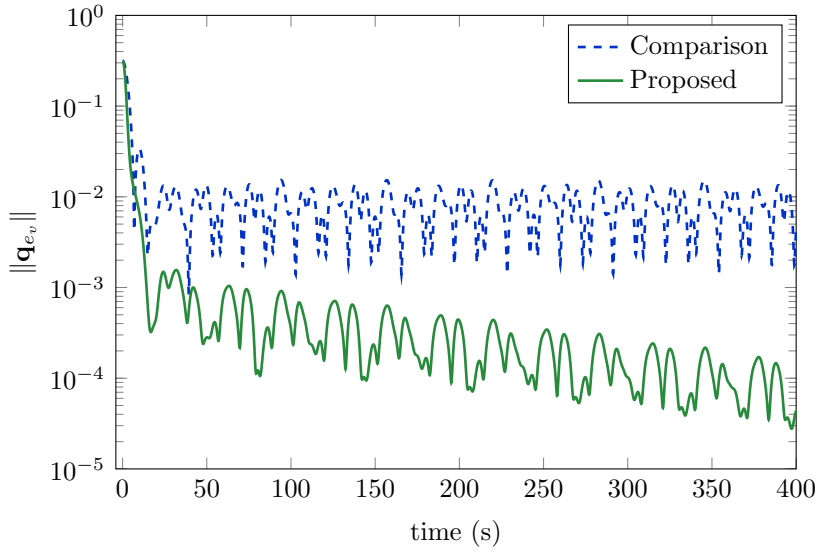

(b) Norm of quaternion error vector

Figure 3.5: Adaptive attitude-tracking control simulation for spacecraft with time-dependent inertia matrix variations due to mass displacement.

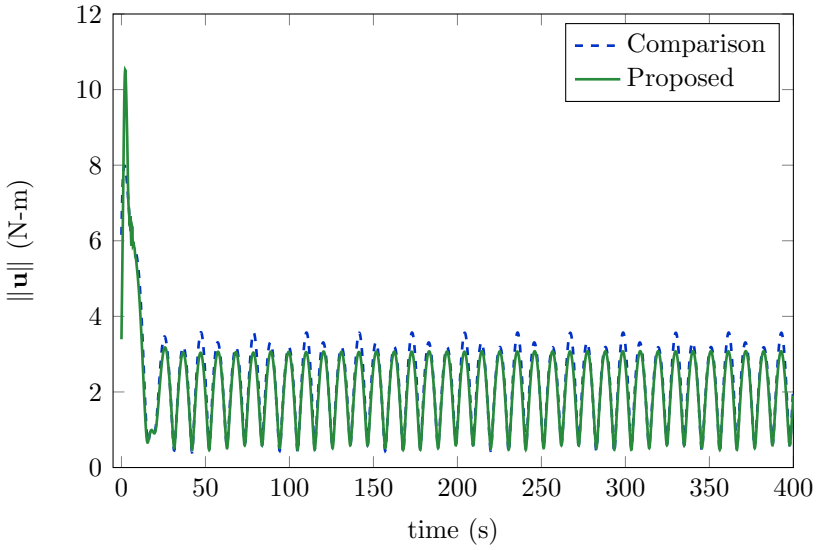

(a) Norm of control vector

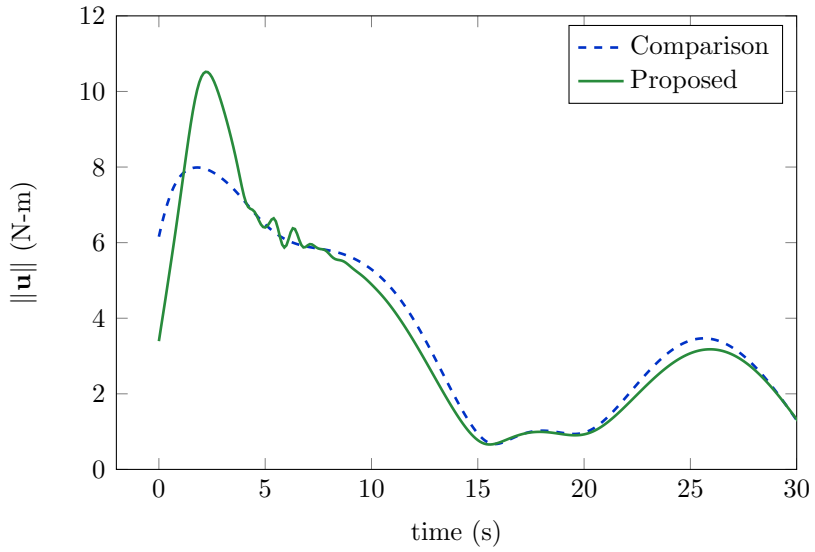

(b) Initial transient of control norm

Figure 3.6: Commanded control effort for adaptive control simulation of spacecraft with time-dependent inertia variations.

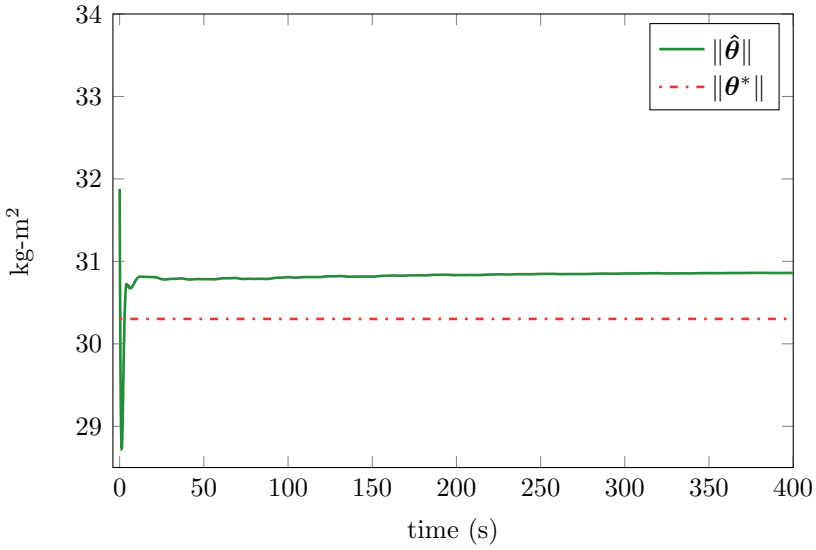

(a) Norm of $\mathbf{J}_0$ parameter estimates, $\|\hat{\boldsymbol{\theta}}\|$

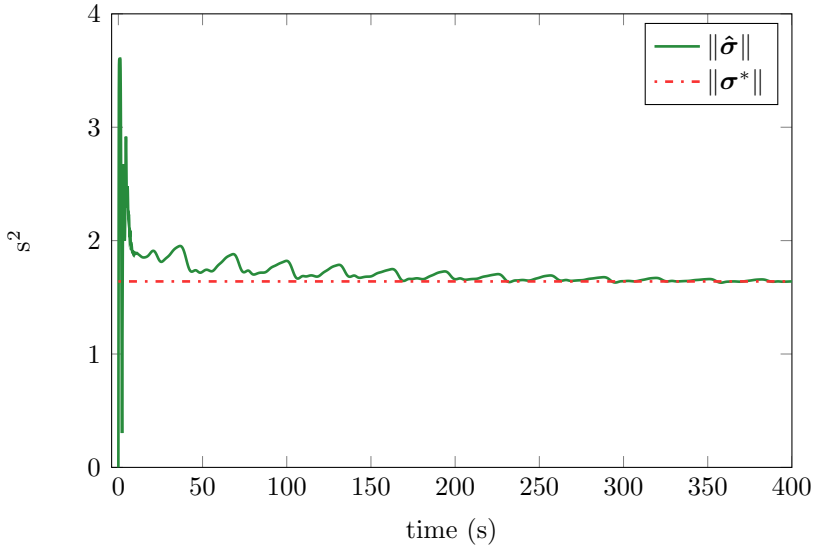

(b) Norm of $\mathbf{J}_1$ parameter estimates, $\|\hat{\boldsymbol{\sigma}}\|$

Figure 3.7: Parameter estimates of the unknown $\mathbf{J}_0$ and $\mathbf{J}_1$ matrices for mass displacement example.

The degradation of performance in the comparison control is consid-

ered to be a direct result of significant inertia matrix changes, which are not explicitly taken into account as they are in the proposed control law. Thus, at best, the comparison controller is only able to drive the tracking errors to within a bounded set.

In Fig. 3.6b, observe that the proposed controller has a slightly higher overshoot in the initial transient regime. However, the steady state regime in Fig. 3.6a seems to indicate that the comparison controller actually commands a higher overall control torque norm than the proposed controller. The higher control demand stems from the fact that because the comparison controller does not directly take into account the time-varying inertia components, it expends a significant amount of effort adapting to parameters that are rapidly varying. Note that the steady-state control is time-varying since a time-varying trajectory is being tracked. Finally, it is noted that since the underlying reference trajectory does not satisfy PE conditions, the parameter estimates are not expected to converge to their true values. This is clearly the case for $\hat{\boldsymbol{\theta}}$ in Fig. 3.7a. However, as illustrated in Fig. 3.7b, the added excitation due to the sinusoidal variation in $\boldsymbol{\Psi}$ allows $\mathbf{J}_1$ estimates, $\hat{\boldsymbol{\sigma}}$, to converge to their true values.

3.4.2 Fuel Loss Compensation

Next, numerical simulations are conducted for a spacecraft undergoing inertia matrix changes due to fuel-mass loss. In particular, the inertia matrix variations are described by Eq. (3.13), the adaptive control is given by Eq. (3.33)

and Eq. (3.40), and the parameter estimation update laws with smooth projection in Eqs. (3.26) and (3.30) are simulated. The unknown matrix $\mathbf{J}_1$ is taken as

$$\mathbf{J}_1 = \begin{bmatrix} 4 \times 10^{-3} & 0 & 0 \\ 0 & 4 \times 10^{-3} & 0 \\ 0 & 0 & 5 \times 10^{-3} \end{bmatrix}$$

which essentially models a fuel tank in the shape of a cylinder. Consistent with the remarks made following Theorem 3.3.1, the constant $\lambda_{\max}$ is taken to be the maximum eigenvalue of $\mathbf{J}_0$, that is, $\lambda_{\max} = 20.7352$, while the minimum eigenvalue is taken as $\lambda_{\min} = 0.5$, and is assumed to be the eigenvalue associated with the dry mass inertia matrix of the spacecraft.

The constants for convex sets $\boldsymbol{\Omega}_{\boldsymbol{\theta}^*}$ and $\boldsymbol{\Omega}_{\hat{\boldsymbol{\theta}}}$ are $\epsilon_1 = (40)^2$ and $\delta_1 = (10)^2$, while those for $\boldsymbol{\Omega}_{\boldsymbol{\sigma}^*}$ and $\boldsymbol{\Omega}_{\hat{\boldsymbol{\sigma}}}$ are given by $\epsilon_2 = (0.008)^2$ and $\delta_2 = (0.008)^2$. Note that $\|\boldsymbol{\theta}^*\|^2 \in \boldsymbol{\Omega}_{\boldsymbol{\theta}^*}$, $\|\boldsymbol{\sigma}^*\|^2 \in \boldsymbol{\Omega}_{\boldsymbol{\sigma}^*}$ while the initial conditions $\hat{\boldsymbol{\theta}}(0) = [21.1, 1.9, 1.4, 17.8, 2.9, 15.5]^{\mathrm{T}}$ and $\hat{\boldsymbol{\sigma}}(0) = 0$ belong respectively to sets $\boldsymbol{\Omega}_{\hat{\boldsymbol{\theta}}}$ and $\boldsymbol{\Omega}_{\hat{\boldsymbol{\sigma}}}$. Furthermore, $\omega_B = \sup_{t \geq 0} \|\boldsymbol{\omega}_r\| = 1.1832$ and $\zeta^* = 55.56$. The tuning parameters are selected to be

$$\gamma = 100, \quad \gamma_1 = 8, \quad \gamma_2 = 20.5$$

and are chosen in such a manner so as to yield a result closest to the baseline performance for each controller. Moreover, using the selected parameters, the

following inequality is obtained in accordance with Eq. (3.46)

$$\begin{aligned}(\|\boldsymbol{\omega}_e(0)\|+1)^2 < \frac{2}{\lambda_{\max}}\Bigg[&\frac{\lambda_{\min}}{2}(\zeta^*-1)^2 - \frac{\lambda_{\min}}{2} - 4(\beta+k_v) \\ &- \frac{\left(\sqrt{\epsilon_1+\delta_1}+\sqrt{\epsilon_1}\right)^2}{2\gamma_1} - \frac{\left(\sqrt{\epsilon_2+\delta_2}+\sqrt{\epsilon_2}\right)^2}{2\gamma_2}\Bigg] \\ \approx\ & 14.81\end{aligned}$$

which is readily satisfied for $\|\boldsymbol{\omega}_e(0)\| = 0.0024$, thereby ensuring a non-singular control for the entire duration of the simulation. Note that every effort was made by the author to select the best possible tuning parameters for each control method. The results are illustrated in Figs. 3.8-3.10.

As with the appendage deployment case, it is found that whereas the proposed controller is able to drive the attitude and angular velocity errors to the origin in a consistent manner, the comparison controller suffers from an appreciable loss of accuracy both for attitude and angular-velocity tracking. The norms of the control torques commanded by the proposed and comparison controllers are shown in Figs. 3.9a-3.9b. The proposed control law remains well-defined throughout the simulation period. As illustrated in Fig. 3.9b, the torque demands of both controllers are comparable during the initial transient period. In Fig. 3.9a, the monotonic steady-state decay of the control norm for both controllers is consistent with the decrease in the overall rotational inertia of the spacecraft as a consequence of losing mass.

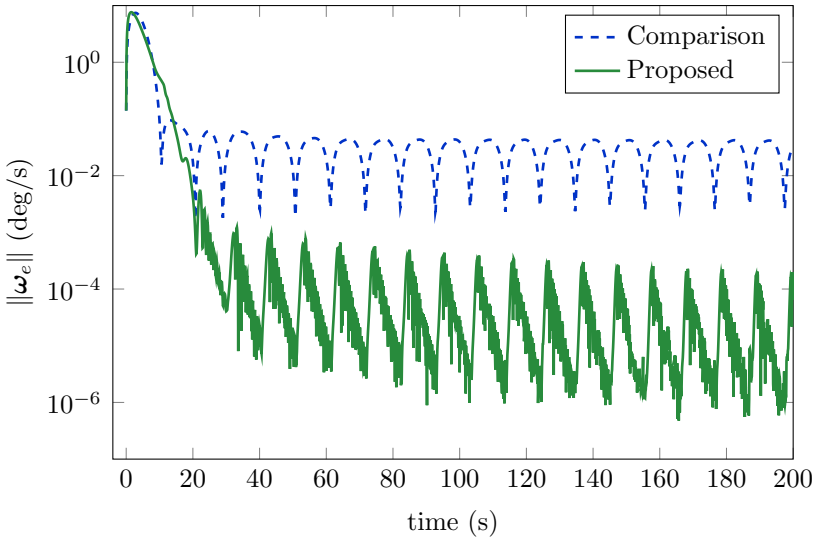

(a) Norm of angular velocity error vector

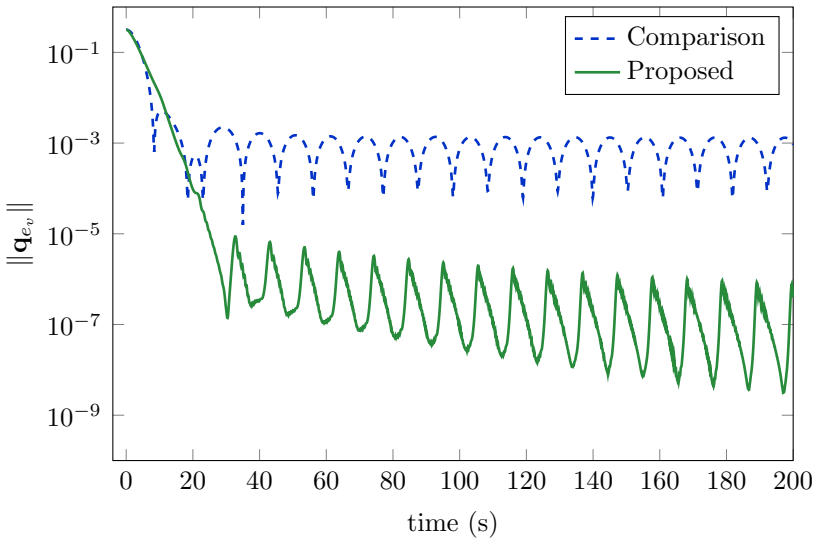

(b) Norm of quaternion error vector

Figure 3.8: Adaptive attitude-tracking control response for a spacecraft with fuel mass-loss induced inertia variations.

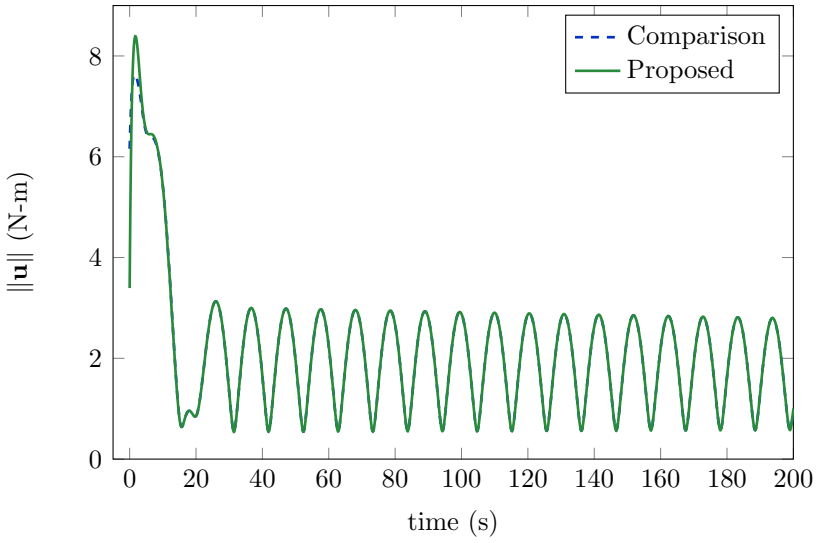

(a) Norm of control vector

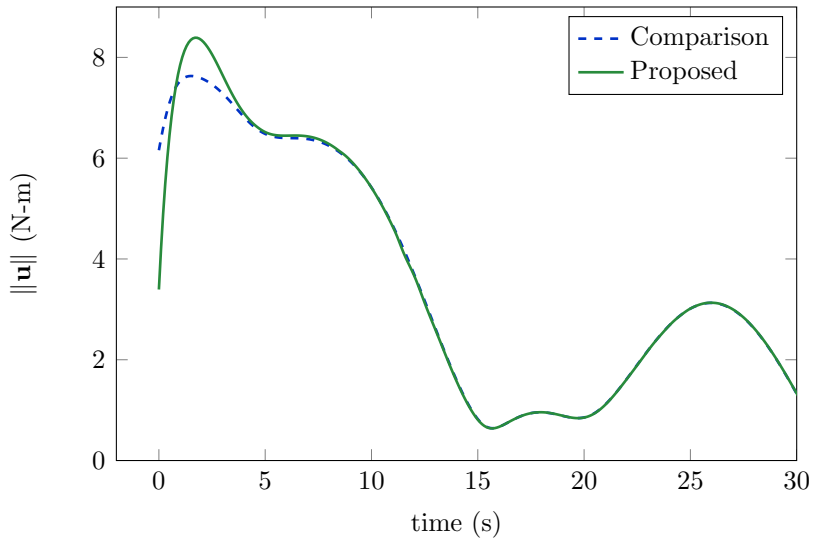

(b) Initial transient of control norm

Figure 3.9: Commanded control effort for adaptive control simulation of a spacecraft with fuel loss tracking a non-PE signal.

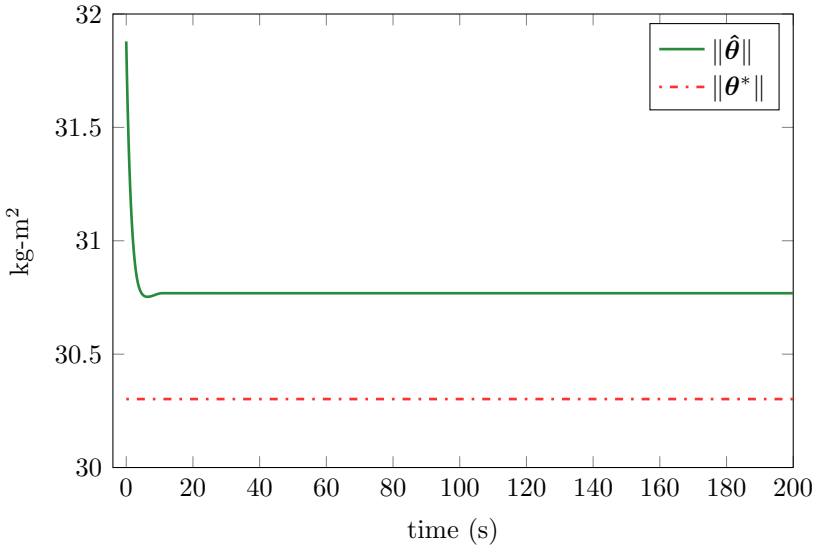

(a) Norm of $\mathbf{J}_0$ parameter estimates, $\|\hat{\boldsymbol{\theta}}\|$

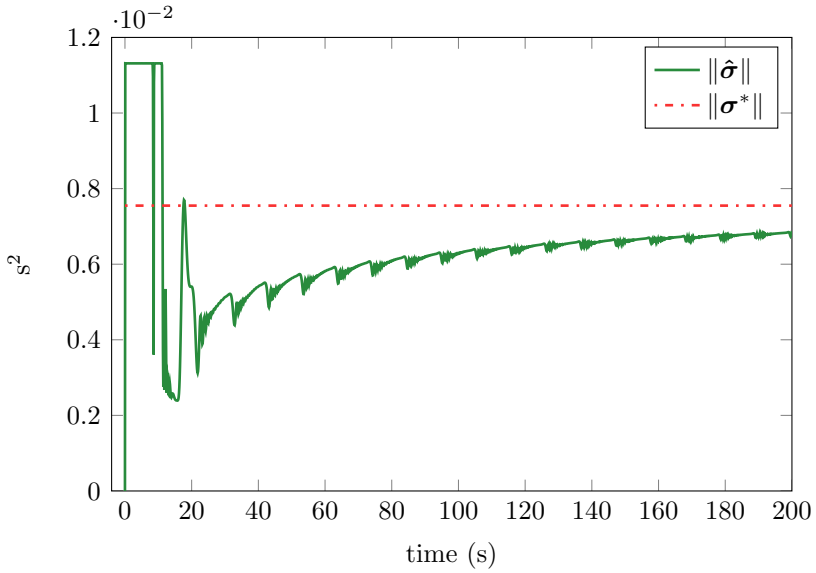

(b) Norm of $\mathbf{J}_1$ parameter estimates, $\|\hat{\boldsymbol{\sigma}}\|$

Figure 3.10: Parameter estimates of unknown $\mathbf{J}_0$ and $\mathbf{J}_1$ matrices (fuel-loss example).

The time evolution of the parameter estimates is shown in Fig. 3.10. In Fig. 3.10b, a similar trend to the deployment scenario is found, where the update law for $\hat{\boldsymbol{\sigma}}$ in the proposed control strategy is able to drive the estimated values to their true values. As mentioned in the previous example, the added persistence of excitation introduced in $\mathbf{W}_2$ and $\mathbf{W}_3$ due to the input dependent $\boldsymbol{\Psi}$ and $\dot{\boldsymbol{\Psi}}$ matrices, contributes to this unique feature despite a non-PE reference trajectory. Furthermore as expected, $\|\hat{\boldsymbol{\sigma}}\|$ is bounded by $\sqrt{\epsilon_2 + \delta_2} = 0.0113$ due to the smooth projection mechanism. Finally, the evolution of the principal moments of inertia of the fuel-mass dependent inertia matrix is illustrated in Fig. 3.11a for the proposed controller, and in Fig. 3.11b for the comparison controller. The simulated inertia matrix remains positive definite and satisfies the triangle inequalities in Eq. 3.5 for all time.

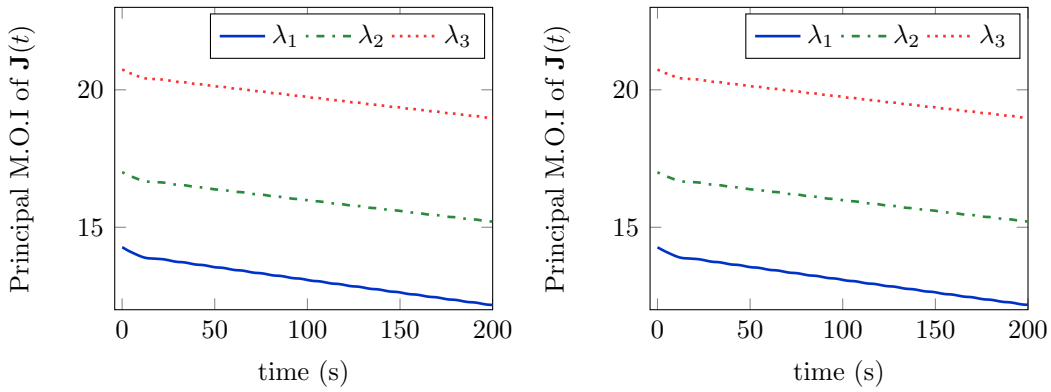

(a) Proposed controller

(b) Comparison controller

Figure 3.11: Principal moments of inertia of the control norm dependent inertia matrix simulating variations due to fuel mass-loss.

3.5 Concluding Remarks

In this chapter, an adaptive attitude control problem is addressed for a spacecraft with a time-varying inertia matrix. The inertia matrix consists of an unknown rigid (constant) matrix component, as well as a variable component with multiplicative uncertainty. The variable inertia term may be purely input dependent, or may display a combination of time and/or state dependencies. The proposed adaptive control delivers consistent tracking performance in the face of arbitrarily large uncertainties in the inertia matrix. When variations occur due to fuel mass-loss, a smooth projection scheme prevents drifting of the parameter estimates and ensures a singularity-free control solution for the coupled dynamics resulting from a control torque-dependent inertia matrix. A complete analysis of the proposed control law depicting asymptotic convergence of the tracking error signals is provided. Numerical simulation examples are provided to highlight the performance gains of the proposed controller when compared to existing adaptive controllers that do not account for inertia variations. The proposed control scheme has many practical advantages, especially in the field of aerospace engineering, where spacecraft often experience mass displacement or variations during flight. Future work for this problem could consider extending the present certainty-equivalence adaptive control solution to a non-certainty equivalence framework for increased performance efficiency, and possibly addressing more complicated inertia matrix models.

Chapter 4

Gyro-Free Rigid Body Attitude Stabilization using only Vector Measurements on $SO(3)$

In this chapter, the attitude stabilization of a rigid body is considered for the case when only a set of unit vector measurements is available for control feedback. In particular, angular velocity information is assumed to be either unavailable or unreliable due to faulty gyroscopes. This chapter provides a detailed development of a novel control scheme for stabilizing the rigid body's orientation to the desired configuration by using unit vector measurements for feedback. That is, rather than relying on an estimated attitude vector or rate gyro measurements, the novel control law is designed such that the unit vector measurements are employed directly for attitude regulation. The

control law is formulated on the special orthogonal group SO(3) and satisfies the so-called self-reduction property, wherein the resulting control law does not require information about the rigid-body inertia parameters. A technically important feature of this control design is that unlike other approaches, this control law is rooted in the passive systems framework and observers are not needed to reconstruct either the attitude or the angular velocity of the rigid body.

The chapter is organized as follows. Sec. 4.1 describes the rigid-body dynamics and kinematics as well as the measurement model. The main results of this chapter are presented along with thorough stability analysis in Sec. 4.2. In Sec. 4.3, numerical simulation studies are presented to help illustrate the technical aspects of this work, as well as to show the performance of the controller under realistic situations like measurement noise. Finally, the chapter in concluded in Sec. 4.4 with remarks that summarize the presented results.

4.1 Problem Formulation

The rigid body dynamics and kinematics are stated in terms of the direction cosine matrix and Euler's rotational equations. For notational convenience in this particular chapter, the subscript 'B' is added to $\mathbf{C}$ such that $\mathbf{C}_{\mathrm{b}}$ denotes the orthogonal matrix transformation from inertial reference frame $\mathcal{I}$ to body-fixed reference $\mathcal{B}$. Thus, the rigid body kinematics are stated as

$$\dot{\mathbf{C}}_{\mathrm{b}} = -S\left(\boldsymbol{\omega}\right)\mathbf{C}_{\mathrm{b}}. \tag{4.1}$$

The attitude dynamics stated in Eq. (2.2) are repeated here for the reader's convenience:

$$\mathbf{J}\dot{\boldsymbol{\omega}} = -S\left(\boldsymbol{\omega}\right)\mathbf{J}\boldsymbol{\omega} + \mathbf{u}. \tag{2.2}$$

The measurement model is discussed in the next section.

4.1.1 Measurement Model and Orientation Error

The rigid body (spacecraft) is assumed to be equipped with a combination of inertial sensors such as star trackers, sun sensors, or horizon sensors that provide at least two *non-collinear* unit vector measurements in the body-fixed frame. In addition, the spacecraft angular velocity measurement is assumed to be unavailable for feedback, either due to faulty or unreliable hardware or because the spacecraft is not equipped with rate gyros. The N unit-length vector measurements are defined through the following equations

$$\mathbf{y}^j = \mathbf{C}_{\mathrm{b}}\mathbf{x}^j, \quad \text{for } j = 1, 2, ..., N, \tag{4.2}$$

where $\mathbf{y}^j \in \mathbb{R}^3$ is the jth measurement expressed in $\mathcal{B}$ and $N \geq 2$. The vectors $\mathbf{x}^j$, $j = 1, \ldots, N$ are non-collinear constant unit vectors governing the inertial direction of the jth observation. The desired measurements are expressed in the desired frame $\mathcal{R}$ as follows

$$\mathbf{y}_r^j = \mathbf{C}_{\mathrm{r}}\mathbf{x}^j, \quad \text{for } j = 1, 2, ..., N, \tag{4.3}$$

where $\mathbf{y}_r^j \in \mathbb{R}^3$ is the jth desired constant measurement and $\mathbf{C}_\mathrm{r} \in SO(3)$, $\dot{\mathbf{C}}_r = 0$ denotes the constant orientation of $\mathcal{R}$ with respect to the inertial frame.

Let $\mathbf{E} = \mathbf{C}_\mathrm{b}\mathbf{C}_\mathrm{r}{}^\mathrm{T} \in SO(3)$ denote the error between the current orientation and the desired orientation. Using Poisson's equation, the dynamical evolution of the orientation error is given by

$$\dot{\mathbf{E}} = -S\left(\boldsymbol{\omega}\right)\mathbf{C}_\mathrm{b}\mathbf{C}_\mathrm{r}{}^\mathrm{T} = -S\left(\boldsymbol{\omega}\right)\mathbf{E}. \tag{4.4}$$

From the definition of $\mathbf{E}$, it follows that $\mathbf{E} = \mathbf{I}$ implies $\mathbf{C}_\mathrm{b} = \mathbf{C}_\mathrm{r}$. Since the true attitude of the vehicle is not directly measured, the attitude stabilization control law will be developed using the measured and desired unit vectors for feedback. For the j^{th} vector $\mathbf{y}^j$, the measurement error considered is given by

$$\begin{aligned} E_j &= 1 - \mathbf{y}_r^{j^\mathrm{T}}\mathbf{y}^j, \\ &= 1 - \mathrm{tr}\left(\mathbf{C}_\mathrm{b}\mathbf{x}^j\mathbf{x}^{j^\mathrm{T}}\mathbf{C}_\mathrm{r}{}^\mathrm{T}\right), \\ &= 1 - \mathrm{tr}\left(\mathbf{C}_\mathrm{b}\mathbf{x}^j\mathbf{x}^{j^\mathrm{T}}\mathbf{C}_\mathrm{b}{}^\mathrm{T}\mathbf{E}\right). \end{aligned}$$

The cost function for all N measurements is expressed as

$$E = \frac{1}{2}\sum_{j=1}^{N} k_j E_j = \frac{1}{2}\sum_{j=1}^{N} k_j\left(1 - \mathbf{y}_r^{j^\mathrm{T}}\mathbf{y}^j\right) = \frac{1}{2}\left[\sum_{j=1}^{N} k_j - \mathrm{tr}\left(\mathbf{M}\mathbf{E}\right)\right], \tag{4.5}$$

where [19, 32]

$$\mathbf{M} = \mathbf{C}_\mathrm{b}\mathbf{M}_0\mathbf{C}_\mathrm{b}{}^\mathrm{T} = \mathbf{M}^\mathrm{T}; \quad \mathbf{M}_0 = \sum_{j=1}^{N} k_j\mathbf{x}^j\mathbf{x}^{j^\mathrm{T}}, \tag{4.6}$$

and the scalar quantities $k_j > 0$ are user-defined weights on the confidence of the measurements. Observe that if $N \geq 3$, then $\mathbf{M} > 0$, and when $N = 2$, $\mathbf{M}$ is only positive semi-definite with one zero eigenvalue [32]. In Eq. (4.5), observe that when $\mathbf{y}^j \neq -\mathbf{y}_r^j \; \forall \; j = 1, \ldots, N$, the total measurement error taken on values such that $E < \sum_{j=1}^{N} k_j$. Subsequent stability analysis will employ this fact to ascertain convergence properties for the control law developed in the proceeding sections.

Given the system governed by Eqs. (4.1)-(2.2), the control objective is to design $\mathbf{u}$ such that $\mathbf{E}(t) \to \mathbf{I}$ ($E(t) \to 0$) and $\boldsymbol{\omega}(t) \to \mathbf{0}$ as $t \to \infty$ for any constant reference $\mathbf{C}_\mathrm{r}$, while ensuring boundedness of all closed loop signals. For control implementation, only the desired and measured unit-length vector measurements are assumed to be perfectly measured (no noise) and available for feedback.

4.2 Velocity-Free Attitude Control

4.2.1 Preliminary Results

Define a signal $\boldsymbol{\Omega}$ in the following manner

$$\boldsymbol{\Omega} = \frac{1}{2} \sum_{j=1}^{N} k_j S\left(\mathbf{y}^j\right) \mathbf{y}_r^j. \tag{4.7}$$

An important lemma is now stated that will be useful later in the convergence analysis of the control law that will be developed subsequently.

Lemma 4.2.1. *Assume that there are two or more ($N \geq 2$) non-collinear*

vector measurements available. Then, $\mathbf{\Omega} = \mathbf{0}$ *implies that either* $\mathbf{E} = \mathbf{I}$ *or* $\mathrm{tr}(\mathbf{E}) = -1$.

Proof. Consider the signal $S(\mathbf{\Omega})$, which, using the identity $S(\mathbf{v}\times\mathbf{w}) = -\mathbf{v}\mathbf{w}^{\mathrm{T}} + \mathbf{w}\mathbf{v}^{\mathrm{T}}$, is expressed as [19]

$$\begin{aligned} S(\mathbf{\Omega}) &= \frac{1}{2}\sum_{j=1}^{N} k_j S(\mathbf{y}^j \times \mathbf{y}_r^j), \\ &= \frac{1}{2}\sum_{j=1}^{N} k_j \left[-\mathbf{y}^j \mathbf{y}_r^{j\,\mathrm{T}} + \mathbf{y}_r^j \mathbf{y}^{j\,\mathrm{T}}\right], \\ &= \frac{1}{2}\sum_{j=1}^{N} k_j \left[-\mathbf{C}_{\mathrm{b}} \mathbf{x}^j \mathbf{x}^{j\,\mathrm{T}} \mathbf{C}_{\mathrm{r}}{}^{\mathrm{T}} + \mathbf{C}_{\mathrm{r}} \mathbf{x}^j \mathbf{x}^{j\,\mathrm{T}} \mathbf{C}_{\mathrm{b}}{}^{\mathrm{T}}\right] \\ &= \frac{1}{2}\left[-\mathbf{M}\mathbf{E} + \mathbf{E}^{\mathrm{T}}\mathbf{M}^{\mathrm{T}}\right] \end{aligned} \tag{4.8}$$

Observe that when $\mathbf{\Omega} = \mathbf{0}$, $S(\mathbf{\Omega}) = \mathbf{0}$. Then, from Eq. (4.8) it follows that $\mathbf{M}\mathbf{E} = \mathbf{E}^{\mathrm{T}}\mathbf{M}^{\mathrm{T}}$. Following the procedure of [19, 22, 32], we show next that this implies $\mathbf{E} = \mathbf{I}$ or $\mathrm{tr}(\mathbf{E}) = -1$. Since $\mathbf{E}$ is a real-valued matrix, its eigenvalues and eigenvectors satisfy $\mathbf{E}\mathbf{e}_k = \sigma_k \mathbf{e}_k$ and $\mathbf{e}_k^{\mathrm{H}}\mathbf{E}^{\mathrm{T}} = \sigma_k^{\mathrm{H}}\mathbf{e}_k^{\mathrm{H}}$, where σ_k^{H} for $k = 1, 2, 3$ denotes the complex conjugate of the eigenvalue σ_k, while $\mathbf{e}_k^{\mathrm{H}}$ denotes the complex conjugate transpose of the eigenvector $\mathbf{e}_k$ associated with σ_k. Pre-multiplying and post-multiplying $\mathbf{M}\mathbf{E} = \mathbf{E}^{\mathrm{T}}\mathbf{M}^{\mathrm{T}}$ respectively by $\mathbf{e}_k^{\mathrm{H}}$ and $\mathbf{e}_k$, recognizing that $\mathbf{M}^{\mathrm{T}} = \mathbf{M}$, and following through with appropriate substitutions leads to $\mathbf{e}_k^{\mathrm{H}}\mathbf{M}\mathbf{e}_k\sigma_k = \sigma_k^{\mathrm{H}}\mathbf{e}_k^{\mathrm{H}}\mathbf{M}\mathbf{e}_k$. When $N \geq 3$, $\mathbf{M} > 0$ and $\mathbf{e}_k^{\mathrm{H}}\mathbf{M}\mathbf{e}_k > 0 \;\forall\; k = 1, 2, 3$. Consequently, $\sigma_k = \sigma_k^{\mathrm{H}}$ and all eigenvalues of $\mathbf{E}$ are real. When only two vector measurements are available ($N = 2$), two of the eigenvalues are real. Since complex eigenvalues must appear in

complex conjugate pairs, it follows that the third eigenvalue is also real. Observe that since $\mathbf{E}$ is a rotation matrix, its eigenvalues are of the form $\text{eig}(\mathbf{E}) = (1, \cos(\phi) + i\sin(\phi), \cos(\phi) - i\sin(\phi))$ where ϕ is the angle associated with the angle/axis representation of $\mathbf{E}$. Then, since the eigenvalues of $\mathbf{E}$ are all real, $\phi = 0$ or $\phi = \pm 180^\circ$. As a result, $\boldsymbol{\Omega} = \mathbf{0}$ implies that $\mathbf{E} = \mathbf{I}$ or $\text{tr}(\mathbf{E}) = -1$. For further details, the reader is referred to [22, 32]. □

Using the facts that $\dot{\mathbf{y}}^j = S(\mathbf{y}^j)\boldsymbol{\omega}$ and $\dot{\mathbf{y}}_r^j = \mathbf{0}$ along with the identity $S(\mathbf{v})S(\mathbf{w}) = \mathbf{w}\mathbf{v}^T - (\mathbf{v}^{\mathrm{T}}\mathbf{w})\mathbf{I}$ for $\mathbf{v}, \mathbf{w} \in \mathbb{R}^3$, the dynamical equation governing the evolution of $\boldsymbol{\Omega}$ is derived as follows:

$$\begin{aligned}
\dot{\boldsymbol{\Omega}} &= -\frac{1}{2}\sum_{j=1}^{N} k_j S\left(\mathbf{y}_r^j\right)\dot{\mathbf{y}}^j \\
&= -\frac{1}{2}\sum_{j=1}^{N} k_j S\left(\mathbf{y}_r^j\right) S\left(\mathbf{y}^j\right)\boldsymbol{\omega} \\
&= -\frac{1}{2}\sum_{j=1}^{N} k_j \left[\mathbf{y}^j\mathbf{y}_r^{j\mathrm{T}} - \left(\mathbf{y}_r^{j\mathrm{T}}\mathbf{y}^j\right)\mathbf{I}\right]\boldsymbol{\omega} \\
&= -\frac{1}{2}\sum_{j=1}^{N} k_j \left[\mathbf{C}_{\mathrm{b}}\mathbf{x}^j\mathbf{x}^{j\mathrm{T}}\mathbf{C}_{\mathrm{r}}{}^{\mathrm{T}} - \text{tr}\left(\mathbf{C}_{\mathrm{b}}\mathbf{x}^j\mathbf{x}^{j\mathrm{T}}\mathbf{C}_{\mathrm{r}}{}^{\mathrm{T}}\right)\mathbf{I}\right]\boldsymbol{\omega} \\
&= -\frac{1}{2}\sum_{j=1}^{N} k_j \left[\mathbf{C}_{\mathrm{b}}\mathbf{x}^j\mathbf{x}^{j\mathrm{T}}\mathbf{C}_{\mathrm{b}}{}^{\mathrm{T}}\mathbf{E} - \text{tr}\left(\mathbf{C}_{\mathrm{b}}\mathbf{x}^j\mathbf{x}^{j\mathrm{T}}\mathbf{C}_{\mathrm{b}}{}^{\mathrm{T}}\mathbf{E}\right)\mathbf{I}\right]\boldsymbol{\omega} \\
&= -\frac{1}{2}\left[\mathbf{M}\mathbf{E} - \text{tr}\left(\mathbf{M}\mathbf{E}\right)\mathbf{I}\right]\boldsymbol{\omega}
\end{aligned} \tag{4.9}$$

A second important lemma is stated next that will be utilized in the stability analysis of the forthcoming attitude control law development.

Lemma 4.2.2. *Suppose that there are two or more ($N \geq 2$) non-collinear*

vector measurements available. Then, $\dot{\boldsymbol{\Omega}}(t) \to \mathbf{0}$ *as* $t \to \infty$ *implies that either one or both of the following conditions must hold:* $\boldsymbol{\omega}(t) \to \mathbf{0}$ *and/or* $\mathrm{tr}(\mathbf{E}(t)) \to -1$ *as* $t \to \infty$*.*

Proof. When $\dot{\boldsymbol{\Omega}} = \mathbf{0}$, Eq. (4.9) yields

$$\mathbf{ME}\boldsymbol{\omega} = \mathrm{tr}\,(\mathbf{ME})\,\boldsymbol{\omega}. \tag{4.10}$$

Pre-multiplying both sides of Eq. (4.10) by $\boldsymbol{\omega}^{\mathrm{T}}\mathbf{E}^{\mathrm{T}}$, recognizing that $\mathbf{M}^{\mathrm{T}} = \mathbf{M}$, and using Eq. (4.10) to substitute for $\mathbf{ME}\boldsymbol{\omega}$ leads to

$$\mathrm{tr}\,(\mathbf{ME})\,\boldsymbol{\omega}^{\mathrm{T}}\mathbf{E}\boldsymbol{\omega} = \mathrm{tr}\,(\mathbf{ME})\,\boldsymbol{\omega}^{\mathrm{T}}\mathbf{E}^{\mathrm{T}}\boldsymbol{\omega}, \tag{4.11}$$

which may be satisfied by one or a combination of the following solutions: (i) $\mathbf{E} = \mathbf{E}^{\mathrm{T}}$, (ii) $\mathrm{tr}(\mathbf{ME}) = 0$, and (iii) $\boldsymbol{\omega} = \mathbf{0}$. We now examine the solutions (i) and (ii) and show that $\mathbf{E} = \mathbf{E}^{\mathrm{T}}$ leads to $\boldsymbol{\omega} = \mathbf{0}$ or $\mathrm{tr}(\mathbf{E}) = -1$, while $\mathrm{tr}(\mathbf{ME}) = 0$ always leads to $\boldsymbol{\omega} = \mathbf{0}$.

Consider solution (i) where $\mathbf{E} = \mathbf{E}^{\mathrm{T}}$. As discussed in the proof for Lemma 4.2.1, the eigenvalues of $\mathbf{E}$ are of the form

$$\mathrm{eig}\,(\mathbf{E}) = (1, \cos(\phi) + i\sin(\phi), \cos(\phi) - i\sin(\phi))\,.$$

If $\mathbf{E} = \mathbf{E}^{\mathrm{T}}$, then the eigenvalues of $\mathbf{E}$ are real and $\phi = 0$ or $\phi = \pm 180°$. Therefore, $\mathbf{E} = \mathbf{I}$ or $\mathrm{tr}(\mathbf{E}) = -1$. Substituting for $\mathbf{E} = \mathbf{I}$ in Eq. (4.10) and slightly rearranging terms yields

$$[\mathbf{M} - \mathrm{tr}\,(\mathbf{M})\,\mathbf{I}]\,\boldsymbol{\omega} = \mathbf{0}. \tag{4.12}$$

Next, denote the eigenvalues of $\mathbf{M}$ as λ_k, $k = 1, 2, 3$. For $\boldsymbol{\omega} \neq \mathbf{0}$, observe that Eq. (4.12) is a simple eigenvalue problem. Therefore, without loss of generality, we can write $\lambda_1 = \mathrm{tr}\,(\mathbf{M})$. Using the definition of the matrix trace as the sum of the matrix eigenvalues, that is, $\mathrm{tr}\,(\mathbf{M}) = \sum_{k=1}^{3} \lambda_k$, and substituting this definition into $\lambda_1 = \mathrm{tr}\,(\mathbf{M})$ and simplifying yields $\lambda_2 + \lambda_3 = 0$. However, recall that when $N \geq 3$, $\mathbf{M} > 0$ which means $\lambda_k > 0 \ \forall \ k = 1, 2, 3$. Similarly, when $N = 2$, $\mathbf{M}$ has exactly one zero eigenvalue and two positive eigenvalues. Consequently, it must be that $\lambda_2 + \lambda_3 > 0$ is always true which implies that $\mathrm{tr}\,(\mathbf{M})$ cannot be an eigenvalue of $\mathbf{M}$. Thus, it follows that the only solution to Eq. (4.12) is $\boldsymbol{\omega} = \mathbf{0}$. Therefore, the solution (i) $\mathbf{E} = \mathbf{E}^{\mathrm{T}}$ leads to either $\boldsymbol{\omega} = \mathbf{0}$ or $\mathrm{tr}(\mathbf{E}) = -1$.

We now consider the solution (ii) $\mathrm{tr}\,(\mathbf{ME}) = 0$. When $\mathrm{tr}\,(\mathbf{ME}) = 0$, Eq. (4.10) simplifies to

$$\mathbf{ME}\boldsymbol{\omega} = \mathbf{0}. \tag{4.13}$$

Since $\mathbf{M} > 0$ for $N \geq 3$, it is simple to show that Eq. (4.13) leads to $\boldsymbol{\omega} = \mathbf{0}$ owing to the fact that $(\mathbf{ME})^{-1} = \mathbf{E}^{\mathrm{T}}\mathbf{M}^{-1}$ is well defined. Deriving a similar result for the case when $N = 2$ requires more involved analysis. When $N = 2$, Eq. (4.13) is expressed as

$$k_1 \mathbf{y}^1 (\mathbf{y}_r^{1^{\mathrm{T}}} \boldsymbol{\omega}) = -k_2 \mathbf{y}^2 (\mathbf{y}_r^{2^{\mathrm{T}}} \boldsymbol{\omega}) \tag{4.14}$$

which follows directly from substituting the definitions of $\mathbf{M}$ and $\mathbf{E}$ into Eq. (4.13) and rearranging terms. Since $\mathbf{y}^1$ and $\mathbf{y}^2$ are non-collinear, and

$\mathbf{y}_r^1$ and $\mathbf{y}_r^2$ are non-collinear, the potential solutions for Eq. (4.14) are $\boldsymbol{\omega} = \mathbf{0}$ or $\boldsymbol{\omega} = \alpha \mathbf{y}_r^1 \times \mathbf{y}_r^2$, where α is any nonzero and potentially time-varying scalar. We now show through a contradiction argument that $\boldsymbol{\omega} = \alpha \mathbf{y}_r^1 \times \mathbf{y}_r^2$ is not a feasible solution of the system and that Eq. (4.14) always leads to $\boldsymbol{\omega} = \mathbf{0}$. To this end, note that if $\mathrm{tr}\,(\mathbf{ME}) = 0$ for all $t \geq 0$, it must be that $d/dt\,(\mathrm{tr}\,(\mathbf{ME})) = 0 \;\forall\; t \geq 0$. Recalling that by definition $\mathrm{tr}\,(\mathbf{ME}) = \sum_{j=1}^{N} k_j \mathbf{y}_r^{j^{\mathrm{T}}} \mathbf{y}^j$, we have

$$\begin{aligned}
\frac{\mathrm{d}}{\mathrm{d}t}\left(\sum_{j=1}^{N} k_j \mathbf{y}_r^{j^{\mathrm{T}}} \mathbf{y}^j\right) &= \sum_{j=1}^{N} k_j \mathbf{y}_r^{j^{\mathrm{T}}} \dot{\mathbf{y}}^j \\
&= -\sum_{j=1}^{N} k_j \left(S(\mathbf{y}^j)\mathbf{y}_r^j\right)^{\mathrm{T}} \boldsymbol{\omega} \\
&= -\boldsymbol{\Omega}^{\mathrm{T}} \boldsymbol{\omega},
\end{aligned}$$

from which it follows that $\boldsymbol{\Omega}^{\mathrm{T}}\boldsymbol{\omega} = 0$ since $\mathrm{tr}\,(\mathbf{ME}) = 0$. Next, define a unit vector $\mathbf{e}_\omega$ such that $\mathbf{e}_\omega = \mathbf{y}_r^1 \times \mathbf{y}_r^2 / \|\mathbf{y}_r^1 \times \mathbf{y}_r^2\|$. Observe that the unit vectors $\{\mathbf{y}_r^1,\ \mathbf{y}_r^2,\ \mathbf{e}_\omega\}$ form a basis in $\mathbb{R}^3$, which can be used to express $\mathbf{y}^1$ and $\mathbf{y}^2$ as follows

$$\mathbf{y}^1 = (\mathbf{y}^{1^{\mathrm{T}}} \mathbf{y}_r^1)\mathbf{y}_r^1 + (\mathbf{y}^{1^{\mathrm{T}}} \mathbf{y}_r^2)\mathbf{y}_r^2 + (\mathbf{y}^{1^{\mathrm{T}}} \mathbf{e}_\omega)\mathbf{e}_\omega, \tag{4.15}$$

$$\mathbf{y}^2 = (\mathbf{y}^{2^{\mathrm{T}}} \mathbf{y}_r^1)\mathbf{y}_r^1 + (\mathbf{y}^{2^{\mathrm{T}}} \mathbf{y}_r^2)\mathbf{y}_r^2 + (\mathbf{y}^{2^{\mathrm{T}}} \mathbf{e}_\omega)\mathbf{e}_\omega. \tag{4.16}$$

Substituting Eqs. (4.15)-(4.16) into the definition of $\boldsymbol{\Omega}$ in Eq. (4.7) and simplifying gives

$$\boldsymbol{\Omega} = k_1 \left[-\beta(\mathbf{y}^{1^{\mathrm{T}}} \mathbf{y}_r^2)\mathbf{e}_\omega + (\mathbf{y}^{1^{\mathrm{T}}} \mathbf{e}_\omega)\mathbf{e}_\omega \times \mathbf{y}_r^1\right] + k_2 \left[\beta(\mathbf{y}^{2^{\mathrm{T}}} \mathbf{y}_r^1)\mathbf{e}_\omega + (\mathbf{y}^{2^{\mathrm{T}}} \mathbf{e}_\omega)\mathbf{e}_\omega \times \mathbf{y}_r^2\right], \tag{4.17}$$

where $\beta = \|\mathbf{y}_r^1 \times \mathbf{y}_r^2\|$. Premultiplying both sides of Eq. (4.17) by $\mathbf{e}_\omega^{\mathrm{T}}$ leads to

$$\mathbf{e}_\omega^{\mathrm{T}}\boldsymbol{\Omega} = -k_1\beta(\mathbf{y}^{1^{\mathrm{T}}}\mathbf{y}_r^2) + k_2\beta(\mathbf{y}^{2^{\mathrm{T}}}\mathbf{y}_r^1). \tag{4.18}$$

Since $\boldsymbol{\omega}^{\mathrm{T}}\boldsymbol{\Omega} = \alpha\beta\mathbf{e}_\omega^{\mathrm{T}}\boldsymbol{\Omega} = 0$, from Eq. (4.18) we have

$$-k_1(\mathbf{y}^{1^{\mathrm{T}}}\mathbf{y}_r^2) + k_2(\mathbf{y}^{2^{\mathrm{T}}}\mathbf{y}_r^1) = 0. \tag{4.19}$$

Next, observe that the orientation error matrix $\mathbf{E}$ may be parameterized in terms of its corresponding quaternion $\mathbf{q} = \begin{bmatrix} q_0, & \mathbf{q}_v^{\mathrm{T}} \end{bmatrix}^{\mathrm{T}}$, where $q_0 \in \mathbb{R}$, $\mathbf{q}_v \in \mathbb{R}^3$, and $q_0^2 + \mathbf{q}_v^{\mathrm{T}}\mathbf{q}_v = 1$, as follows

$$\mathbf{E} = \left(q_0^2 - \mathbf{q}_v^{\mathrm{T}}\mathbf{q}_v\right)\mathbf{I} + 2\mathbf{q}_v\mathbf{q}_v^{\mathrm{T}} + 2q_0 S(\mathbf{q}_v). \tag{4.20}$$

Using Eq. (4.20), along with the fact that $\mathbf{y}^j = \mathbf{C}_{\mathrm{b}}\mathbf{x}^j = \mathbf{C}_{\mathrm{b}}\mathbf{C}_{\mathrm{r}}{}^{\mathrm{T}}\mathbf{C}_{\mathrm{r}}\mathbf{x}^j = \mathbf{E}\mathbf{y}_r^j$, one can express $\mathrm{tr}(\mathbf{ME})$ for $N = 2$ as follows:

$$\begin{aligned}
\mathrm{tr}\,(\mathbf{ME}) &= k_1\mathbf{y}_r^{1^{\mathrm{T}}}\mathbf{y}^1 + k_2\mathbf{y}_r^{2^{\mathrm{T}}}\mathbf{y}^2 \\
&= k_1\mathbf{y}_r^{1^{\mathrm{T}}}\mathbf{E}\mathbf{y}_r^1 + k_2\mathbf{y}_r^{2^{\mathrm{T}}}\mathbf{E}\mathbf{y}_r^2 \\
&= k_1\left[(q_0^2 - \mathbf{q}_v^{\mathrm{T}}\mathbf{q}_v) + 2(\mathbf{y}_r^{1^{\mathrm{T}}}\mathbf{q}_v)^2\right] + k_2\left[(q_0^2 - \mathbf{q}_v^{\mathrm{T}}\mathbf{q}_v) + 2(\mathbf{y}_r^{2^{\mathrm{T}}}\mathbf{q}_v)^2\right].
\end{aligned} \tag{4.21}$$

Observe that q_0 and $\mathbf{q}_v$ can be expressed in terms of the eigenaxis $\mathbf{e}_v$ and eigenangle ϕ associated with $\mathbf{E}$ according to $q_0 = \cos(\phi/2)$ and $\mathbf{q}_v = \mathbf{e}_v \sin(\phi/2)$, where $\|\mathbf{e}_v\| = 1$ by definition. Substituting these expressions into the right-hand side of Eq. (4.21) along with using some trigonometric identities, and recognizing that the right-hand side of Eq. (4.21) is identically zero since

$\mathrm{tr}(\mathbf{ME}) = 0$, we get the following expression

$$k_1 \left[\cos(\phi)\left(1 - (\mathbf{y}_r^{1^{\mathrm{T}}}\mathbf{e}_v)^2\right) + (\mathbf{y}_r^{1^{\mathrm{T}}}\mathbf{e}_v)^2\right] + k_2 \left[\cos(\phi)\left(1 - (\mathbf{y}_r^{2^{\mathrm{T}}}\mathbf{e}_v)^2\right) + (\mathbf{y}_r^{2^{\mathrm{T}}}\mathbf{e}_v)^2\right] = 0. \quad (4.22)$$

Recall that the rotation matrix $\mathbf{E}$ evolves according to $\dot{\mathbf{E}} = -S(\boldsymbol{\omega})\mathbf{E}$. Since $\boldsymbol{\omega} = \alpha\beta\mathbf{e}_\omega$ is an inertially fixed vector, $\mathbf{E}$ describes the orientation of a rigid body executing pure-spin about the axis $\mathbf{e}_\omega$. It follows then that $\mathbf{e}_\omega$ describes the eigenaxis associated with $\mathbf{E}$, i.e., $\mathbf{e}_v = \mathbf{e}_\omega$. Since $\mathbf{e}_\omega = \mathbf{y}_r^1 \times \mathbf{y}_r^2 / \|\mathbf{y}_r^1 \times \mathbf{y}_r^2\|$, we then have $\mathbf{y}_r^{1^{\mathrm{T}}}\mathbf{e}_v = \mathbf{y}_r^{2^{\mathrm{T}}}\mathbf{e}_v = 0$. Thus, Eq. (4.22) simplifies to $(k_1 + k_2)\cos(\phi) = 0$, and since $k_1 + k_2 > 0$, it follows that $\cos(\phi) = 0$ or that $\phi = \pm 90°, \pm 270°$.

Next, using Eq. (4.19) together with $\mathbf{y}^j = \mathbf{E}\mathbf{y}_r^j$ and Eq. (4.20), substituting for $q_0 = \cos(\phi/2)$ and $\mathbf{q}_v = \mathbf{e}_v \sin(\phi/2)$, and once again applying some common trigonometric identities leads to

$$-k_1 \left[\mathbf{y}_r^{1^{\mathrm{T}}}\mathbf{y}_r^2 \cos(\phi) + (\mathbf{y}_r^{1^{\mathrm{T}}}\mathbf{e}_v)(\mathbf{y}_r^{2^{\mathrm{T}}}\mathbf{e}_v)\,(1 - \cos(\phi)) + \sin(\phi)\mathbf{y}_r^{2^{\mathrm{T}}}(\mathbf{e}_v \times \mathbf{y}_r^1)\right] + k_2 \left[\mathbf{y}_r^{1^{\mathrm{T}}}\mathbf{y}_r^2 \cos(\phi) + (\mathbf{y}_r^{1^{\mathrm{T}}}\mathbf{e}_v)(\mathbf{y}_r^{2^{\mathrm{T}}}\mathbf{e}_v)\,(1 - \cos(\phi)) - \sin(\phi)\mathbf{y}_r^{2^{\mathrm{T}}}(\mathbf{e}_v \times \mathbf{y}_r^1)\right] = 0. \quad (4.23)$$

Substituting $\mathbf{y}_r^{1^{\mathrm{T}}}\mathbf{e}_v = \mathbf{y}_r^{2^{\mathrm{T}}}\mathbf{e}_v = 0$ and $\cos(\phi) = 0$ into Eq. (4.23) yields

$$(k_1 + k_2)\sin(\phi)\mathbf{y}_r^{2^{\mathrm{T}}}(\mathbf{e}_v \times \mathbf{y}_r^1) = 0. \quad (4.24)$$

Since $k_1, k_2 > 0$ and $\cos(\phi) = 0$, it follows that $(k_1 + k_2)\sin(\phi) \neq 0$, and from Eq. (4.24) we have $\mathbf{y}_r^{2^{\mathrm{T}}}(\mathbf{e}_v \times \mathbf{y}_r^1) = 0$, which when combined with $\mathbf{e}_v = \mathbf{y}_r^1 \times \mathbf{y}_r^2 / \|\mathbf{y}_r^1 \times \mathbf{y}_r^2\|$ leads to $(\mathbf{y}_r^{1^{\mathrm{T}}}\mathbf{y}_r^2)^2 = 1$ after applying the vector triple

product identity $\mathbf{a} \times (\mathbf{b} \times \mathbf{c}) = \mathbf{b}(\mathbf{a}^{\mathrm{T}}\mathbf{c}) - \mathbf{c}(\mathbf{a}^{\mathrm{T}}\mathbf{b})$ for any $\mathbf{a}, \mathbf{b}, \mathbf{c} \in \mathbb{R}^3$. Finally, observe that $({\mathbf{y}_r^1}^{\mathrm{T}}\mathbf{y}_r^2)^2 = 1$ would only be satisfied if $\mathbf{y}_r^1$ and $\mathbf{y}_r^2$ are collinear vectors, which brings us to a direct contradiction since $\mathbf{y}_r^1$ and $\mathbf{y}_r^2$ are assumed to be non-collinear directions. Consequently, it follows that the only feasible solution of $\mathbf{\Omega}^{\mathrm{T}}\boldsymbol{\omega} = 0$ is $\boldsymbol{\omega} = \mathbf{0}$ and, therefore, the only possible solution of Eq. (4.14) is $\boldsymbol{\omega} = \mathbf{0}$. Thus, the solution (ii) $\mathrm{tr}(\mathbf{ME}) = 0 \ \forall \ t \geq 0$ results in $\boldsymbol{\omega} = \mathbf{0}$ when $N \geq 2$.

We have shown that when at least two vector measurements are available, Eq. (4.10) leads to either one or both of the following two conditions being satisfied: $\boldsymbol{\omega} = \mathbf{0}$ and $\mathrm{tr}(\mathbf{E}) = -1$. Thus, when $N \geq 2$, $\dot{\mathbf{\Omega}}(t) \to \mathbf{0}$ as $t \to \infty$ implies that $\boldsymbol{\omega}(t) \to \mathbf{0}$ and/or $\mathrm{tr}(\mathbf{E}(t)) \to -1$ as $t \to \infty$. □

4.2.2 Gyro-Free Attitude Stabilization Control Law

We now state the main result of this chapter in the form of an asymptotically stabilizing angular-velocity free feedback control input presented below in Theorem 4.2.3.

Theorem 4.2.3. *Consider the system governed by Eqs.* (4.1)-(2.2) *and let the control input torque* $\mathbf{u}$ *be determined by*

$$\mathbf{u} = -k_p\mathbf{\Omega} - k_z\tilde{\mathbf{M}}^{\mathrm{T}}\boldsymbol{\zeta} \tag{4.25}$$

with $\tilde{\mathbf{M}} = -(1/2)\left[\mathbf{ME} - \mathrm{tr}(\mathbf{ME})\mathbf{I}\right]$, *any positive scalars* k_p *and* k_z, *and* $\boldsymbol{\zeta}$

determined as the output of the linear time-invariant system

$$\dot{\mathbf{z}} = \mathbf{A}_m \mathbf{z} + \mathbf{B}\boldsymbol{\Omega}, \tag{4.26a}$$

$$\boldsymbol{\zeta} = \mathbf{B}^{\mathrm{T}} \mathbf{P} \dot{\mathbf{z}} \tag{4.26b}$$

with any Hurwitz $\mathbf{A}_m \in \mathbb{R}^{3\times3}$*, any full rank matrix* $\mathbf{B}$*, and a symmetric and positive-definite matrix* $\mathbf{P} \in \mathbb{R}^{3\times3}$ *that solves the equation* $\mathbf{A}_m^{\mathrm{T}}\mathbf{P} + \mathbf{P}\mathbf{A}_m = -\mathbf{Q}$*, for any symmetric, positive-definite matrix* $\mathbf{Q} \in \mathbb{R}^{3\times3}$*. Then, the closed-loop system is asymptotically stable, i.e.,* $[\mathbf{E}(t), \boldsymbol{\omega}(t)] \to [\mathbf{I}, \mathbf{0}]$ *as* $t \to \infty$ *for any constant reference orientation* $\mathbf{C}_{\mathrm{r}}$ *and all initial conditions* $[\mathbf{E}(0), \boldsymbol{\omega}(0)]$ *satisfying*

$$\frac{1}{2}\boldsymbol{\omega}(0)^{\mathrm{T}}\mathbf{J}\boldsymbol{\omega}(0) + \frac{1}{2}k_p \sum_{j=1}^{N} k_j \left(1 - \mathbf{y}(0)^{j^{\mathrm{T}}} \mathbf{y}_r(0)^j\right) + \frac{1}{2}k_z \dot{\mathbf{z}}(0)^{\mathrm{T}}\mathbf{P}\dot{\mathbf{z}}(0) < k_p \sum_{j=1}^{N} k_j. \tag{4.27}$$

Proof. Consider the following positive definite Lyapunov function candidate

$$V = \frac{1}{2}\boldsymbol{\omega}^{\mathrm{T}}\mathbf{J}\boldsymbol{\omega} + \frac{1}{2}k_p \sum_{j=1}^{N} k_j \left(1 - \mathbf{y}^{j^{\mathrm{T}}} \mathbf{y}_r^j\right) + \frac{1}{2}k_z \dot{\mathbf{z}}^{\mathrm{T}}\mathbf{P}\dot{\mathbf{z}}. \tag{4.28}$$

Taking the time-derivative of V along Eqs. (2.2), (4.9), (5.27), and (4.26) and

using the property $S^{\mathrm{T}}(\mathbf{v}) = -S(\mathbf{v})$ for any $\mathbf{v} \in \mathbb{R}^3$ yields

$$\begin{aligned}
\dot{V} &= \boldsymbol{\omega}^{\mathrm{T}}\mathbf{J}\dot{\boldsymbol{\omega}} - \frac{1}{2}k_p\sum_{j=1}^{N} k_j\dot{\mathbf{y}}^{j^{\mathrm{T}}}\mathbf{y}_r^j + \frac{1}{2}k_z\dot{\mathbf{z}}^{\mathrm{T}}\left(\mathbf{P}\mathbf{A}_m + \mathbf{A}_m^{\mathrm{T}}\mathbf{P}\right)\dot{\mathbf{z}} + k_z\dot{\mathbf{z}}^{\mathrm{T}}\mathbf{P}\mathbf{B}\dot{\boldsymbol{\Omega}} \\
&= \boldsymbol{\omega}^{\mathrm{T}}\left(-S(\boldsymbol{\omega})\mathbf{J}\boldsymbol{\omega} + \mathbf{u}\right) - \frac{1}{2}k_p\sum_{j=1}^{N} k_j\left(S(\mathbf{y}^j)\boldsymbol{\omega}\right)^{\mathrm{T}}\mathbf{y}_r^j - \frac{1}{2}k_z\dot{\mathbf{z}}^{\mathrm{T}}\mathbf{Q}\dot{\mathbf{z}} \\
&\quad - \frac{1}{2}k_z\dot{\mathbf{z}}^{\mathrm{T}}\mathbf{P}\mathbf{B}\left[\mathbf{M}\mathbf{E} - \mathrm{tr}(\mathbf{M}\mathbf{E})\mathbf{I}\right]\boldsymbol{\omega} \\
&= \boldsymbol{\omega}^{\mathrm{T}}\left(-k_p\boldsymbol{\Omega} - k_z\tilde{\mathbf{M}}^{\mathrm{T}}\boldsymbol{\zeta}\right) + \frac{1}{2}k_p\boldsymbol{\omega}^{\mathrm{T}}\sum_{j=1}^{N} k_j S\left(\mathbf{y}^j\right)\mathbf{y}_r^j - \frac{1}{2}k_z\dot{\mathbf{z}}^{\mathrm{T}}\mathbf{Q}\dot{\mathbf{z}} + k_z\dot{\mathbf{z}}^{\mathrm{T}}\mathbf{P}\mathbf{B}\tilde{\mathbf{M}}\boldsymbol{\omega} \\
&= \boldsymbol{\omega}^{\mathrm{T}}\left(-k_p\boldsymbol{\Omega} - k_z\tilde{\mathbf{M}}^{\mathrm{T}}\boldsymbol{\zeta}\right) + k_p\boldsymbol{\omega}^{\mathrm{T}}\boldsymbol{\Omega} - \frac{1}{2}k_z\dot{\mathbf{z}}^{\mathrm{T}}\mathbf{Q}\dot{\mathbf{z}} + k_z\boldsymbol{\omega}^{\mathrm{T}}\tilde{\mathbf{M}}^{\mathrm{T}}\boldsymbol{\zeta} \\
&= -\frac{1}{2}k_z\dot{\mathbf{z}}^{\mathrm{T}}\mathbf{Q}\dot{\mathbf{z}} \leq 0.
\end{aligned}$$

Thus, $\boldsymbol{\omega}$, $\dot{\mathbf{z}}$, $\mathbf{z}$, and $\boldsymbol{\Omega}$ are all uniformly bounded. It follows then from Eq. (5.27) that $\mathbf{u}$ is uniformly bounded. Since $V \geq 0$, and $\dot{V} \leq 0$, $\int_0^\infty \dot{V}(t)\,\mathrm{d}t$ exists and is finite which implies that $\dot{\mathbf{z}} \in \mathcal{L}_2$. From Eq. (4.26), we have $\ddot{\mathbf{z}} = \mathbf{A}_m\dot{\mathbf{z}} + \mathbf{B}\dot{\boldsymbol{\Omega}}$ which together with Eq. (4.9) and $\dot{\mathbf{z}}, \boldsymbol{\omega} \in \mathcal{L}_\infty$ implies $\ddot{\mathbf{z}} \in \mathcal{L}_\infty$. Using the corollary to Barbalat's lemma for $\dot{\mathbf{z}} \in \mathcal{L}_2 \cap \mathcal{L}_\infty$ and $\ddot{\mathbf{z}} \in \mathcal{L}_\infty$ yields $\lim_{t\to\infty}\dot{\mathbf{z}}(t) = \mathbf{0}$. By taking the third time derivative of the function $\mathbf{z}(t)$, one may show that $\dddot{\mathbf{z}} \in \mathcal{L}_\infty$ which implies that $\ddot{\mathbf{z}}$ is uniformly continuous. Using this result along with $\lim_{t\to\infty}\dot{\mathbf{z}}(t) = \dot{\mathbf{z}}(0) + \lim_{t\to\infty}\int_0^t \ddot{\mathbf{z}}(\tau)\,\mathrm{d}\tau = \mathbf{0}$ and applying Barbalat's lemma, leads to $\lim_{t\to\infty}\ddot{\mathbf{z}}(t) = \mathbf{0}$. Since $\ddot{\mathbf{z}} = \mathbf{A}_m\dot{\mathbf{z}} + \mathbf{B}\dot{\boldsymbol{\Omega}}$ and $\mathbf{B}$ is invertible, it follows that $\lim_{t\to\infty}\dot{\boldsymbol{\Omega}}(t) = \mathbf{0}$. As shown in Lemma 4.2.2, $\dot{\boldsymbol{\Omega}}(t) \to \mathbf{0}$ as $t \to \infty$ means that $\boldsymbol{\omega}(t) \to \mathbf{0}$ and/or $\mathrm{tr}(\mathbf{E}(t)) \to -1$ as $t \to \infty$. Recall from Lemma 4.2.2 that $\mathrm{tr}(\mathbf{E}) = -1$ implies that $\phi = \pm 180^\circ$, where ϕ is the rotation angle associated with $\mathbf{E}$, which specifically describes the scenario

$\mathbf{y}^j = -\mathbf{y}_r^j \ \forall \ j = 1, 2, ..., N$. However, this condition is prohibited by the initial condition constraint in Eq. (4.27), which can be seen by the fact that $V(t) \leq V(0) < k_p \sum_{j=1}^{N} k_j \ \forall \ t \geq 0$ which means $E(t) < \sum_{j=1}^{N} k_j \ \forall \ t \geq 0$, and therefore $\mathbf{y}^j \neq -\mathbf{y}_r^j \ \forall \ j = 1, 2, ..., N$, for all $t \geq 0$. Consequently, $\dot{\boldsymbol{\Omega}}(t) \to \mathbf{0}$ as $t \to \infty$ implies that $\lim_{t\to\infty} \boldsymbol{\omega}(t) = \mathbf{0}$. Next, by differentiating Eq. (2.2), one may easily show $\ddot{\boldsymbol{\omega}} \in \mathcal{L}_\infty$ which implies that $\dot{\boldsymbol{\omega}}$ is uniformly continuous and by once again applying Barbalat's lemma, we have $\dot{\boldsymbol{\omega}}(t) \to \mathbf{0}$ as $t \to \infty$. Finally, the last two results can be used in Eq. (2.2) along with Eq. (5.27) to demonstrate that $\boldsymbol{\Omega}(t) \to \mathbf{0}$ as $t \to \infty$. As shown in Lemma 4.2.1, $\boldsymbol{\Omega} = \mathbf{0}$ implies that $\mathbf{E} = \mathbf{I}$ or $\text{tr}(\mathbf{E}) = -1$. As discussed previously in this proof, the condition $\text{tr}(\mathbf{E}) = -1$ is precluded by the initial condition constraint in Eq. (4.27).

Thus, one may conclude that

$$[\mathbf{E}(t), \boldsymbol{\omega}(t)] \to [\mathbf{I}, \mathbf{0}] \quad \text{as} \quad t \to \infty$$

which completes the proof. □

Remark 4.2.1. The initial condition constraint in Eq. (4.27) is a mild requirement as will be shown next. It is always possible to choose the initial condition $\mathbf{z}(0) = -\mathbf{A}_m^{-1}\mathbf{B}\boldsymbol{\Omega}$ such that $\dot{\mathbf{z}}(0) = \mathbf{0}$. In this case, Eq. (4.27) simplifies to a less restrictive condition

$$\frac{1}{2}\boldsymbol{\omega}(0)^{\mathrm{T}}\mathbf{J}\boldsymbol{\omega}(0) + \frac{1}{2}k_p \sum_{j=1}^{N} k_j \left(1 - \mathbf{y}(0)^{j^{\mathrm{T}}}\mathbf{y}_r(0)^j\right) < k_p \sum_{j}^{N} k_j,$$

from which the following upper bound on $\boldsymbol{\omega}(0)$ can be obtained

$$\|\boldsymbol{\omega}(0)\|^2 < \frac{k_p}{2j_{\max}} \sum_{j=1}^{N} k_j \left(1 + \mathbf{y}(0)^{j^{\mathrm{T}}} \mathbf{y}_r(0)^j\right) \tag{4.29}$$

where $j_{\max}$ is the maximum eigenvalue of $\mathbf{J}$. If the control gain k_p is sufficiently large, we may easily accommodate the lack or unreliability of $\boldsymbol{\omega}(0)$ measurement by scaling up the right hand side of the strict inequality in Eq. (4.29).

Remark 4.2.2. Although an upper bound on the maximum eigenvalue of the inertia matrix is needed to satisfy Eq. (4.29), the controller does not require full knowledge of the inertia matrix. Therefore, the control scheme possesses the so-called *self-reduction property*; that is, for the regulation problem, the control law is independent of the inertia parameters of the spacecraft.

Remark 4.2.3. Since the attitude control law Eq. (5.27) is configured directly using vector measurements, the closed-loop system does not suffer from the so-called "unwinding" phenomenon [10] typically observed with quaternions, where even when the body starts arbitrarily close to the desired orientation, rotation through large angles may be executed before coming to rest to the desired attitude.

Remark 4.2.4. Two critical obstacles have been identified within the current framework that prevent the extension of the control law Eq. (5.27) to the general tracking problem. Observe that since the mapping $\boldsymbol{\omega}_r^B = \mathbf{C}_{\mathrm{b}} \mathbf{C}_{\mathrm{r}}{}^{\mathrm{T}} \boldsymbol{\omega}_r$ is not available, the rigid body dynamics for the general tracking problem will be expressed in terms of the algebraic angular velocity tracking error signal

$\boldsymbol{\omega}_e := \boldsymbol{\omega} - \boldsymbol{\omega}_r$. Furthermore, for stability analysis, the Lyapunov function candidate would be expressed as

$$V = \frac{1}{2}\boldsymbol{\omega}_e^{\mathrm{T}}\mathbf{J}\boldsymbol{\omega}_e + \frac{1}{2}k_p\sum_j^N k_j\left(1 - \mathbf{y}^{j^{\mathrm{T}}}\mathbf{y}_r^j\right) + k_z\dot{\mathbf{z}}^{\mathrm{T}}\mathbf{P}\dot{\mathbf{z}}. \tag{4.30}$$

which has the derivative

$$\dot{V} = \boldsymbol{\omega}_e^{\mathrm{T}}\left(-S\left(\boldsymbol{\omega}\right)\mathbf{J}\boldsymbol{\omega} + \mathbf{u} - \dot{\boldsymbol{\omega}}_r\right) + k_p\boldsymbol{\omega}_e^{\mathrm{T}}\boldsymbol{\Omega} - k_z\dot{\mathbf{z}}^{\mathrm{T}}\mathbf{Q}\dot{\mathbf{z}} + k_z\dot{\mathbf{z}}^{\mathrm{T}}\mathbf{P}\mathbf{B}\dot{\boldsymbol{\Omega}}. \tag{4.31}$$

The first obstacle comes from the derivative of $\boldsymbol{\Omega}$ for a time-varying reference angular velocity, $\boldsymbol{\omega}_r$, given by $\dot{\boldsymbol{\Omega}} = \tilde{\mathbf{M}}\boldsymbol{\omega} - \tilde{\mathbf{M}}^{\mathrm{T}}\boldsymbol{\omega}_r$. In its current form, $\dot{\boldsymbol{\Omega}}$ is not a function in the error signal $\boldsymbol{\omega}_e$. Using the equation above, that last term of $\dot{V}$ can be written as

$$k_z\dot{\mathbf{z}}^{\mathrm{T}}\mathbf{P}\mathbf{B}\dot{\boldsymbol{\Omega}} = k_z\dot{\mathbf{z}}^{\mathrm{T}}\mathbf{P}\mathbf{B}\left[\tilde{\mathbf{M}}\boldsymbol{\omega} - \tilde{\mathbf{M}}^{\mathrm{T}}\boldsymbol{\omega}_r\right].$$

Clearly, this term could not be cancelled by $\mathbf{u}$. Instead, an additional input signal must be introduced in the linear system Eq. (4.26) so as to be able to neatly cancel the term in the Lyapunov analysis. One possible way to do this would be to introduce a new dynamic auxiliary signal $\boldsymbol{\Gamma}$:

$$\dot{\boldsymbol{\Gamma}} = \tilde{\mathbf{M}}^{\mathrm{T}}\boldsymbol{\omega}_r - \tilde{\mathbf{M}}\boldsymbol{\omega}_r, \tag{4.32}$$

with any initial condition $\boldsymbol{\Gamma}(0)$ and to redefine $\dot{\mathbf{z}}$ as

$$\dot{\mathbf{z}} = \mathbf{A}_m\mathbf{z} + \mathbf{B}\left(\boldsymbol{\Omega} + \boldsymbol{\Gamma}\right). \tag{4.33}$$

Observing that $\dot{\boldsymbol{\Omega}} + \dot{\boldsymbol{\Gamma}} = \tilde{\mathbf{M}}\boldsymbol{\omega}_e$, and letting $\mathbf{u} = -k_p\boldsymbol{\Omega} + \dot{\boldsymbol{\omega}}_r - \tilde{\mathbf{M}}^{\mathrm{T}}\mathbf{y} + S(\boldsymbol{\omega}_r)\mathbf{J}\boldsymbol{\omega}_r$

and doing a few tedious but straightforward algebraic manipulations $\dot{V}$ now becomes

$$\begin{aligned}\dot{V} &= \boldsymbol{\omega}_e^{\mathrm{T}} \left(-S\left(\boldsymbol{\omega}\right)\mathbf{J}\boldsymbol{\omega} + \mathbf{u} - \dot{\boldsymbol{\omega}}_r\right) + k_p \boldsymbol{\omega}_e^{\mathrm{T}} \boldsymbol{\Omega} - k_z \dot{\mathbf{z}}^{\mathrm{T}} \mathbf{Q} \dot{\mathbf{z}} + k_z \dot{\mathbf{z}}^{\mathrm{T}} \mathbf{P} \mathbf{B} \left(\dot{\boldsymbol{\Omega}} + \dot{\boldsymbol{\Gamma}}\right) \\ &= -\boldsymbol{\omega}_e^{\mathrm{T}} \left(S\left(\boldsymbol{\omega}_r\right)\mathbf{J}\boldsymbol{\omega}_e\right) - k_z \dot{\mathbf{z}}^{\mathrm{T}} \mathbf{Q} \dot{\mathbf{z}}.\end{aligned}$$

The second obstacle and the true bottleneck to extending the proposed control law to the general tracking case comes from the following term in $\dot{V}$:

$$-\boldsymbol{\omega}_e^{\mathrm{T}} \left(S\left(\boldsymbol{\omega}_r\right)\mathbf{J}\boldsymbol{\omega}_e\right) \tag{4.34}$$

which could not be canceled in any way through the control torque input $\mathbf{u}$ since $\boldsymbol{\omega}_e$ (or rather $\boldsymbol{\omega}$) is not an available quantity for feedback. Therefore, it is not possible to obtain a negative semi-definite $\dot{V}$.

Of the two obstacles outlined above, the former may be overcome through the solution provided above or one similar to it. However, the true hinderance comes from the cross term $-\boldsymbol{\omega}_e^{\mathrm{T}} \left(S\left(\boldsymbol{\omega}_r\right)\mathbf{J}\boldsymbol{\omega}_e\right)$ that appears in the derivative of the Lyapunov function candidate, and cannot be canceled in order to obtain a negative semi-definite $\dot{V}$ in the current framework. A solution to overcome this limitation may be found through a clever manipulation or augmentation of the Lyapunov function construction provided here. Note that the approach by [62] also suffers from similar obstacles which prevent the extension of their stabilization control law to the general attitude tracking case.

4.3 Numerical Simulations

Two sets of numerical simulation studies are presented to validate the theoretical development of the novel unit vector measurement-only control law presented in this chapter. First, a set point regulation scenario is tested assuming perfect measurements without noise. Next, noise is introduced into the given unit vector measurements and numerical simulations are carried out for the same attitude regulation scenario. For comparison, the performance of the proposed gyro-free controller is contrasted with a full-state feedback proportional-derivative type control law given by [19]

$$\mathbf{u}_f = -k_p \boldsymbol{\Omega} - k_\omega \boldsymbol{\omega}.$$

The spacecraft inertia matrix is selected as $\mathbf{J} = \text{diag}\{0.29,\ 0.29,\ 0.5\}\ \text{kg} \cdot \text{m}^2$. The initial angular velocity of the rigid body is set to

$$\boldsymbol{\omega}(0) = [-0.02,\ -0.02,\ -0.02]^{\text{T}}\ \text{rad/s},$$

while the initial and desired orientations are given respectively as follows

$$\mathbf{C}_{\text{b}}(0) = \begin{bmatrix} 0 & 1 & 0 \\ 0 & 0 & 1 \\ 1 & 0 & 0 \end{bmatrix}, \quad \mathbf{C}_{\text{r}} = \begin{bmatrix} 0.3601 & 0.8968 & -0.2569 \\ -0.2569 & 0.3601 & 0.8968 \\ 0.8968 & -0.2569 & 0.3601 \end{bmatrix}.$$

The desired orientation, $\mathbf{C}_{\text{r}}$, corresponds with a rotation of 87.7° about the eigenaxis $\mathbf{e} = [1/\sqrt{3},\ 1/\sqrt{3},\ 1/\sqrt{3}]^{\text{T}}$. For both controllers, we assume that

three vector measurements are available

$$\mathbf{x}_1 = [0,\ 0,\ 1]^{\mathrm{T}}; \quad \mathbf{x}_2 = [1,\ 0,\ 0]^{\mathrm{T}}; \quad \mathbf{x}_2 = \left[1/\sqrt{2},\ 1/\sqrt{2},\ 0\right]^{\mathrm{T}},$$

with weights $k_1 = k_2 = k_3 = 1$. After some trial and error, through numerical simulations, we select $\mathbf{A} = \mathrm{diag}\{-3,\ -10,\ -5\}$, $\mathbf{B} = \mathbf{I}$, and $\mathbf{Q} = 10.5\mathbf{I}$, from which we can solve for $\mathbf{P}$ to obtain $\mathbf{P} = \mathrm{diag}\{1.75,\ 0.525,\ 1.05\}$. The control gains are selected as $k_p = 0.03$, $k_z = 0.6$, and $k_\omega = 0.06$, while the initial condition $\mathbf{z}(0)$ is taken to be $\mathbf{z}(0) = -\mathbf{A}_m^{-1}\mathbf{r}(0)$ such that $\dot{\mathbf{z}}(0) = 0$. The convergence of the orientation error quantity $\mathbf{E} = \mathbf{C}_{\mathrm{b}}\mathbf{C}_{\mathrm{r}}{}^{\mathrm{T}}$ is illustrated by plotting the time evolution of the rotation angle, ϕ, associated with $\mathbf{E}$, which is obtained through the relation [58]

$$\cos(\phi) = 0.5\,(\mathrm{tr}(\mathbf{E}) - 1)\,.$$

Recall that when $\mathbf{E} = \mathbf{I}$, the rotation angle takes on the value $\phi = 0$.

4.3.1 Vector Measurement Only Feedback Control with Perfect Measurements

The first set of simulations is conducted assuming that there is no noise in the observed vector measurements. The plots in Figs. 4.1-4.2 show the closed-loop system performance for the chosen tuning parameters. As shown in Fig. 4.2a, for both controllers, the maximum control torque commanded during the maneuver is less than 1.5×10^{-2} N-m, which is highly realistic for a low-thrust spacecraft implementation.

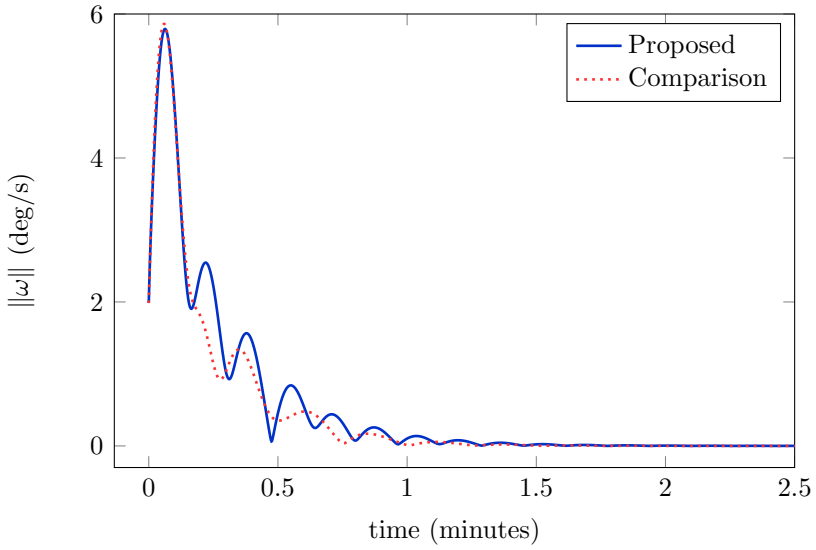

(a) Norm of angular velocity

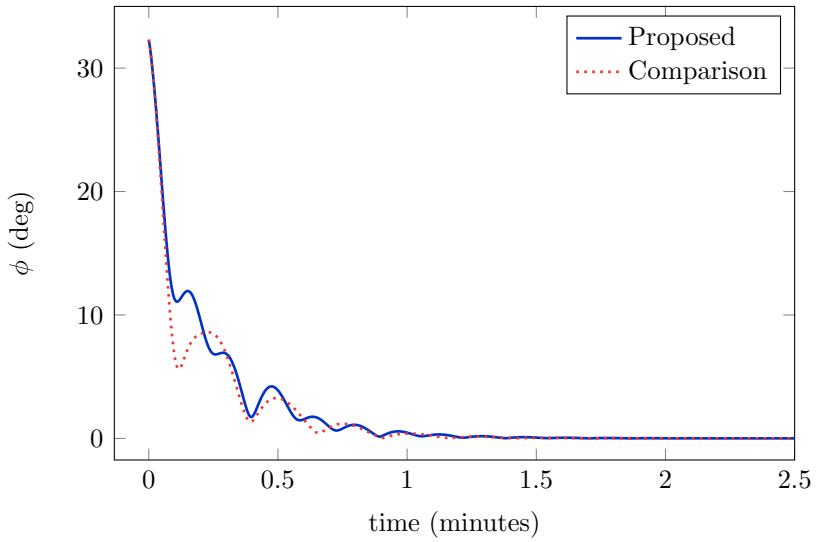

(b) Principal rotation angle

Figure 4.1: Comparison of the novel gyro-free controller with a full state feedback controller without measurement noise.

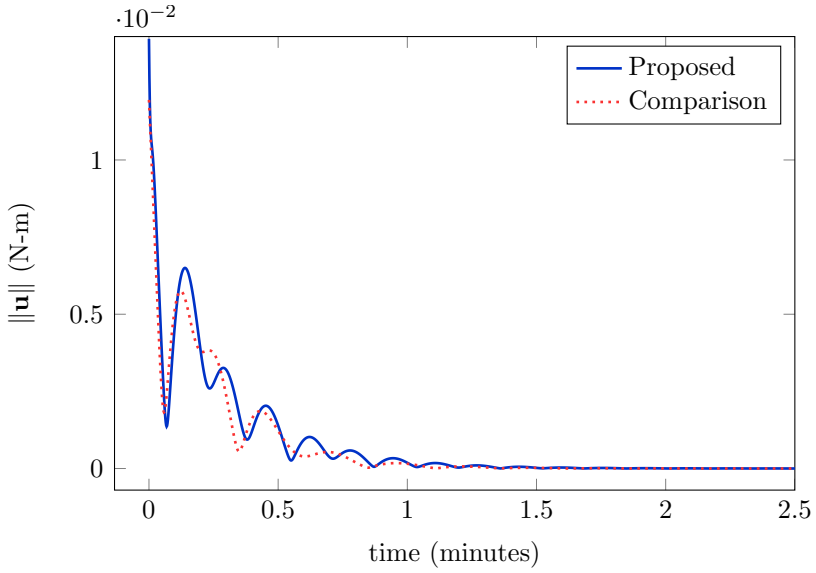

(a) Norm of commanded control

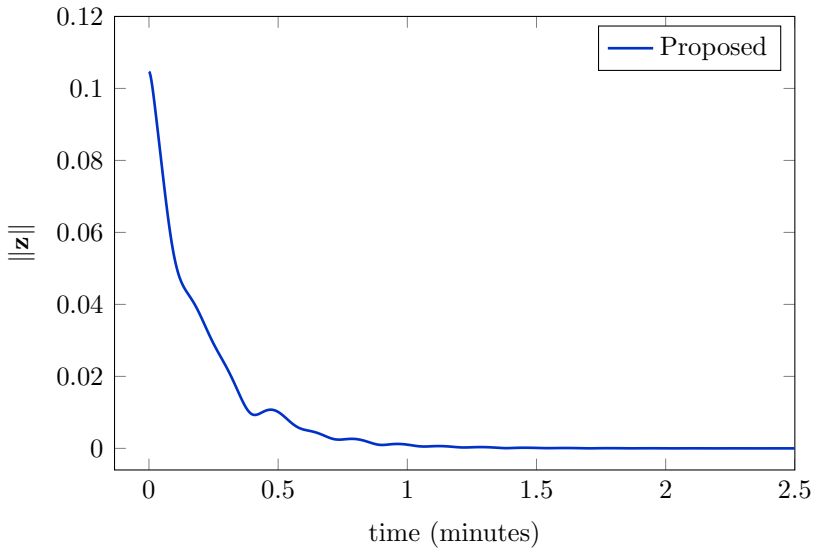

(b) Norm of linear auxiliary signal, $\mathbf{z}$

Figure 4.2: Commanded control effort and time evolution of the auxiliary state $\mathbf{z}(t)$ when no measurement noise is present.

For both controller schemes, the angular velocity and orientation errors

are observed to be driven to the origin within two minutes of the attitude control maneuver. The proposed gyro-free control law commands a slightly higher initial torque norm by approximately 0.002 N-m, but overall both the gyro-free and full-state feedback controllers have comparable torque requirements. The results verify that the proposed velocity-free attitude control law asymptotically stabilizes the spacecraft to its desired orientation using only vector measurements. Moreover, the novel control law performs with a large degree of comparability to a full-state feedback control law, and does so without the need for an attitude vector or angular velocity feedback.

4.3.2 Vector Measurement Only Feedback Control with Noisy Measurements

The next set of simulations is carried out with noise added to the unit vector measurements available for control feedback. The measurement noise is parameterized as a normal distribution contained in a cone of prescribed half-cone angle about $\mathbf{y}^j$. All of the gain values and initial conditions remain the same. A half-cone angle of 0.05 deg is selected, and the resulting performance of the closed-loop system is illustrated in Figs. 4.3-4.4 over a longer simulation period. The angular velocity norm and the absolute value of the rotation angle are plotted on a semilogarithmic scale to highlight the differences in the steady-state behaviors of the two control systems.

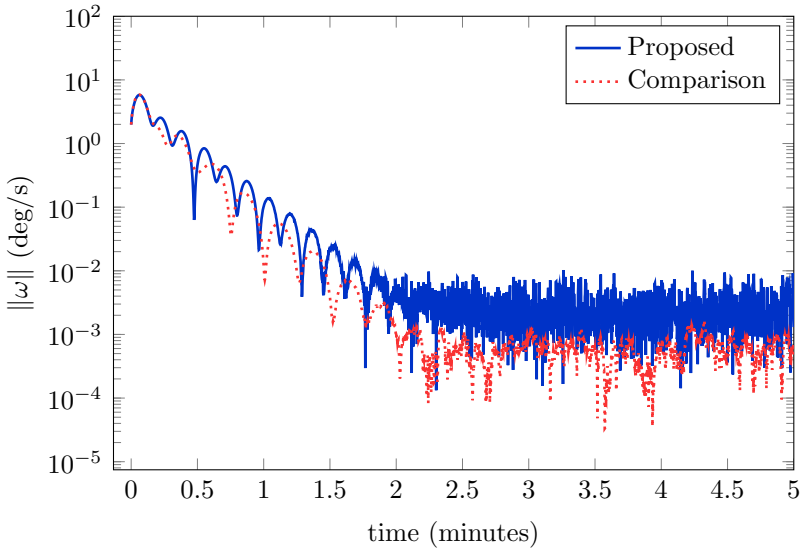

(a) Norm of angular velocity

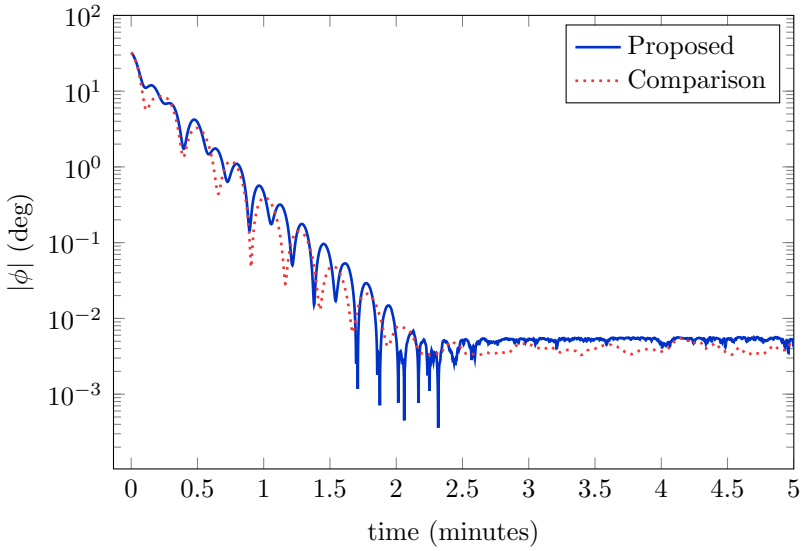

(b) Principal rotation angle

Figure 4.3: Comparison of the novel gyro-free controller with a full state feedback controller in the presence of measurement noise.

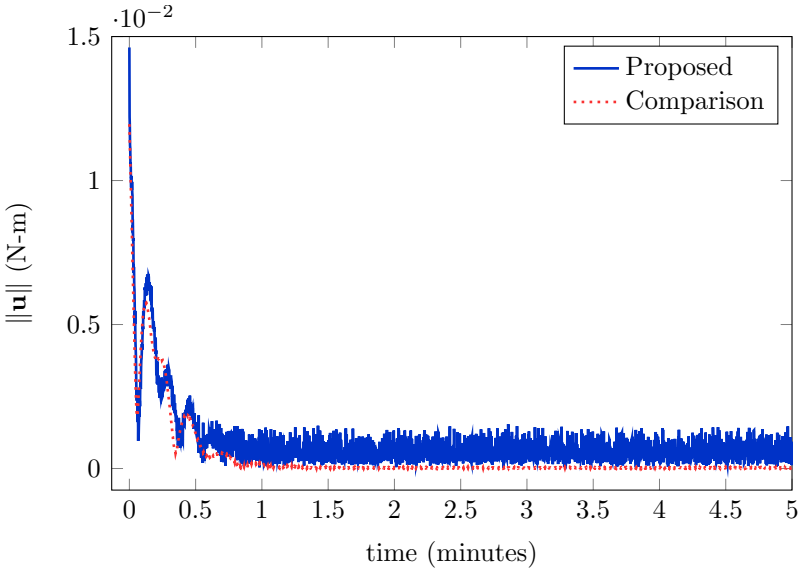

(a) Norm of commanded control

Figure 4.4: Control magnitude for closed-loop system when measurements are noisy.

While the transient behavior of the system states is relatively unaffected by the added measurement noise, the angular velocity and attitude norm clearly converge to a nonzero steady-state value for the both the proposed and comparison methods as shown in Figs. 4.3a-4.3b. Thus, empirical evidence suggests that the addition of measurement of noise to the proposed method causes the attitude and angular velocity states to converge to a residual set which may grow or shrink depending on the size of cone used for noise parameterization. Further, it is clear that noise in the unit vector measurement does not affect the performance of the proposed method any worse than a full-state feedback controller.

The plots in Figs. 4.3-4.4 illustrate the evolution of the system states

for a single initial condition. In order to further corroborate the boundedness characteristics of the closed-loop signals subject to noise in the unit vector measurements, simulations are conducted with 10 random initial conditions using the proposed control law with the same noise characteristics discussed earlier, and all other simulation parameters remaining the same. The results are shown in Figs. 4.5-4.6. As expected, the angular velocity and attitude norms for each of the ten simulations with random initial conditions remain bounded within a residual set. Finally, observe that the proposed control method is immune to measurement noise in the angular velocity vector since it does not use angular velocity for feedback, making it a useful strategy in the event that gyro-rate measurements are too noisy for reliable feedback.

4.4 Conclusion

In this chapter, a novel attitude-stabilization controller is presented that utilizes vector measurements obtained from inertial sensors directly for feedback, without relying on the estimated attitude vector or angular velocity feedback. The control law is formulated in the classical passive systems framework, and does not rely on observers of any kind. Although many classical results for angular velocity-free control laws are available in existing literature, they are typically formulated using some kind of attitude parameterization. As such, these control laws must be integrated with an attitude estimation scheme that can provide the attitude of the vehicle using a combination of gyro-rate and vector measurements. Thus, regardless of the approach, most existing control

laws have either an explicit or implicit requirement for angular velocity measurements. The attitude control law proposed in this chapter truly eliminates the need for either direct or indirect angular velocity information as it solely and directly employs vector measurements for control feedback. The proposed controller requires a minimum of two non-collinear vector measurements to satisfy the attitude stabilization objective. Under this setting, rigorous analysis proves that the spacecraft converges to the desired attitude and zero angular velocity as long as some mild constraints on the initial conditions are satisfied. A simulation study conducted in the presence of measurement error shows that our control law drives the states to a bounded residual set in this case. Some technical limitations that prevent the extension of this control law to the full tracking case have been discussed in the chapter. The work presented here presents an important step towards dealing with a very realistic scenario for spacecraft missions in which failed or unreliable gyroscopes prevent traditional control methods from being implemented for onboard attitude stabilization. A natural future direction for this research would be to further explore the full tracking case through a different Lyapunov function construction or a modified control law.

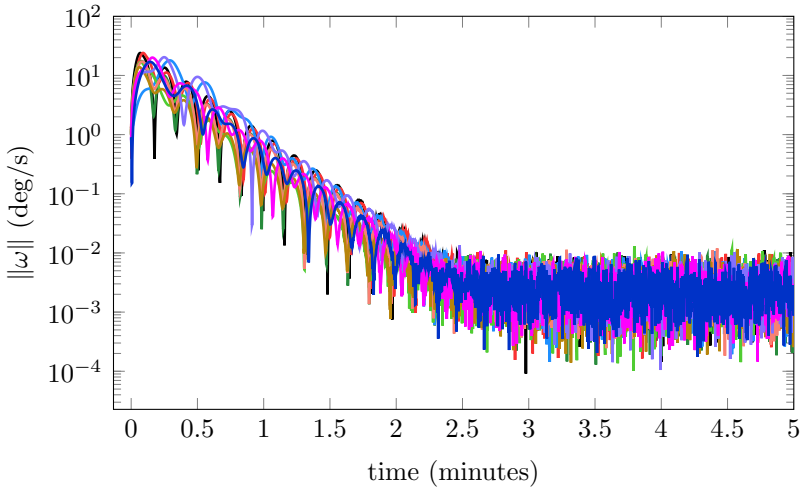

(a) Norm of angular velocity

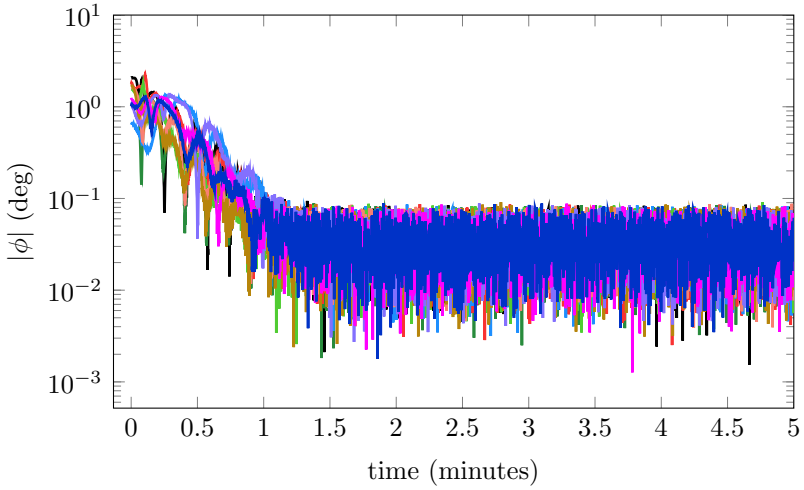

(b) Principal rotation angle

Figure 4.5: Attitude and angular velocity stabilization simulation for proposed controller using 10 random initial conditions subject to measurement noise.

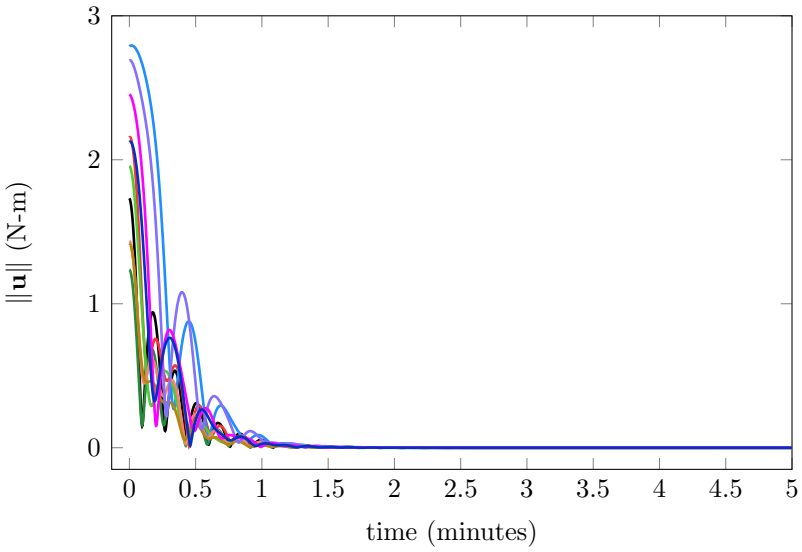

(a) Norm of commanded control

Figure 4.6: Control history for proposed controller simulation using 10 random initial conditions and noisy measurements.

Chapter 5

Partial Lyapunov Strictification: Smooth Angular Velocity Observers for Attitude Tracking Control

This chapter considers the classical problem of angular velocity observer design for attitude tracking control when angular velocity is unavailable. The attitude is parameterized in terms of a quaternion and is available through measurements. While several angular velocity observers are available in literature, the existence of a separation-type property for the combined stable implementation of a separately designed observer with an attitude tracking controller was, until recently, unproven. The result by Chunodkar and Akella

[15] established for the first time a separation property for a switching observer when combined with a PD attitude tracking control law. While this result presents an important advancement in this area, the switching-based observer construction has its drawbacks, primarily due to the fact that the underlying physical system could experience undesirable chattering behavior. Thus, when consistent performance and robustness are of concern, the design of a smooth angular velocity observer that ensures $\mathcal{C}^\infty$ continuity of estimated states is highly desirable and is the subject of this chapter.

A novel angular velocity observer is proposed here for global asymptotic convergence of angular velocity state estimation errors through a switching-free structure that ensures $\mathcal{C}^\infty$ continuity of estimated states. We prove global asymptotic convergence of estimation errors irrespective of the prescribed control torque and initial state of the spacecraft. The fundamental contribution of the proposed observer formulation is that, unlike Reference [15], the design here has a smooth construction. Furthermore, the observer satisfies an important "separation" property when combined with an independently designed PD attitude tracking control law. More specifically, a PD attitude tracking control law using angular velocity estimates generated from the proposed observer for feedback in place of actual angular velocity measurements leads to (almost) global asymptotic stability for the overall closed-loop tracking error dynamics. To the best knowledge of the author, this is the first time a "separation" property has been established for the rigid-body dynamics through the use of a *smooth* angular velocity observer.

The separation-property result is realized through the use of a partial Lyapunov "strictification" [34, 38, 39] strategy, a process by which a non-strict Lyapunov function is transformed into a strict Lyapunov function whose derivative contains additional non-positive terms in the system states. Within the context of the smooth observer, the introduction of additional non-positive terms of the estimation error states in the Lyapunov function derivative helps dominate undesirable mixed/cross terms arising due to the observer implementation, and is critical for establishing the "separation" property result. Moreover, the strictification process directly relies on our novel use of a spiral logic procedure, wherein certain intermediate signal boundedness results must be established prior to proving overall closed-loop system stability. In particular, first, we prove boundedness of spacecraft angular velocity when the PD control law employs estimates generated from the proposed observer for feedback. Subsequently, we use this result to carry out Lyapunov strictification to obtain a *partially* strict Lyapunov function for the observer through the judicious introduction of a mixed term in the estimation error states. We use the word partial to emphasize that only non-positive terms in the angular velocity estimation error state and the *vector* component of the quaternion estimation error state are contained in the "strictified" Lyapunov function derivative. Finally, by using a composite Lyapunov function consisting of the controller Lyapunov function and the new partially strict observer Lyapunov function, the combined observer-controller scheme is shown to result in asymptotic convergence of all estimation and tracking-error states, and accordingly

the "separation" property.

The chapter is organized as follows. In Sec. 5.1, a brief review of a standard full-state proportional-derivative controller for attitude tracking is provided. In Sec. 5.2, the main contributions of this research are presented. The estimation framework is developed and thorough details are provided regarding the construction of the novel smooth angular velocity observer along with a rigorous convergence analysis. In Sec. 5.3, a separation property is formally stated and proved for a PD control employing angular velocity estimates generated from the novel observer. Numerical simulation studies are conducted in Sec. 5.4 in order to illustrate the observer-based controller performance as well as to highlight certain features of the observer. Finally, concluding remarks are made in Sec. 5.5.

5.1 Preliminaries

This section provides important mathematical background that will be useful in the upcoming developments. The rigid body dynamics are restated for the reader's convenience and a brief overview is provided of a proportional-derivative attitude tracking control law using both angular velocity and quaternion for feedback.

5.1.1 Rigid Body Dynamics

The attitude tracking error dynamics Eqs. (2.12)-(2.13) are restated below for the reader's convenience:

$$\dot{\mathbf{q}}_e = \frac{1}{2}\mathbf{E}(\mathbf{q}_e)\boldsymbol{\omega}_e \tag{2.12}$$

$$\mathbf{J}\dot{\boldsymbol{\omega}}_e = -S(\boldsymbol{\omega})\mathbf{J}\boldsymbol{\omega} + \mathbf{u} + \mathbf{J}\left[S(\boldsymbol{\omega}_e)\boldsymbol{\omega}_r^B - C(\mathbf{q}_e)\dot{\boldsymbol{\omega}}_r\right]. \tag{2.13}$$

5.1.2 Full-State PD Attitude Control

A brief overview of a proportional derivative (PD) attitude tracking control law is provided here, which is based on feedback of true attitude and angular velocity values [77]. Let the desired angular velocity $\boldsymbol{\omega}_r^B = \mathbf{C}(\mathbf{q}_e)\boldsymbol{\omega}_r$ be bounded and at least twice differentiable with bounded derivatives. The full-state PD controller is summarized below in Proposition 5.1.1.

Proposition 5.1.1. *Let the control law* $\mathbf{u}(t)$ *be prescribed according to*

$$\mathbf{u} = -k_p\mathbf{q}_{e_v} - k_v\boldsymbol{\omega}_e + \mathbf{J}\mathbf{C}(\mathbf{q}_e)\dot{\boldsymbol{\omega}}_r + S(\boldsymbol{\omega}_r^B)\mathbf{J}\boldsymbol{\omega}_r^B \tag{5.1}$$

for any $k_p, k_v > 0$. *Then the system described by Eqs.* (2.12)-(2.13) *is (almost) globally asymptotically stabilized to the origin.*

Proof. Consider the following positive-definite Lyapunov function candidate

$$V_c = k_p\left[(1-q_{e_0})^2 + \mathbf{q}_{e_v}^T\mathbf{q}_{e_v}\right] + \frac{1}{2}\boldsymbol{\omega}_e^{\mathrm{T}}\mathbf{J}\boldsymbol{\omega}_e. \tag{5.2}$$

Differentiating V_c with respect to time along with Eqs. (2.12),(2.13), and (5.1)

yields

$$\begin{aligned}\dot{V}_c &= k_p \mathbf{q}_{e_v}^{\mathrm{T}} \boldsymbol{\omega}_e + \boldsymbol{\omega}_e^{\mathrm{T}} \left(-S(\boldsymbol{\omega}) \mathbf{J} \boldsymbol{\omega} + \mathbf{u} + \mathbf{J} \left[S(\boldsymbol{\omega}_e) \boldsymbol{\omega}_r^B - C(\mathbf{q}_e) \dot{\boldsymbol{\omega}}_r \right] \right) \\ &= \boldsymbol{\omega}_e^{\mathrm{T}} \left(-S(\boldsymbol{\omega}) \mathbf{J} \boldsymbol{\omega} - k_v \boldsymbol{\omega}_e + S(\boldsymbol{\omega}_r^B) \mathbf{J} \boldsymbol{\omega}_r^B + \mathbf{J} S(\boldsymbol{\omega}_e) \boldsymbol{\omega}_r^B \right) \\ &= -k_v \|\boldsymbol{\omega}_e\|^2, \end{aligned} \tag{5.3}$$

where we have used the identity

$$\boldsymbol{\omega}_e^{\mathrm{T}} \left(-S(\boldsymbol{\omega}) \mathbf{J} \boldsymbol{\omega} + S(\boldsymbol{\omega}_r^B) \mathbf{J} \boldsymbol{\omega}_r^B + \mathbf{J} S(\boldsymbol{\omega}_e) \boldsymbol{\omega}_r^B \right) = 0 \tag{5.4}$$

which can be shown through tedious but straightforward algebra. Since $\dot{V}_c \leq 0$, it follows that $\boldsymbol{\omega}_e, \dot{\boldsymbol{\omega}}_e \in \mathcal{L}_\infty$. Recall that $\mathbf{q}_v$ is always bounded due to the unit norm constraint on the unit quaternion. Further, since V_c is lower bounded, $\int_0^\infty \dot{V}_c(t)\, \mathrm{d}t$ exists and is finite which together with Eq. (5.3) implies $\boldsymbol{\omega}_e \in \mathcal{L}_2 \cap \mathcal{L}_\infty$. Invoking Barbalat's lemma for $\boldsymbol{\omega}_e \in \mathcal{L}_2 \cap \mathcal{L}_\infty$ and $\dot{\boldsymbol{\omega}}_e \in \mathcal{L}_\infty$ leads to

$$\lim_{t \to \infty} \boldsymbol{\omega}_e(t) = 0.$$

Using the fact that $\boldsymbol{\omega}_r^B$ is bounded and twice differentiable, it follows that $\ddot{\boldsymbol{\omega}}_e \in \mathcal{L}_\infty$. Applying Barbalat's lemma for a second time ensures that $\dot{\boldsymbol{\omega}}_e(t) \to 0$ as $t \to \infty$. Finally, it follows from Eqs. (2.13) and (5.1) that

$$\lim_{t \to \infty} \mathbf{q}_{e_v}(t) = 0,$$

which completes the proof. □

5.2 Angular Velocity Observer Development

The development of the smooth observer proceeds with the derivation of the estimation error quantities, followed by the construction details of the observer dynamics and associated convergence analysis.

5.2.1 Estimation Framework

A detailed development of the estimation framework is provided here. The estimates for the angular velocity are generated in a separate frame defined as $\mathcal{E}$. Let $\hat{\mathbf{q}} = [\hat{q}_0, \hat{\mathbf{q}}_v^{\mathrm{T}}]^{\mathrm{T}}$ and $\hat{\boldsymbol{\omega}}$ define the estimates of $\mathbf{q}$ and $\boldsymbol{\omega}$, respectively. Denote $\hat{\boldsymbol{e}}$ as the unit-vector triad in the reference frame $\mathcal{E}$ and define the following rotation matrices:

$$\begin{aligned} \mathcal{N} \overset{\hat{\mathbf{q}}}{\rightarrow} \mathcal{E} \Rightarrow \{\hat{\boldsymbol{e}}\} &= \mathbf{C}(\hat{\mathbf{q}})\{\hat{\boldsymbol{n}}\}, \\ \mathcal{E} \overset{\tilde{\mathbf{q}}}{\rightarrow} \mathcal{B} \Rightarrow \{\hat{\boldsymbol{b}}\} &= \mathbf{C}(\tilde{\mathbf{q}})\{\hat{\boldsymbol{e}}\}. \end{aligned}$$

Since the direction cosine matrix $\mathbf{C}(\hat{\mathbf{q}})$ gives the rotation sequence from the inertial frame $\mathcal{N}$ to the estimation frame $\mathcal{E}$, the combined rotation from $\mathcal{E}$ to $\mathcal{B}$ is given by

$$\mathbf{C}(\tilde{\mathbf{q}}) = \mathbf{C}(\mathbf{q})\mathbf{C}^{\mathrm{T}}(\hat{\mathbf{q}}). \tag{5.5}$$

which gives rise to the definition of the quaternion attitude estimation error $\tilde{\mathbf{q}} = [\tilde{q}_0, \tilde{\mathbf{q}}_v^{\mathrm{T}}]^{\mathrm{T}}$. Using the composite rotation property of Euler-parameters we

can write [53, 58]

$$\mathbf{q} = \tilde{\mathbf{q}} \otimes \hat{\mathbf{q}} \tag{5.6}$$

which can be expressed using the rules of quaternion multiplication as [58]

$$\mathbf{q} = \begin{bmatrix} \hat{q}_0 & -\hat{\mathbf{q}}_v^{\mathrm{T}} \\ \hat{\mathbf{q}}_v & S(\hat{\mathbf{q}}_v) + \hat{q}_0 \mathbf{I}_{3\times 3} \end{bmatrix} \tilde{\mathbf{q}}. \tag{5.7}$$

Recalling that the matrix in Eq. (5.7) is orthogonal [58], the following explicit expression for $\tilde{\mathbf{q}}$ can be obtained

$$\tilde{\mathbf{q}} = \begin{bmatrix} \hat{q}_0 q_0 + \hat{\mathbf{q}}_v^{\mathrm{T}} \mathbf{q}_v \\ -q_0 \hat{\mathbf{q}}_v - S(\hat{\mathbf{q}}_v)\mathbf{q}_v + \hat{q}_0 \mathbf{q}_v \end{bmatrix}. \tag{5.8}$$

Finally, the angular velocity estimation error, $\tilde{\boldsymbol{\omega}}$, is defined as

$$\tilde{\boldsymbol{\omega}} = \boldsymbol{\omega} - \mathbf{C}(\tilde{\mathbf{q}})\hat{\boldsymbol{\omega}} \tag{5.9}$$

$$= \boldsymbol{\omega} - \hat{\boldsymbol{\omega}}^{\mathrm{B}}, \tag{5.10}$$

where $\hat{\boldsymbol{\omega}}^{\mathrm{B}} \equiv \mathbf{C}(\tilde{\mathbf{q}})\hat{\boldsymbol{\omega}}$ is defined for ease of notation.

5.2.2 Smooth Observer

The following theorem summarizes a primary contribution of this chapter: a smooth angular velocity observer that ensures convergence of estimation errors irrespective of the control input.

Theorem 5.2.1. *Consider a smooth angular velocity observer that evolves*

according to the following dynamics:

$$\dot{\hat{\mathbf{q}}} = \frac{1}{2}E(\hat{\mathbf{q}})\Big(\hat{\boldsymbol{\omega}} + \lambda \mathbf{C}^{\mathrm{T}}(\tilde{\mathbf{q}})\tilde{\mathbf{q}}_v\Big) \tag{5.11}$$

$$\dot{\hat{\boldsymbol{\omega}}} = \mathbf{C}^{\mathrm{T}}(\tilde{\mathbf{q}})\mathbf{J}^{-1}\Bigg[\gamma\tilde{\mathbf{q}}_v - S(\hat{\boldsymbol{\omega}}^{\mathrm{B}})\mathbf{J}\hat{\boldsymbol{\omega}}^{\mathrm{B}} + \mathbf{u} - \lambda\mathbf{J}S(\tilde{\mathbf{q}}_v)\hat{\boldsymbol{\omega}}^{\mathrm{B}}\Bigg], \tag{5.12}$$

with any $\lambda, \gamma > 0$. *Then the estimation errors* $\tilde{\mathbf{q}}$, $\tilde{\boldsymbol{\omega}}$ *asymptotically converge to the origin, that is,*

$$\lim_{t\to\infty}\left[\tilde{\mathbf{q}}_v(t), \tilde{\boldsymbol{\omega}}(t)\right] = 0$$

for any $\hat{\boldsymbol{\omega}}(0)$ *and* $\hat{\mathbf{q}}(0)$.

Proof. To begin with, the dynamics of the quaternion and angular velocity estimation error quantities are derived using Eqs. (5.11)-(5.12). The dynamics of $\tilde{\mathbf{q}}$ are derived by following similar steps described in Eq. (2.11). Taking the time derivative of Eq. (5.5) and using Eqs. (2.1) and Eq. (5.11) leads to

$$\begin{aligned}
\dot{\mathbf{C}}(\tilde{\mathbf{q}}) &= -S(\boldsymbol{\omega})\mathbf{C}(\tilde{\mathbf{q}}) + \mathbf{C}(\tilde{\mathbf{q}})S\left(\hat{\boldsymbol{\omega}} + \lambda\mathbf{C}^{\mathrm{T}}(\tilde{\mathbf{q}})\tilde{\mathbf{q}}_v\right) \\
&= -S(\boldsymbol{\omega})\mathbf{C}(\tilde{\mathbf{q}}) + S\left(\mathbf{C}(\tilde{\mathbf{q}})\left(\hat{\boldsymbol{\omega}} + \lambda\mathbf{C}^{\mathrm{T}}(\tilde{\mathbf{q}})\tilde{\mathbf{q}}_v\right)\right)\mathbf{C}(\tilde{\mathbf{q}}) \\
&= -S(\boldsymbol{\omega} - \mathbf{C}(\tilde{\mathbf{q}})\hat{\boldsymbol{\omega}} - \lambda\tilde{\mathbf{q}}_v)\mathbf{C}(\tilde{\mathbf{q}}) \\
&= -S(\tilde{\boldsymbol{\omega}} - \lambda\tilde{\mathbf{q}}_v)\mathbf{C}(\tilde{\mathbf{q}}).
\end{aligned} \tag{5.13}$$

The corresponding quaternion dynamics of Eq. (5.13) are given by

$$\dot{\tilde{\mathbf{q}}} = \frac{1}{2}\mathbf{E}(\tilde{\mathbf{q}})\left[\tilde{\boldsymbol{\omega}} - \lambda\tilde{\mathbf{q}}_v\right]. \tag{5.14}$$

Recognizing that $S(\tilde{\mathbf{q}}_v)\tilde{\mathbf{q}}_v = 0$, Eq. (5.14) simplifies to

$$\dot{\tilde{q}}_0 = -\frac{1}{2}\tilde{\mathbf{q}}_v^{\mathrm{T}}\left(\tilde{\boldsymbol{\omega}} - \lambda\tilde{\mathbf{q}}_v\right) \tag{5.15}$$

$$\dot{\tilde{\mathbf{q}}}_v = -\frac{\lambda}{2}\tilde{q}_0\tilde{\mathbf{q}}_v + \frac{1}{2}\Big(\tilde{q}_0\mathbf{I}_{3\times 3} + S(\tilde{\mathbf{q}}_v)\Big)\tilde{\boldsymbol{\omega}}. \tag{5.16}$$

Next, using Eq. (2.2) along with Eq. (5.13), the time-derivative of $\tilde{\boldsymbol{\omega}}$ is found to be

$$\begin{aligned}\mathbf{J}\dot{\tilde{\boldsymbol{\omega}}} &= \mathbf{J}\dot{\boldsymbol{\omega}} - \mathbf{J}\dot{\mathbf{C}}(\tilde{\mathbf{q}})\hat{\boldsymbol{\omega}} - \mathbf{J}\mathbf{C}(\tilde{\mathbf{q}})\dot{\hat{\boldsymbol{\omega}}} \\ &= -S(\boldsymbol{\omega})\mathbf{J}\boldsymbol{\omega} + \mathbf{u} + \mathbf{J}S(\tilde{\boldsymbol{\omega}} - \lambda\tilde{\mathbf{q}}_v)\hat{\boldsymbol{\omega}}^B - \mathbf{J}\mathbf{C}(\tilde{\mathbf{q}})\dot{\hat{\boldsymbol{\omega}}}\end{aligned} \tag{5.17}$$

Substituting the update law Eq. (5.12) for $\dot{\hat{\boldsymbol{\omega}}}$ into Eq. (5.17) yields the angular velocity estimation error dynamics

$$\mathbf{J}\dot{\tilde{\boldsymbol{\omega}}} = -S(\boldsymbol{\omega})\mathbf{J}\boldsymbol{\omega} + \mathbf{J}S(\tilde{\boldsymbol{\omega}})\hat{\boldsymbol{\omega}}^{\mathrm{B}} - \gamma\tilde{\mathbf{q}}_v + S(\hat{\boldsymbol{\omega}}^{\mathrm{B}})\mathbf{J}\hat{\boldsymbol{\omega}}^{\mathrm{B}}. \tag{5.18}$$

Define a Lyapunov function candidate V_o as follows

$$V_o = \gamma\Big[\tilde{\mathbf{q}}_v^{\mathrm{T}}\tilde{\mathbf{q}}_v + (\tilde{q}_0 - 1)^2\Big] + \frac{1}{2}\tilde{\boldsymbol{\omega}}^{\mathrm{T}}\mathbf{J}\tilde{\boldsymbol{\omega}}. \tag{5.19}$$

Differentiating V_o with respect to time and substituting Eqs. (5.15) and (5.18) results in

$$\begin{aligned}\dot{V}_o &= -2\gamma\dot{\tilde{q}}_0 + \tilde{\boldsymbol{\omega}}^{\mathrm{T}}\mathbf{J}\dot{\tilde{\boldsymbol{\omega}}} \\ &= \gamma\tilde{\mathbf{q}}_v^{\mathrm{T}}\left(\tilde{\boldsymbol{\omega}} - \lambda\tilde{\mathbf{q}}_v\right) + \tilde{\boldsymbol{\omega}}^{\mathrm{T}}\left(-S(\omega)\mathbf{J}\omega + \mathbf{J}S(\tilde{\boldsymbol{\omega}})\hat{\boldsymbol{\omega}}^{\mathrm{B}} - \gamma\tilde{\mathbf{q}}_v + S(\hat{\boldsymbol{\omega}}^{\mathrm{B}})\mathbf{J}\hat{\boldsymbol{\omega}}^{\mathrm{B}}\right) \\ &= -\gamma\lambda\|\tilde{\mathbf{q}}_v\|^2 + \tilde{\boldsymbol{\omega}}^{\mathrm{T}}\left(-S(\omega)\mathbf{J}\omega + \mathbf{J}S(\tilde{\boldsymbol{\omega}})\hat{\boldsymbol{\omega}}^{\mathrm{B}} + S(\hat{\boldsymbol{\omega}}^{\mathrm{B}})\mathbf{J}\hat{\boldsymbol{\omega}}^{\mathrm{B}}\right).\end{aligned} \tag{5.20}$$

Observe that the gyroscopic term $-S(\boldsymbol{\omega})\mathbf{J}\boldsymbol{\omega}$ can be expressed as

$$\begin{aligned}-S(\boldsymbol{\omega})\mathbf{J}\boldsymbol{\omega} &= -\left(\tilde{\boldsymbol{\omega}} + \hat{\boldsymbol{\omega}}^{\mathrm{B}}\right) \times \mathbf{J}\left(\tilde{\boldsymbol{\omega}} + \hat{\boldsymbol{\omega}}^{\mathrm{B}}\right) \\ &= -S(\tilde{\boldsymbol{\omega}})\mathbf{J}\tilde{\boldsymbol{\omega}} - S(\tilde{\boldsymbol{\omega}})\mathbf{J}\hat{\boldsymbol{\omega}}^{\mathrm{B}} - S(\hat{\boldsymbol{\omega}}^{\mathrm{B}})\mathbf{J}\tilde{\boldsymbol{\omega}} - S(\hat{\boldsymbol{\omega}}^{\mathrm{B}})\mathbf{J}\hat{\boldsymbol{\omega}}^{\mathrm{B}},\end{aligned}$$

which can be substituted into the right-hand side of Eq. (5.20) to obtain

$$\dot{V}_o = -\gamma\lambda\|\tilde{\mathbf{q}}_v\|^2 + \tilde{\boldsymbol{\omega}}^{\mathrm{T}}\left(-S(\tilde{\boldsymbol{\omega}})\mathbf{J}\tilde{\boldsymbol{\omega}} - S(\tilde{\boldsymbol{\omega}})\mathbf{J}\hat{\boldsymbol{\omega}}^{\mathrm{B}} - \left[S(\hat{\boldsymbol{\omega}}^{\mathrm{B}})\mathbf{J} + \mathbf{J}S(\hat{\boldsymbol{\omega}}^{\mathrm{B}})\right]\tilde{\boldsymbol{\omega}}\right). \tag{5.21}$$

After recognizing that $\left[S(\hat{\boldsymbol{\omega}}^{\mathrm{B}})\mathbf{J} + \mathbf{J}S(\hat{\boldsymbol{\omega}}^{\mathrm{B}})\right]$ is also a skew-symmetric matrix, it is easily seen that the second term on the right-hand side of Eq. (5.21) is identically zero, which leads to

$$\dot{V}_o = -\gamma\lambda\|\tilde{\mathbf{q}}_v\|^2 \leq 0. \tag{5.22}$$

Thus, $\tilde{\mathbf{q}}_v$ and $\tilde{\boldsymbol{\omega}}$ are uniformly bounded. From Eq. (5.14) it follows that $\dot{\tilde{\mathbf{q}}}_v$ is also uniformly bounded. Since $V_o \geq 0$ and $\dot{V}_o \leq 0$, we have that $\lim_{t\to\infty} V_o(t) = V_{o_\infty}$ exists for some finite $V_{o_\infty} \in \mathcal{R}^+$. Hence, $\int_0^\infty \dot{V}_o(t)\,\mathrm{d}t = V_{o_\infty} - V_o(0)$ which implies that $\tilde{\mathbf{q}}_v \in \mathcal{L}_2$. Invoking Barbalat's lemma for $\tilde{\mathbf{q}}_v \in \mathcal{L}_2 \cap \mathcal{L}_\infty, \dot{\tilde{\mathbf{q}}}_v \in \mathcal{L}_\infty$ leads to $\lim_{t\to\infty} \tilde{\mathbf{q}}_v(t) = 0$.

Ascertaining convergence properties of $\tilde{\boldsymbol{\omega}}$ requires more involved analysis. Using $\tilde{\mathbf{q}}_v(t) \to 0$ as $t \to \infty$ in Eq. (5.15) leads to $\lim_{t\to\infty} \dot{\tilde{q}}_0(t) = 0$. Using

the kinematic property $\mathbf{E}^{\mathrm{T}}(\tilde{\mathbf{q}})\mathbf{E}(\tilde{\mathbf{q}}) = \mathbf{I}_{3\times 3}$, Eq. (5.14) can be expressed as

$$\begin{aligned}\tilde{\boldsymbol{\omega}} - \lambda\tilde{\mathbf{q}}_v &= 2\mathbf{E}^{\mathrm{T}}(\tilde{\mathbf{q}})\dot{\tilde{\mathbf{q}}} \\ &= 2\Big[-\tilde{\mathbf{q}}_v\dot{\tilde{q}}_0 + \Big(\tilde{q}_0\mathbf{I}_{3\times 3} - S(\tilde{\mathbf{q}}_v)\Big)\dot{\tilde{\mathbf{q}}}_v\Big] \end{aligned} \tag{5.23}$$

which may be combined with $\lim_{t\to\infty}\tilde{\mathbf{q}}_v(t) = 0$ to obtain

$$\lim_{t\to\infty}\tilde{\boldsymbol{\omega}}(t) = 2\lim_{t\to\infty}\Big[\tilde{q}_0(t)\dot{\tilde{\mathbf{q}}}_v(t)\Big]. \tag{5.24}$$

Next, observe that the dynamics of $\dot{\tilde{\mathbf{q}}}_v$ in Eq. (5.16) may be written as

$$\dot{\tilde{\mathbf{q}}}_v = -\frac{\lambda}{2}\tilde{\mathbf{q}}_v + \boldsymbol{\delta}; \qquad \boldsymbol{\delta} \triangleq \frac{1}{2}\Big[\Big(\tilde{q}_0\mathbf{I}_{3\times 3} + S(\tilde{\mathbf{q}}_v)\Big)\tilde{\boldsymbol{\omega}} + \lambda(-\tilde{q}_0 + 1)\tilde{\mathbf{q}}_v\Big], \tag{5.25}$$

where $\boldsymbol{\delta}$ is a bounded signal consisting of the bounded states $\tilde{\mathbf{q}}_v$, $\tilde{q}_0$, and $\tilde{\boldsymbol{\omega}}$. Thus, $\tilde{\mathbf{q}}_v$ has the dynamics of an asymptotically stable first-order linear filter with bounded input $\boldsymbol{\delta}$. Since $\tilde{\mathbf{q}}_v(t) \to 0$ as $t \to \infty$, it readily follows that $\lim_{t\to\infty}\boldsymbol{\delta}(t) = 0$. Further, using the definition of $\boldsymbol{\delta}$ in Eq. (5.25) together with $\lim_{t\to\infty}[\boldsymbol{\delta}(t), \tilde{\mathbf{q}}_v(t)] = 0$ leads to

$$\lim_{t\to\infty}\tilde{q}_0(t)\tilde{\boldsymbol{\omega}}(t) = 0. \tag{5.26}$$

Finally, from the quaternion unit norm constraint $\tilde{\mathbf{q}}_v^{\mathrm{T}}\tilde{\mathbf{q}}_v + \tilde{q}_0^2 = 1$, $\lim_{t\to\infty}\tilde{\mathbf{q}}_v(t) = 0$ implies that $\lim_{t\to\infty}\tilde{q}_0(t) = \pm 1$, which can be applied to Eq. (5.26) to ascertain

$$\lim_{t\to\infty}\tilde{\boldsymbol{\omega}}(t) = 0,$$

thereby ensuring $\hat{\boldsymbol{\omega}}(t) \to \hat{\boldsymbol{\omega}}^B(t)$ asymptotically. This completes the proof. □

A few important remarks are now in order.

Remark 5.2.1. Suppose it is known initially that $\hat{\boldsymbol{\omega}}^B(0) = \boldsymbol{\omega}(0)$ (this is a likely scenario if it is known that the body starts from rest) and $\hat{\mathbf{q}}_v(0) = \mathbf{q}(0)$ is selected. Then by the definition of the error states, $\tilde{\boldsymbol{\omega}}(0) = \tilde{\mathbf{q}}_v(0) = 0$. Further, from Eqs. (5.14) and (5.18), $\dot{\tilde{\mathbf{q}}} = 0$ and $\dot{\tilde{\boldsymbol{\omega}}} = 0$. Thus, when the initial value of the body angular velocity is known, the estimation errors never deviate from zero and $\hat{\boldsymbol{\omega}}^B(t) = \boldsymbol{\omega}(t)$ for all $t \geq 0$.

Remark 5.2.2. The observer in Eqs. (5.11)-(5.12) is smooth and involves no switches to guarantee convergence of the angular velocity and attitude estimates to their respective true values independent of the control torque.

Remark 5.2.3. Observe that V_o is a non-strict Lyapunov function since its time derivative only contains negative terms in $\tilde{\mathbf{q}}_v$. A partially strict Lyapunov function would additionally have negative terms in $\tilde{\boldsymbol{\omega}}$ in its time derivative, which is not the case here.

Remark 5.2.4. The observer depends on perfect knowledge of the inertia matrix $\mathbf{J}$. Thus, errors or uncertainties in $\mathbf{J}$ have a potential impact on the overall observer convergence properties. This will be further evaluated in the numerical simulations section.

5.2.3 Towards a Strict Lyapunov Function

In order to circumvent the non-strictness issue with regards to V_o, a strictification approach is pursued in order to transform V_o into a partially strict

Lyapunov function whose derivative contains additional negative terms in $\tilde{\boldsymbol{\omega}}$. In the specific context of rigid-body attitude dynamics using quaternion parameterization, the term "partial" is used to emphasize the fact that convergence of the estimation error states $\tilde{\mathbf{q}}$ and $\tilde{\boldsymbol{\omega}}$ corresponds with $\tilde{\mathbf{q}} = [\pm 1, 0, 0, 0]^{\mathrm{T}}$ and $\tilde{\boldsymbol{\omega}} = [0, 0, 0]^{\mathrm{T}}$. That is, only a partial component of the attitude state $\tilde{\mathbf{q}}$, namely the vector component, $\tilde{\mathbf{q}}_v$, is driven to the origin. Since a Lyapunov function containing only negative terms in $\tilde{\boldsymbol{\omega}}$ and $\tilde{\mathbf{q}}_v$ does not conform with the precise definition of strict Lyapunov functions as stated in Definition 2.3.4, the qualifier "partial" is used for technical consistency.

The crucial advantage gained by constructing a (partially) strict Lyapunov function will become clear subsequently when a separation property is established when the observer is used in conjunction with a separately designed PD control law employing estimates generated by the smooth observer. The construction of the partially strict Lyapunov function proceeds in a novel fashion that is based upon "spiral" logic. To be more specific, first, by using the results of Theorem 5.2.1, an intermediate result is presented which shows that the PD control in Eq. (5.1) employing the output of the observer ensures closed-loop boundedness of the body angular velocity. This intermediate result is then directly applied towards the generation of a mixed/cross term in V_o as a means to partially strictify V_o.

Proposition 5.2.2. *Consider the tracking error dynamics described by Eqs.* (2.12)-(2.13). *Let the control input* $\mathbf{u}(t)$ *be computed by using angular velocity esti-*

mates and prescribed according to

$$\mathbf{u} = -k_p \mathbf{q}_{e_v} - k_v \hat{\boldsymbol{\omega}}_e + \mathbf{J}\mathbf{C}(\mathbf{q}_e)\dot{\boldsymbol{\omega}}_r + S(\boldsymbol{\omega}_r^B)\mathbf{J}\boldsymbol{\omega}_r^B, \tag{5.27}$$

with $k_p > 0$, $k_v > 0$, *and where*

$$\hat{\boldsymbol{\omega}}_e = \hat{\boldsymbol{\omega}}^B - \boldsymbol{\omega}_r^B. \tag{5.28}$$

Suppose that the angular velocity estimate $\hat{\boldsymbol{\omega}}^B = \mathbf{C}(\boldsymbol{\epsilon})\hat{\boldsymbol{\omega}}$ *is determined through Eqs.* (5.11)-(5.12)*, then* $\boldsymbol{\omega}_e$ *and* $\boldsymbol{\omega}$ *are uniformly bounded.*

Proof. Consider the following Lyapunov function candidate

$$V_c = k_p \left[(1 - q_{e_0})^2 + \mathbf{q}_{e_v}^T \mathbf{q}_{e_v}\right] + \frac{1}{2}\boldsymbol{\omega}_e^{\mathrm{T}} \mathbf{J} \boldsymbol{\omega}_e \tag{5.29}$$

Differentiating V_c with respect to time along Eqs. (2.12),(2.13),(5.27), and (5.28) yields

$$\begin{aligned}
\dot{V}_c &= k_p \mathbf{q}_{e_v}^{\mathrm{T}} \boldsymbol{\omega}_e + \boldsymbol{\omega}_e^{\mathrm{T}} \Big(- S(\boldsymbol{\omega})\mathbf{J}\boldsymbol{\omega} + \mathbf{u} + \mathbf{J}\left[S(\boldsymbol{\omega}_e)\boldsymbol{\omega}_r^B - C(\delta\mathbf{q})\dot{\boldsymbol{\omega}}_r\right] \Big) \\
&= \boldsymbol{\omega}_e^{\mathrm{T}} \Big(- S(\boldsymbol{\omega})\mathbf{J}\boldsymbol{\omega} - k_v \hat{\boldsymbol{\omega}}_e + S(\boldsymbol{\omega}_r^B)\mathbf{J}\boldsymbol{\omega}_r^B + \mathbf{J}S(\boldsymbol{\omega}_e)\boldsymbol{\omega}_r^B \Big) \\
&= -k_v \boldsymbol{\omega}_e^{\mathrm{T}} \hat{\boldsymbol{\omega}}_e,
\end{aligned} \tag{5.30}$$

where, the following identity is used to obtain Eq. (5.30):

$$\boldsymbol{\omega}_e^{\mathrm{T}} \Big(- S(\boldsymbol{\omega})\mathbf{J}\boldsymbol{\omega} + S(\boldsymbol{\omega}_r^B)\mathbf{J}\boldsymbol{\omega}_r^B + \mathbf{J}S(\boldsymbol{\omega}_e)\boldsymbol{\omega}_r^B \Big) = 0,$$

which can be shown using similar steps used to obtain Eq. (5.22). After

recognizing that $\hat{\boldsymbol{\omega}}_e = \boldsymbol{\omega}_e - \tilde{\boldsymbol{\omega}}$ and substituting into Eq. (5.30), one obtains

$$\begin{aligned}\dot{V}_c &= -k_v \boldsymbol{\omega}_e^{\mathrm{T}} \boldsymbol{\omega}_e + k_v \boldsymbol{\omega}_e^{\mathrm{T}} \tilde{\boldsymbol{\omega}} \\ &\leq -k_v \|\boldsymbol{\omega}_e\|^2 + k_v \|\boldsymbol{\omega}_e\| \|\tilde{\boldsymbol{\omega}}\|. \end{aligned} \tag{5.31}$$

Define a scalar constant c_1 according to $c_1 = \sup_{t \geq 0} \|\tilde{\boldsymbol{\omega}}(t)\|$, which is positive and well-defined since $\tilde{\boldsymbol{\omega}} \in \mathcal{L}_\infty$ as shown in Theorem 5.2.1. Using c_1, the following upper bound is obtained on Eq. (5.31)

$$\begin{aligned}\dot{V}_c &\leq -k_v \|\boldsymbol{\omega}_e\|^2 + k_v \|\boldsymbol{\omega}_e\| c_1 \\ &= -\frac{k_v}{2} \|\boldsymbol{\omega}_e\|^2 - \frac{k_v}{2} \left(\|\boldsymbol{\omega}_e\|^2 - 2\|\boldsymbol{\omega}_e\| c_1 + c_1^2 \right) + \frac{k_v}{2} c_1^2 \\ &\leq -\frac{k_v}{2} \|\boldsymbol{\omega}_e\|^2 + \frac{k_v}{2} c_1^2 \\ &= -\left[\frac{k_v}{2} \|\boldsymbol{\omega}_e\|^2 + \frac{4 k_p k_v}{J_{\max}} \right] + \sigma; \qquad \sigma = (k_v/2) c_1^2 + (4 k_p k_v / J_{\max}) \end{aligned} \tag{5.32}$$

where $J_{\max}$ is the maximum eigenvalue of $\mathbf{J}$, and the constant $\sigma > 0$ is well-defined and finite. Further, since V_c is upper bounded as follows

$$\begin{aligned} V_c &\leq 4k_p + \frac{1}{2} J_{\max} \|\boldsymbol{\omega}_e\|^2 \\ &= \frac{J_{\max}}{k_v} \left[\frac{k_v}{2} \|\boldsymbol{\omega}_e\|^2 + \frac{4 k_p k_v}{J_{\max}} \right], \end{aligned}$$

we use Eq. (5.32) to express an upper-bound on $\dot{V}_c$ as follows

$$\dot{V}_c \leq \frac{-k_v}{J_{\max}} V_c + \sigma, \tag{5.33}$$

which shows that V_c and $\boldsymbol{\omega}_e$ are uniformly bounded functions. Further, since $\boldsymbol{\omega}_r$ is bounded, it follows that $\boldsymbol{\omega}$ is bounded. This completes the proof. $\square$

A few important observations are made regarding Proposition 5.2.2.

Remark 5.2.5. The use of the scalar constant c_1 is essential in showing boundedness of the closed-loop signal $\boldsymbol{\omega}$. It is important to remark that claiming c_1 is well-defined is possible only through the results of Theorem 5.2.1. Hence, the ordered logic procedure is critical.

Remark 5.2.6. To further motivate the need for a strict Lyapunov function for the observer dynamics, we examine the current obstacle that prevents us from obtaining closed-loop stability and convergence for a combined observer-controller implementation. Consider a composite Lyapunov function V_{oc} defined as the sum of V_o and V_c.

$$V_{oc} = V_o + V_c. \tag{5.34}$$

where V_o and V_c are previously defined in Eqs.(5.19) and (5.29). Differentiating V_{oc} along Eqs. (2.12), (2.13), (5.14), (5.18) results in

$$\dot{V}_{oc} \leq -\gamma\lambda\|\tilde{\mathbf{q}}_v\|^2 - k_v\|\boldsymbol{\omega}_e\|^2 + k_v\|\boldsymbol{\omega}_e\|\|\tilde{\boldsymbol{\omega}}\| \tag{5.35}$$

Observe that the term $k_v\|\boldsymbol{\omega}_e\|\|\tilde{\boldsymbol{\omega}}\|$ in Eq. (5.35) cannot be dominated in any way since there is no negative term in $\tilde{\boldsymbol{\omega}}$. At best, after assuming that the initial estimation and tracking errors are known, it may be possible to obtain some local stability result. Hence, the current non-strict nature of V_o poses a hard obstacle in this regard.

The strictification process proceeds as follows. Define a scalar time-

varying signal, N, as a cross term in the observer states $\tilde{\mathbf{q}}_v$ and $\tilde{\boldsymbol{\omega}}$ given by

$$N = -2\tilde{q}_0 \tilde{\mathbf{q}}_v^{\mathrm{T}} \tilde{\boldsymbol{\omega}}. \tag{5.36}$$

Next, using the uniform boundedness properties of $\tilde{\boldsymbol{\omega}}$ and $\boldsymbol{\omega}_e$, it is possible to derive an upper bounding function for $\dot{N}$. Differentiating N with respect to time and evaluating along Eqs. (5.14) gives the following:

$$\begin{aligned} \dot{N} &= -2\tilde{q}_0 \tilde{\mathbf{q}}_v^{\mathrm{T}} \dot{\tilde{\boldsymbol{\omega}}} + \tilde{\mathbf{q}}_v^{\mathrm{T}} \left(\tilde{\boldsymbol{\omega}} - \lambda \tilde{\mathbf{q}}_v\right) \tilde{\mathbf{q}}_v^{\mathrm{T}} \tilde{\boldsymbol{\omega}} - \tilde{q}_0 \tilde{\boldsymbol{\omega}}^{\mathrm{T}} \left(\tilde{q}_0 \mathbf{I} + S(\tilde{\mathbf{q}}_v)\right) \left(\tilde{\boldsymbol{\omega}} - \lambda \tilde{\mathbf{q}}_v\right) \\ &= -2\tilde{q}_0 \tilde{\mathbf{q}}_v^{\mathrm{T}} \dot{\tilde{\boldsymbol{\omega}}} + (\tilde{\mathbf{q}}_v^{\mathrm{T}} \tilde{\boldsymbol{\omega}})^2 - \lambda \|\tilde{\mathbf{q}}_v\|^2 \tilde{\mathbf{q}}_v^{\mathrm{T}} \tilde{\boldsymbol{\omega}} - \tilde{q}_0^2 \|\tilde{\boldsymbol{\omega}}\|^2 + \lambda \tilde{q}_0^2 \tilde{\boldsymbol{\omega}}^{\mathrm{T}} \tilde{\mathbf{q}}_v. \end{aligned} \tag{5.37}$$

Substituting $\tilde{q}_0^2 = \left(1 - \tilde{\mathbf{q}}_v^{\mathrm{T}} \tilde{\mathbf{q}}_v\right)$ into Eq. (5.37) and carrying out minor algebra yields

$$\begin{aligned} \dot{N} = -2\tilde{q}_0 \tilde{\mathbf{q}}_v^{\mathrm{T}} \dot{\tilde{\boldsymbol{\omega}}} + (\tilde{\mathbf{q}}_v^{\mathrm{T}} \tilde{\boldsymbol{\omega}})^2 - 2\lambda \|\tilde{\mathbf{q}}_v\|^2 \tilde{\mathbf{q}}_v^{\mathrm{T}} \tilde{\boldsymbol{\omega}} - \|\tilde{\boldsymbol{\omega}}\|^2 \\ + \|\tilde{\mathbf{q}}_v\|^2 \|\tilde{\boldsymbol{\omega}}\|^2 + \lambda \tilde{\mathbf{q}}_v^{\mathrm{T}} \tilde{\boldsymbol{\omega}}. \end{aligned} \tag{5.38}$$

The following bounds are established by applying the Cauchy-Schwarz inequality along with the unit norm bounds $\tilde{q}_0 \leq 1$ and $\|\tilde{\mathbf{q}}_v\| \leq 1$ when appropriate:

$$-2\tilde{q}_0 \tilde{\mathbf{q}}_v^{\mathrm{T}} \dot{\tilde{\boldsymbol{\omega}}} \leq 2\|\tilde{\mathbf{q}}_v\| \|\dot{\tilde{\boldsymbol{\omega}}}\| \tag{5.39}$$

$$(\tilde{\mathbf{q}}_v^{\mathrm{T}} \tilde{\boldsymbol{\omega}})^2 \leq \|\tilde{\mathbf{q}}_v\|^2 \|\tilde{\boldsymbol{\omega}}\|^2 \leq \|\tilde{\mathbf{q}}_v\|^2 c_1^2 \tag{5.40}$$

$$-2\lambda \|\tilde{\mathbf{q}}_v\|^2 \tilde{\mathbf{q}}_v^{\mathrm{T}} \tilde{\boldsymbol{\omega}} \leq 2\lambda \|\tilde{\mathbf{q}}_v\|^2 \|\tilde{\mathbf{q}}_v\| \|\tilde{\boldsymbol{\omega}}\| \leq 2\lambda \|\tilde{\mathbf{q}}_v\|^2 c_1 \tag{5.41}$$

$$\lambda \tilde{\mathbf{q}}_v^{\mathrm{T}} \tilde{\boldsymbol{\omega}} \leq \lambda \|\tilde{\mathbf{q}}_v\| \|\tilde{\boldsymbol{\omega}}\| \tag{5.42}$$

$$\|\tilde{\mathbf{q}}_v\|^2 \|\tilde{\boldsymbol{\omega}}\|^2 \leq \|\tilde{\mathbf{q}}_v\|^2 c_1^2 \tag{5.43}$$

Inserting the bounds Eq. (5.39)-(5.43) into Eq. (5.38) yields

$$N \leq 2\|\tilde{\mathbf{q}}_v\|\|\dot{\tilde{\boldsymbol{\omega}}}\| + 2\left(c_1^2 + \lambda c_1\right)\|\tilde{\mathbf{q}}_v\|^2 - \|\tilde{\boldsymbol{\omega}}\|^2 + \lambda\|\tilde{\mathbf{q}}_v\|\|\tilde{\boldsymbol{\omega}}\|.$$

An appropriate upper bound for the term $\|\dot{\tilde{\boldsymbol{\omega}}}\|$ is yet to be determined. Consider a closer examination of Eq. (5.18) which can be simplified as follows:

$$\begin{aligned}
\mathbf{J}\dot{\tilde{\boldsymbol{\omega}}} &= -S(\omega)\mathbf{J}\omega + \mathbf{J}S(\tilde{\boldsymbol{\omega}})\hat{\boldsymbol{\omega}}^{\mathrm{B}} - \gamma\tilde{\mathbf{q}}_v + S(\hat{\boldsymbol{\omega}}^{\mathrm{B}})\mathbf{J}\hat{\boldsymbol{\omega}}^{\mathrm{B}} \\
&= -S(\omega)\mathbf{J}\omega + \mathbf{J}S(\tilde{\boldsymbol{\omega}})(\boldsymbol{\omega} - \tilde{\boldsymbol{\omega}}) - \gamma\tilde{\mathbf{q}}_v + S(\boldsymbol{\omega} - \tilde{\boldsymbol{\omega}})\mathbf{J}(\boldsymbol{\omega} - \tilde{\boldsymbol{\omega}}) \\
&= \Big[\mathbf{J}S(\tilde{\boldsymbol{\omega}}) + S(\mathbf{J}\tilde{\boldsymbol{\omega}}) - S(\tilde{\boldsymbol{\omega}})\mathbf{J}\Big]\boldsymbol{\omega} - \gamma\tilde{\mathbf{q}}_v + S(\tilde{\boldsymbol{\omega}})\mathbf{J}\tilde{\boldsymbol{\omega}}
\end{aligned} \tag{5.44}$$

Using the triangle inequality, the norm of $\dot{\tilde{\boldsymbol{\omega}}}$ may be expressed as

$$\begin{aligned}
\|\dot{\tilde{\boldsymbol{\omega}}}\| \leq \|S(\tilde{\boldsymbol{\omega}})\boldsymbol{\omega}\| + \|\mathbf{J}^{-1}S(\mathbf{J}\tilde{\boldsymbol{\omega}})\boldsymbol{\omega}\| + \|\mathbf{J}^{-1}S(\tilde{\boldsymbol{\omega}})\mathbf{J}\boldsymbol{\omega}\| \\
+ \|\gamma\mathbf{J}^{-1}\tilde{\mathbf{q}}_v\| + \|\mathbf{J}^{-1}S(\tilde{\boldsymbol{\omega}})\dot{\tilde{\boldsymbol{\omega}}}\mathbf{J}\tilde{\boldsymbol{\omega}}\|.
\end{aligned} \tag{5.45}$$

Using again the Cauchy-Schwarz inequality along with $\|\mathbf{J}\| \leq J_{\max}$ and $\|\mathbf{J}^{-1}\| \leq 1/J_{\min}$, where $J_{\min}$ is the the minimum eigenvalue of $\mathbf{J}$, the following upper bounds are established:

$$\|S(\tilde{\boldsymbol{\omega}})\boldsymbol{\omega}\| \leq \|\tilde{\boldsymbol{\omega}}\|\|\boldsymbol{\omega}\| \leq \|\tilde{\boldsymbol{\omega}}\|c_2 \tag{5.46}$$

$$\|\mathbf{J}^{-1}S(\mathbf{J}\tilde{\boldsymbol{\omega}})\boldsymbol{\omega}\| \leq \frac{J_{\max}}{J_{\min}}\|\tilde{\boldsymbol{\omega}}\|\|\boldsymbol{\omega}\| \leq \frac{J_{\max}}{J_{\min}}\|\tilde{\boldsymbol{\omega}}\|c_2 \tag{5.47}$$

$$\|\mathbf{J}^{-1}S(\tilde{\boldsymbol{\omega}})\mathbf{J}\boldsymbol{\omega}\| \leq \frac{J_{\max}}{J_{\min}}\|\tilde{\boldsymbol{\omega}}\|\|\boldsymbol{\omega}\| \leq \frac{J_{\max}}{J_{\min}}\|\tilde{\boldsymbol{\omega}}\|c_2 \tag{5.48}$$

$$\|\gamma\mathbf{J}^{-1}\tilde{\mathbf{q}}_v\| \leq \frac{\gamma}{J_{\min}}\|\tilde{\mathbf{q}}_v\| \tag{5.49}$$

$$\|\mathbf{J}^{-1}S(\tilde{\boldsymbol{\omega}})\mathbf{J}\tilde{\boldsymbol{\omega}}\| \leq \frac{J_{\max}}{J_{\min}}\|\tilde{\boldsymbol{\omega}}\|^2 \leq \frac{J_{\max}}{J_{\min}}\|\tilde{\boldsymbol{\omega}}\|c_1 \tag{5.50}$$

wherein $c_2 = \sup_{t\geq 0} \boldsymbol{\omega}(t)$ is a well defined, finite positive constant since $\boldsymbol{\omega} \in \mathcal{L}_\infty$ as shown in Proposition 5.2.2. Applying the bounds Eqs. (5.46)-(5.50) to Eq. (5.45) leads to

$$\|\dot{\tilde{\boldsymbol{\omega}}}\| \leq \left(c_2 + \frac{2J_{\max}}{J_{\min}}c_2 + \frac{J_{\max}}{J_{\min}}c_1\right)\|\tilde{\boldsymbol{\omega}}\| + \frac{\gamma}{J_{\min}}\|\tilde{\mathbf{q}}_v\|. \tag{5.51}$$

Substituting Eq. (5.51) into Eq. (5.38) and following through with rearranging terms results in the following upper bound for $\dot{N}$:

$$\begin{aligned}\dot{N} &\leq 2\left(c_2 + \frac{2J_{\max}}{J_{\min}}c_2 + \frac{J_{\max}}{J_{\min}}c_1 + \frac{\lambda}{2}\right)\|\tilde{\mathbf{q}}_v\|\|\tilde{\boldsymbol{\omega}}\| \qquad (5.52)\\ &\quad + 2\left(\frac{\gamma}{J_{\min}} + c_1^2 + \lambda c_1\right)\|\tilde{\mathbf{q}}_v\|^2 - \|\tilde{\boldsymbol{\omega}}\|^2\\ &= \alpha\|\tilde{\mathbf{q}}_v\|\|\tilde{\boldsymbol{\omega}}\| + \beta\|\tilde{\mathbf{q}}_v\|^2 - \|\tilde{\boldsymbol{\omega}}\|^2, \qquad (5.53)\end{aligned}$$

where,

$$\begin{aligned}\alpha &= 2\left(c_2 + \frac{2J_{\max}}{J_{\min}}c_2 + \frac{J_{\max}}{J_{\min}}c_1 + \frac{\lambda}{2}\right),\\ \beta &= 2\left(\frac{\gamma}{J_{\min}} + c_1^2 + \lambda c_1\right).\end{aligned}$$

Observe that the upper bounding function for $\dot{N}$ in Eq. (5.52) contains a nonpositive term in $\tilde{\boldsymbol{\omega}}$. This term plays a critical role in the construction of a strict Lyapunov function as shown next in Proposition 5.2.3.

Proposition 5.2.3. *Consider the observer dynamics described by Eqs.* (5.11) *and* (5.12)*. Using the property* $\tilde{\boldsymbol{\omega}}, \boldsymbol{\omega} \in \mathcal{L}_\infty$ *proved respectively in Theorem 5.2.1*

and Proposition 5.2.2, it can be shown that the function

$$\tilde{V}_o = \mu V_o + N; \qquad \mu = \max\left(\sqrt{\frac{8}{\gamma J_{min}}}, \frac{2\left(\beta + \alpha^2\right)}{\gamma\lambda}\right) \tag{5.54}$$

with V_o and N given respectively by Eqs. (5.19) *and* (5.36) *is a partially strict Lyapunov function for the estimation error dynamics.*

Proof. Consider the augmented function $\tilde{V}_o$ expressed in terms of V_o and N

$$\begin{aligned}\tilde{V}_o &= \mu V_o + N \\ &= \mu\gamma\left[\tilde{\mathbf{q}}_v^T\tilde{\mathbf{q}}_v + (\tilde{q}_0 - 1)^2\right] + \frac{\mu}{2}\tilde{\boldsymbol{\omega}}^{\mathrm{T}}\mathbf{J}\tilde{\boldsymbol{\omega}} - 2\tilde{q}_0\tilde{\mathbf{q}}_v^{\mathrm{T}}\tilde{\boldsymbol{\omega}},\end{aligned}$$

where μ, given by Eq. (5.54), is an artificially constructed positive scalar constant that, while not affecting the observer design, aids in the Lyapunov function strictification process. We can obtain a lower-bounding function for $\tilde{V}_o$ as follows

$$\begin{aligned}\tilde{V}_o &\geq \mu\gamma\|\tilde{\mathbf{q}}_v\|^2 + \mu\gamma(\tilde{q}_0 - 1)^2 + \frac{\mu}{2}J_{\min}\|\tilde{\boldsymbol{\omega}}\|^2 - 2\tilde{q}_0\tilde{\mathbf{q}}_v^T\tilde{\boldsymbol{\omega}} \qquad (5.55)\\ &= \frac{\mu\gamma}{2}\|\tilde{\mathbf{q}}_v\|^2 + \left(\frac{\mu\gamma}{2} - \frac{4}{\mu J_{\min}}\tilde{q}_0^2\right)\|\tilde{\mathbf{q}}_v\|^2 + \mu\gamma(\tilde{q}_0 - 1)^2 + \frac{\mu}{4}J_{\min}\|\tilde{\boldsymbol{\omega}}\|^2 \\ &\quad + \left(\frac{4}{\mu J_{\min}}\|\tilde{\mathbf{q}}_v\|^2\tilde{q}_0^2 - 2\tilde{q}_0\tilde{\mathbf{q}}_v^{\mathrm{T}}\tilde{\boldsymbol{\omega}} + \frac{\mu}{4}J_{\min}\|\tilde{\boldsymbol{\omega}}\|^2\right).\end{aligned}$$

Selecting μ according to Eq. (5.54) leads to the following lower bound for $\tilde{V}_o$:

$$\tilde{V}_o \geq \frac{\mu\gamma}{2}\|\tilde{\mathbf{q}}_v\|^2 + \mu\gamma(\tilde{q}_0 - 1)^2 + \frac{\mu}{4}J_{\min}\|\tilde{\boldsymbol{\omega}}\|^2 \geq 0.$$

Consequently, $\tilde{V}_o$ is a Lyapunov function candidate. Next, differentiating $\tilde{V}_o$

with respect to time and using Eqs. (5.21) and (5.52) leads to

$$\begin{aligned}\dot{\tilde{V}}_o &= \mu\dot{V}_o + \dot{N} \\ &\leq -\left(\mu\gamma\lambda - \beta\right)\|\tilde{\mathbf{q}}_v\|^2 + \alpha\|\tilde{\mathbf{q}}_v\|\|\tilde{\boldsymbol{\omega}}\| - \|\tilde{\boldsymbol{\omega}}\|^2. \end{aligned} \tag{5.56}$$

Completing squares in Eq. (5.56) so that

$$\begin{aligned}\dot{\tilde{V}}_o = &-\frac{\mu\gamma\lambda}{2}\|\tilde{\mathbf{q}}_v\|^2 - \left(\frac{\mu\gamma\lambda}{2} - \beta - \alpha^2\right)\|\tilde{\mathbf{q}}_v\|^2 \\ &- \left(\alpha^2\|\tilde{\mathbf{q}}_v\|^2 - \alpha\|\tilde{\mathbf{q}}_v\|\|\tilde{\boldsymbol{\omega}}\| + \frac{1}{4}\|\tilde{\boldsymbol{\omega}}\|^2\right) - \frac{3}{4}\|\tilde{\boldsymbol{\omega}}\|^2\end{aligned}$$

and choosing μ according to Eq. (5.54) results in

$$\dot{\tilde{V}}_o \leq -\frac{\mu\gamma\lambda}{2}\|\tilde{\mathbf{q}}_v\|^2 - \frac{3}{4}\|\tilde{\boldsymbol{\omega}}\|^2. \tag{5.57}$$

As a result, $\tilde{V}_o$ is a partially strict Lyapunov function due to the presence of non-positive terms of $\tilde{\boldsymbol{\omega}}$ in $\dot{\tilde{V}}_o$. This completes the proof. □

The significance of the preceding result is demonstrated in the next section, where a separation property is established for the globally asymptotically stable implementation of the PD control using angular velocity estimates from the proposed observer.

5.3 Separation Property of Angular Velocity Observer Based Attitude Control

The following result represents the second important contribution of this chapter, a separation property for the nonlinear rigid body attitude tracking control system developed by combining a separately designed PD feedback control employing angular velocity estimates obtained from the smooth observer Eqs. (5.11)-(5.12).

Theorem 5.3.1. *Consider the control input* $\mathbf{u}(t)$ *prescribed according to Eq.* (5.27) *with* $k_p, k_v > 0$. *Further, suppose that the angular velocity estimate* $\hat{\boldsymbol{\omega}}^B$ *is determined through Eqs.* (5.11)-(5.12)*, along with* $\lambda, \gamma > 0$. *Then, the closed-loop tracking error dynamics described by Eq.* (2.12)-(2.13) *are (almost) globally asymptotically stable and estimated states converge to true values, that is,*

$$\lim_{t\to\infty} \left[\tilde{\mathbf{q}}_v(t), \tilde{\boldsymbol{\omega}}(t), \boldsymbol{\omega}_e(t), \mathbf{q}_{e_v}(t)\right] = 0.$$

Proof. Consider the following Lyapunov function candidate

$$V = \nu\tilde{V}_o + V_c = \underbrace{\nu\left(\mu\gamma\left[\tilde{\mathbf{q}}_v^T\tilde{\mathbf{q}}_v + (\tilde{q}_0 - 1)^2\right] + \frac{\mu}{2}\tilde{\boldsymbol{\omega}}^{\mathrm{T}}\mathbf{J}\tilde{\boldsymbol{\omega}} - 2\tilde{q}_0\tilde{\mathbf{q}}_v^{\mathrm{T}}\tilde{\boldsymbol{\omega}}\right)}_{\text{observer part}}$$
$$+ \underbrace{k_p\left[(1-q_{e_0})^2 + \mathbf{q}_{e_v}^T\mathbf{q}_{e_v}\right] + \frac{1}{2}\boldsymbol{\omega}_e^{\mathrm{T}}\mathbf{J}\boldsymbol{\omega}_e}_{\text{controller part}}$$

with some strictly positive scalar ν that is introduced purely for analysis and is not implemented in either the control or observer design. The precise value of ν will be determined in the sequel. The time derivative of the Lyapunov

function V yields the following expression

$$\dot{V} = \nu\dot{\tilde{V}}_o + \dot{V}_c \leq -\frac{\nu\mu\gamma\lambda}{2}\|\tilde{\mathbf{q}}_v\|^2 - \frac{3\nu}{4}\|\tilde{\boldsymbol{\omega}}\|^2 - k_v\|\boldsymbol{\omega}_e\|^2 + k_v\boldsymbol{\omega}_e^{\mathrm{T}}\tilde{\boldsymbol{\omega}}. \tag{5.58}$$

Completion of squares for the cross term in Eq. (5.58) leads to

$$\begin{aligned}\dot{V} \leq -\frac{\nu\mu\gamma\lambda}{2}\|\tilde{\mathbf{q}}_v\|^2 - \frac{3\nu}{8}\|\tilde{\boldsymbol{\omega}}\|^2 - \left(\frac{3\nu}{8} - \frac{k_v}{2}\right)\|\tilde{\boldsymbol{\omega}}\|^2 - \frac{k_v}{2}\|\boldsymbol{\omega}_e\|^2 \\ - \frac{k_v}{2}\left(\|\tilde{\boldsymbol{\omega}}\|^2 - 2\boldsymbol{\omega}_e^{\mathrm{T}}\tilde{\boldsymbol{\omega}} + \|\boldsymbol{\omega}_e\|^2\right).\end{aligned} \tag{5.59}$$

If ν is selected in a manner such that

$$\nu = \frac{4k_v}{3}$$

then $\dot{V}$ in Eq. (5.59) further simplifies to

$$\dot{V} \leq -\frac{\nu\mu\gamma\lambda}{2}\|\tilde{\mathbf{q}}_v\|^2 - \frac{3\nu}{8}\|\tilde{\boldsymbol{\omega}}\|^2 - \frac{k_v}{2}\|\boldsymbol{\omega}_e\|^2. \tag{5.60}$$

As a result, $\tilde{\mathbf{q}}_v$, $\tilde{\boldsymbol{\omega}}$, $\boldsymbol{\omega}_e$, and $\mathbf{q}_{e_v}$ are all bounded signals. Further, from Eqs. (2.12),(2.13),(5.14), and (5.18) it follows that $\dot{\tilde{\mathbf{q}}}_v$, $\dot{\tilde{\boldsymbol{\omega}}}$, $\dot{\boldsymbol{\omega}}_e, \dot{\mathbf{q}}_{e_v} \in \mathcal{L}_\infty$. Since $V \geq 0$, $\int_0^\infty \dot{V}(t)\,\mathrm{d}t$ exists and is finite which together with Eq. (5.60) implies that $\tilde{\mathbf{q}}_v, \tilde{\boldsymbol{\omega}}, \boldsymbol{\omega}_e \in \mathcal{L}_2 \cap \mathcal{L}_\infty$. Invoking Barbalat's lemma yields

$$\lim_{t\to\infty}\left[\tilde{\mathbf{q}}_v(t),\ \tilde{\boldsymbol{\omega}}(t),\ \boldsymbol{\omega}_e(t)\right] = 0. \tag{5.61}$$

Through a recursive application of Barbalat's lemma, it can be shown that $\dot{\boldsymbol{\omega}}_e(t) \to 0$ as $t \to \infty$ owing to the fact that $\ddot{\boldsymbol{\omega}}_e \in \mathcal{L}_\infty$ since $\boldsymbol{\omega}_r$ is bounded and twice differentiable. Then from Eqs. (2.13) and (5.27), it follows that $\mathbf{q}_{e_v}(t) \to 0$ as $t \to \infty$ which completes the proof. □

Remark 5.3.1. It is important to emphasize that the additional negative term in $\tilde{\boldsymbol{\omega}}$ obtained as a result from the strictification process outlined in Proposition 5.2.3, is essential in proving this result. Without this additional negative term, it would not have been possible to dominate the mixed term $k_v \boldsymbol{\omega}_e^{\mathrm{T}} \tilde{\boldsymbol{\omega}}$ and obtain global asymptotic convergence of all the estimation and tracking error states.

Remark 5.3.2. The separation property established in Theorem 5.3.1 for the nonlinear rigid body dynamics is specific to a proportional-derivative control structure. Thus, the notion of "separation property" is used here with a slight caveat as it does not precisely follow the classical linear-systems terminology in which *any* independently designed state-feedback linear control law may be combined with a Luenberger observer to guarantee overall stability of the closed-loop linear system [6, 48].

5.4 Numerical Simulations

In this section, a series of numerical simulation studies are conducted to demonstrate the performance of the novel smooth angular velocity observer developed in the preceding sections for attitude control tasks. The inertia matrix of the rigid spacecraft is selected from literature as [15]

$$\mathbf{J} = \begin{bmatrix} 10 & 1.2 & 0.5 \\ 1.2 & 19 & 1.5 \\ 0.5 & 1.5 & 25 \end{bmatrix}. \tag{5.62}$$

For each set of simulations, the spacecraft is assumed to have the initial attitude $\mathbf{q}(0) = [\sqrt{1-(3(0.1^2))}, -0.1, 0.1, -0.1]^{\mathrm{T}}$ and initial angular velocity $\boldsymbol{\omega}(0) = [0.005, 0.006, 0.004]^{\mathrm{T}}$ rad/s. The initial reference quaternion is selected as $\mathbf{q}_r(0) = [\sqrt{1-3(0.1826^2)}, 0.1826, 0.1826, 0.1826]^{\mathrm{T}}$, while the reference angular velocity profile is generated at each instant by $\boldsymbol{\omega}_r = r(t) \cdot [1,1,1]^{\mathrm{T}}$ rad/s where

$$r(t) = 0.1\cos(t)(1 - e^{0.01t^2}) + (0.08\pi + 0.006\sin(t))te^{-0.01t^2}.$$

The performance of the control law, Eq. (5.27), which uses angular velocity estimates from the new observer Eqs. (5.11)-(5.12), is compared to the control law Eq. (5.1), wherein the angular velocity is perfectly measured and available for feedback. In each of the simulation studies, the control and estimation gain values are selected as

$$k_p = 1.5,\ k_v = 5; \qquad \lambda = 1,\ \gamma = 3.$$

5.4.1 Quaternion Measurements Without Noise

The first set of simulations is conducted for the case when the attitude quaternion $\mathbf{q}$ is assumed to be "measured" perfectly without noise. Note that in reality, no sensor is able to directly measure the attitude vector of a vehicle. Rather, the quaternion is reconstructed from a set of two or more non-collinear unit vector measurements (such as those obtained from a star or sun sensor) using an estimation or observer scheme. Thus, from a practical perspective,

this particular simulation study assumes that the attitude quaternion of the rigid body has already been exactly reconstructed through an observer for control feedback. The observer initial conditions are $\hat{\mathbf{q}}(0) = \mathbf{q}(0)$ and angular velocity estimate $\hat{\boldsymbol{\omega}}(0) = [-0.03, 0.01, -0.02]^{\mathrm{T}}$ rad/s. The plots shown in Figs. 5.1-5.2 illustrate the tracking, observer, and controller performance when the attitude vector is perfectly measured.

It is clear from the results of Fig. 5.1 that both the PD and observer-based controllers are able to command convergence of tracking errors within 60 seconds. The observer-based system achieves estimation error convergence within 50 seconds. Once the estimation errors $\tilde{\boldsymbol{\omega}}$ and $\tilde{\mathbf{q}}$ have converged, the steady-state behaviors of both the tracking errors as well as the control history of the observer-based closed-loop system are identical to the full-state feedback control system. However, note in Figs. 5.1a-5.1b that the transient performance of the closed-loop system that assumes availability of the true angular velocity is slightly faster compared with the observer-based system that is simultaneously compensating for the difference in the true angular velocity and the estimated angular velocity. Indeed, larger transient oscillations are observed, especially for angular velocity tracking error, in the case of the controller based on angular velocity observer. The overall control effort for the observer-based feedback is also slightly higher during the transient period in comparison to the full-state feedback control. In fact, it is observed through additional simulations (omitted here for brevity) that larger initial estimation errors result in larger and more frequent transient oscillations in error states

as well as increased control effort for the observer-based control system. This is expected and reasonable, since an increased control effort is expended in compensating for larger discrepancies in the true and estimated values of the angular velocity.

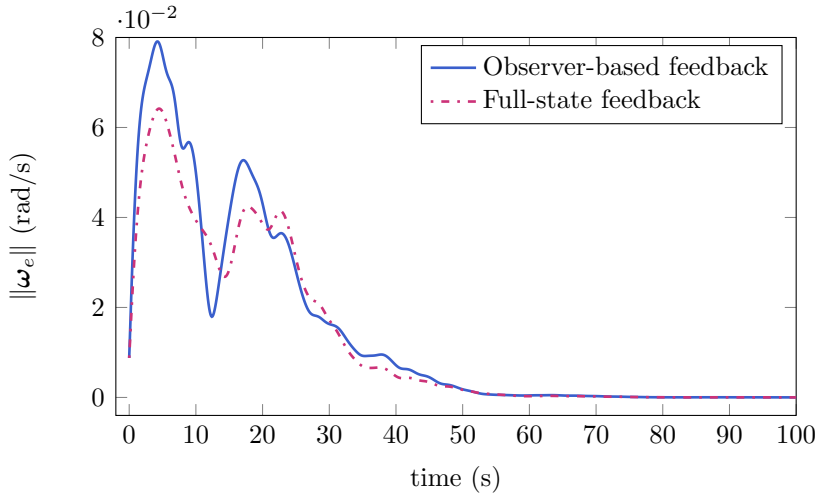

(a) Angular velocity tracking error norm

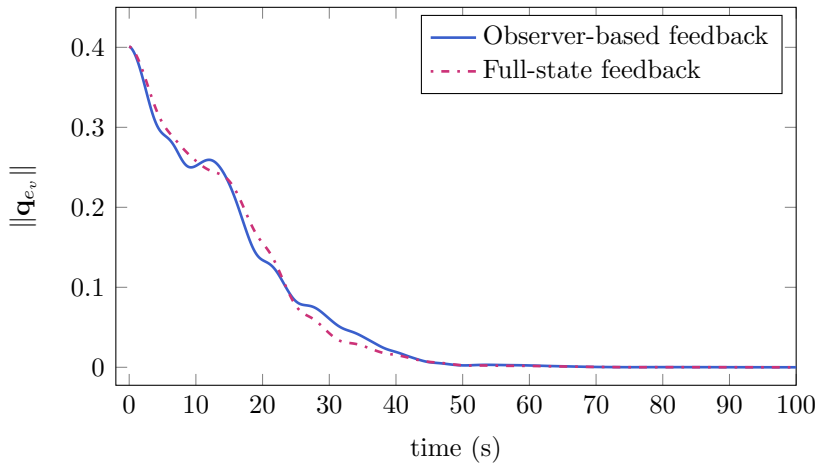

(b) Quaternion tracking error norm

Figure 5.1: Comparison of observer-based PD control with full-state feedback control without measurement noise.

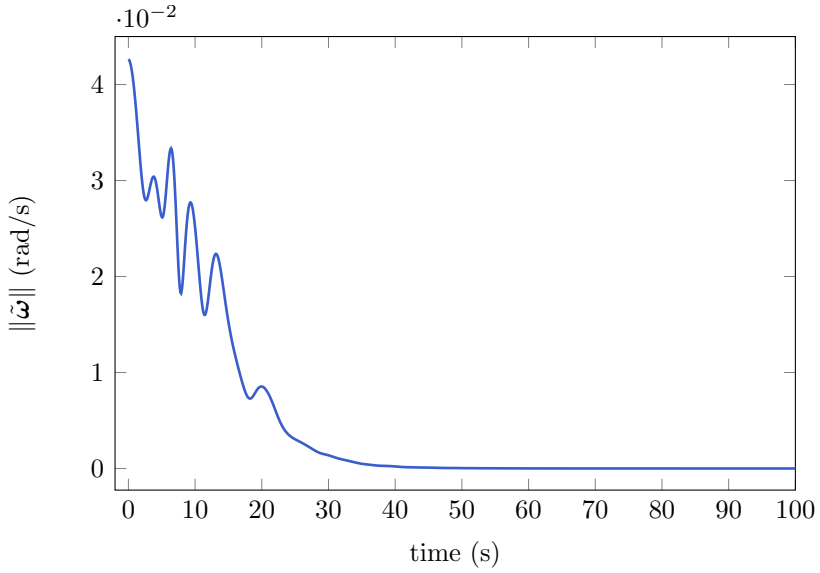

(a) Angular velocity estimation error norm

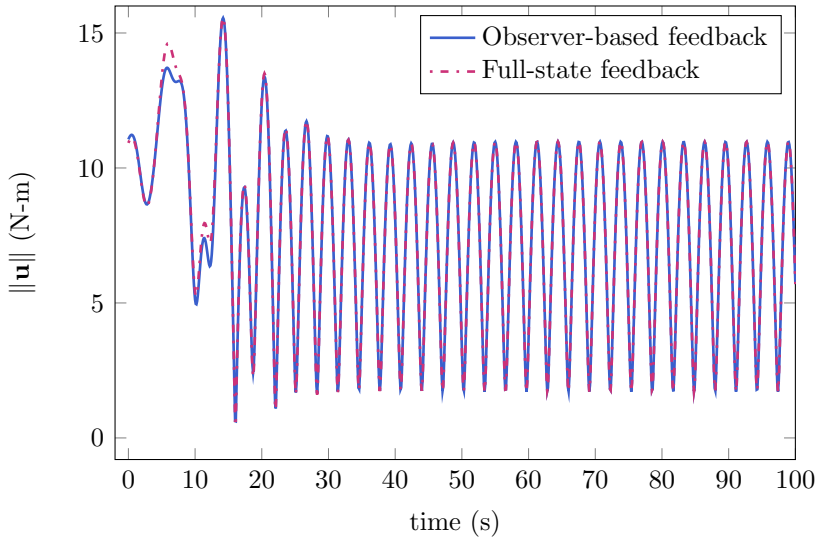

(b) Control torque norm

Figure 5.2: Angular velocity estimation error and commanded control effort for attitude tracking control simulation in the absence of measurement noise.

5.4.2 Quaternion Measurements With Noise

Next, we examine the robustness of the proposed estimation scheme subject to measurement noise/error. The simulations in Figs. 5.1-5.2 are repeated with measurement noise added to $\mathbf{q}$ for both observer and control law feedback. Noisy measurements are generated by randomly perturbing the true unit-length eigenaxis, $\mathbf{e}$, associated with $\mathbf{q}$ [53],

$$\mathbf{e} = \frac{1}{\sin\frac{\theta}{2}}\mathbf{q}_v, \quad \cos\frac{\theta}{2} = q_0,$$

where θ is the eigenangle, within a spherical cone of prescribed cone half-angle and uniform distribution centered around the true eigenaxis at each time t. The cone half-angle is specified as 0.05 deg for this simulation.

In order to clearly illustrate differences between the observer-based and full-state feedback controllers, the norms of all error vectors are plotted on a semilogarithmic scale as shown in Figs. 5.3-5.4. Although each component of the estimation-error and tracking-error states remain bounded, it is evident that both the observer and full-state feedback controllers suffer in overall performance when measurement noise is present. The attitude estimation and tracking errors are only minimized to a non-zero steady-state value. The full-stated feedback control performs only slightly better by minimizing the tracking error to a marginally smaller value.

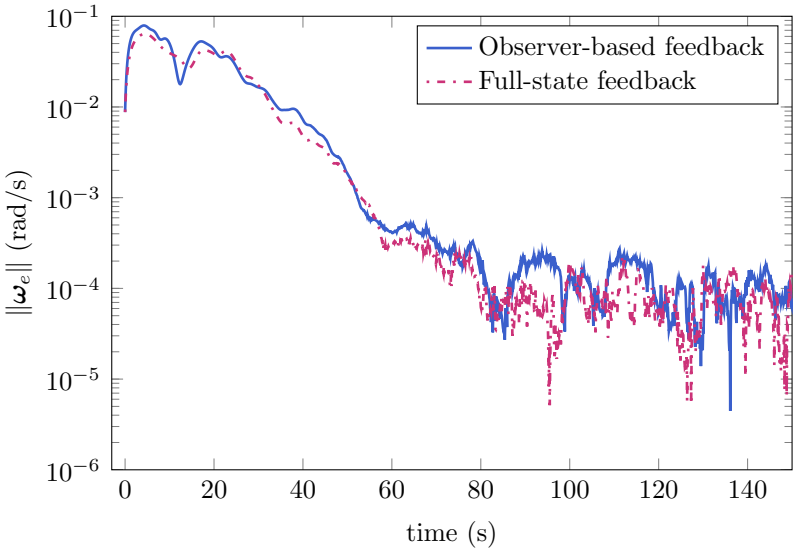

(a) Angular velocity tracking error norm

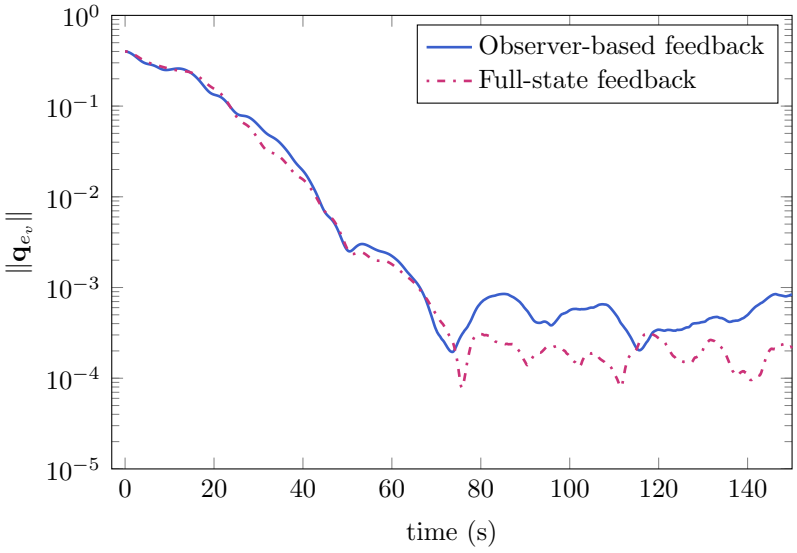

(b) Quaternion tracking error norm

Figure 5.3: Attitude tracking control simulation comparing performance of observer-based and full-state feedback control laws when noise is present in attitude measurements.

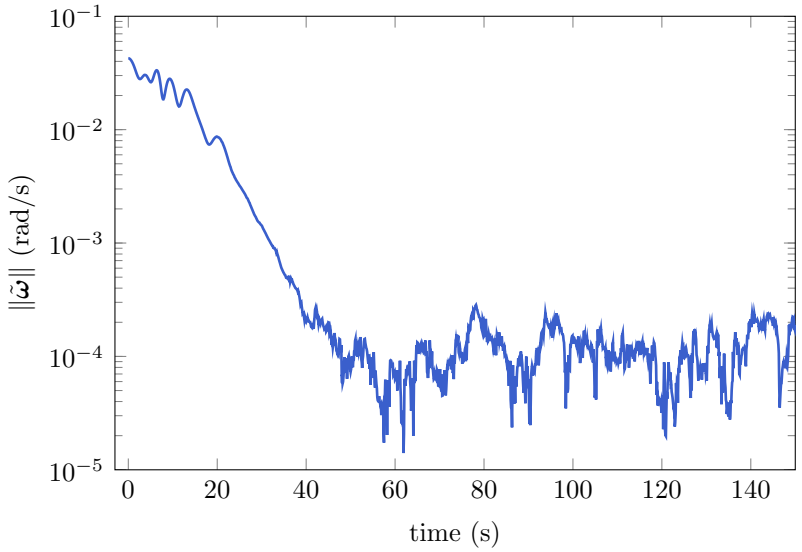

(a) Angular velocity estimation error norm

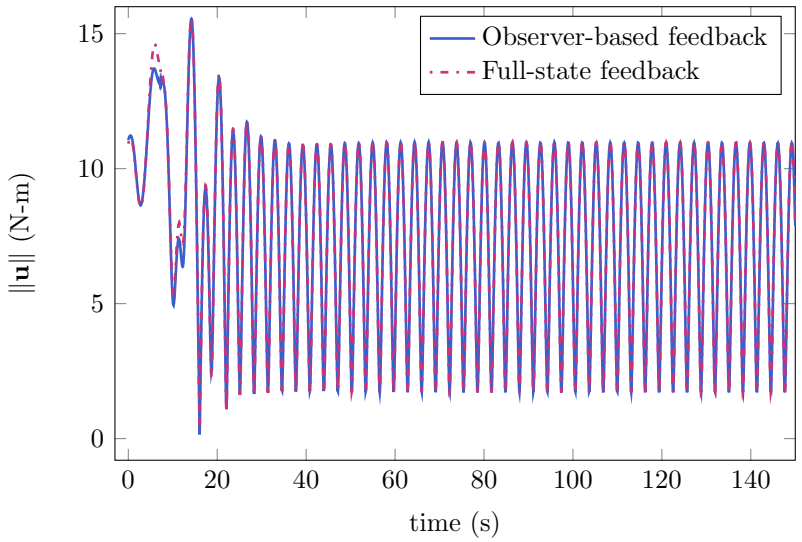

(b) Control torque norm

Figure 5.4: Estimation error evolution and commanded control effort for attitude tracking in the presence of measurement noise.

In order to further corroborate the results in Figs. 5.3-5.4 and show through numerical simulations that measurement noise doesn't result in unbounded tracking and estimation errors, the effects of measurement noise are now investigated for the proposed observer-controller scheme using 10 random initial conditions for $\mathbf{q}(0)$, $\boldsymbol{\omega}(0)$, and $\hat{\boldsymbol{\omega}}(0)$. Using the same cone half-angle for the perturbed eigenaxis, the results are provided in Figs. 5.5-5.6. The plots clearly indicate that both the tracking and estimation errors converge to a bounded residual set.

Finally, as would be expected, it was found through additional simulations (not shown) that increasing the measurement noise cone angle worsened the overall performance of both control schemes by increasing the steady state values of the attitude tracking and estimation error norms. For example, a cone half-angle of 0.5 deg results in increasing the steady-state values of the error norms by almost a full order of magnitude when compared with 0.05 deg cone angle. The magnitude of the estimation and tracking error norms is dictated by the magnitude of measurement noise. Thus, empirical evidence suggests that the observer-based control scheme is not adversely effected any worse than the PD based control in the presence of noisy measurements.

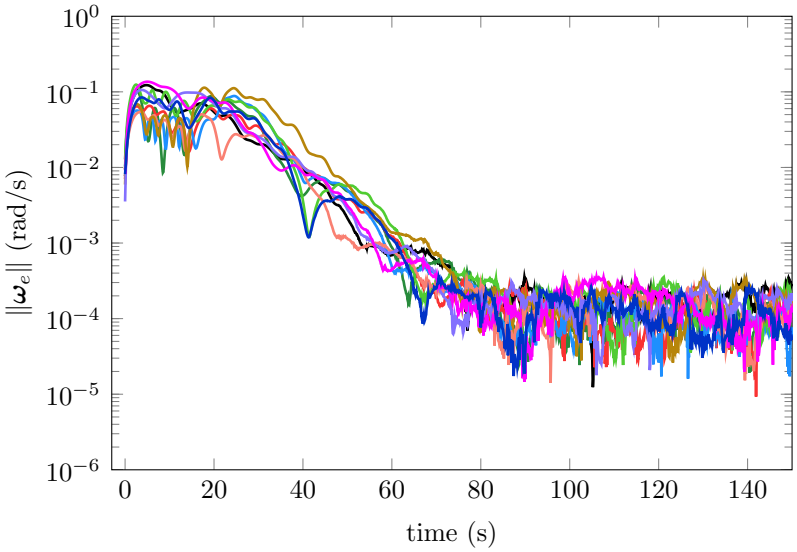

(a) Angular velocity tracking error norm

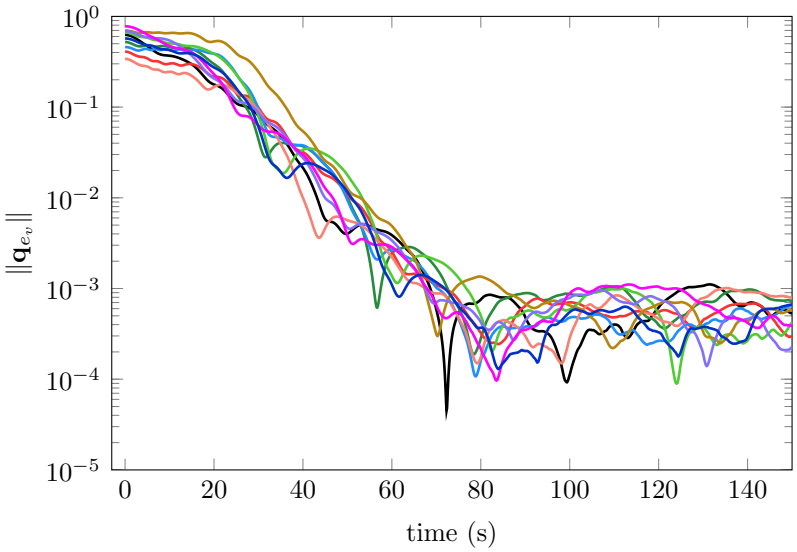

(b) Quaternion tracking error norm

Figure 5.5: Attitude tracking control simulation for proposed observer-controller scheme using 10 random initial conditions with noisy attitude measurements.

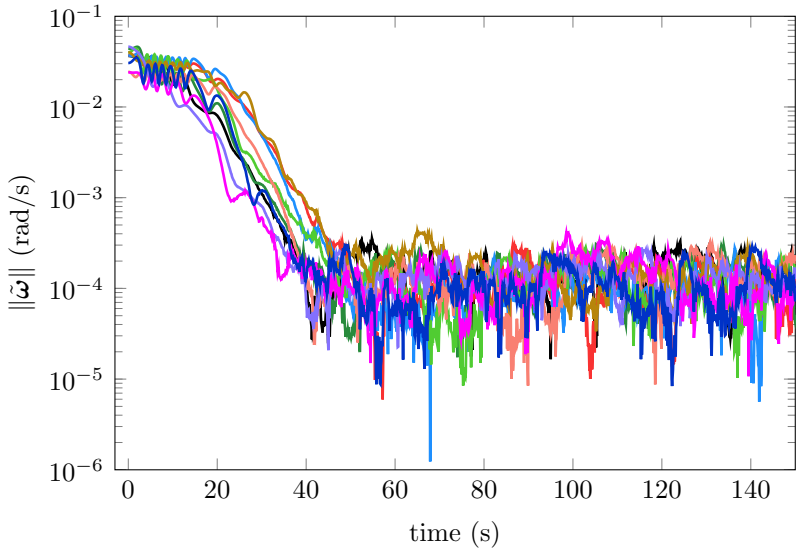

(a) Angular velocity estimation error norm

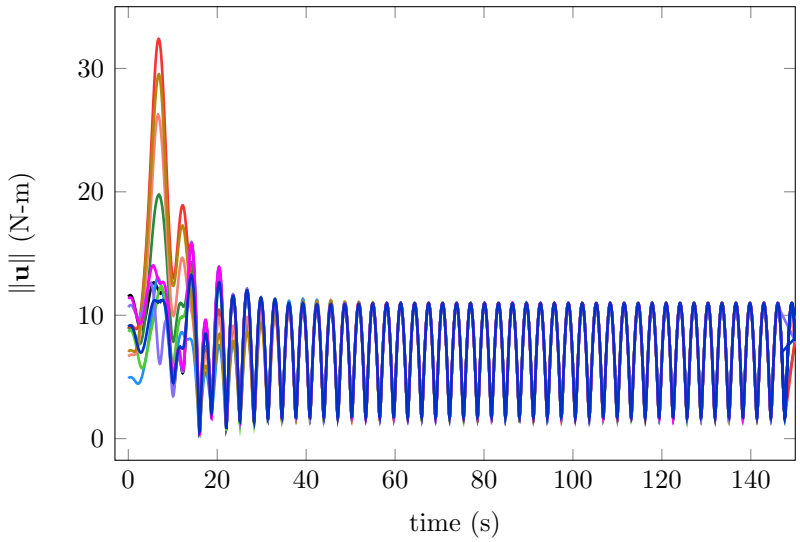

(b) Control torque norm

Figure 5.6: Estimation error evolution and commanded control effort for simulation conducted with the combined observer-controller implementation using 10 random initial conditions.

5.4.3 Estimated Quaternion Using QUEST

In practical spacecraft implementations, since no sensor is directly able to measure the attitude vector (quaternion, MRPs, Gibb's vectors, etc.) of a body, the attitude quaternion is reconstructed using an estimation or observer scheme. Single-frame estimators such as QUEST, ESOQ, ESOQ-2, and their variants are based on Wahba's problem [59, 75]. In this section, a numerical simulation study is conducted in which unit vector measurements are used to construct the body quaternion that is to be used for control feedback. Since rate gyro measurements are unavailable, a point-wise estimation scheme is implemented. In particular, the QUEST algorithm [36, 59] is utilized under the assumption that three unit vector measurements are available at each time, of which at least two are non-collinear. Recalling that the quaternion parameterization in non-unique and each physical attitude may be equivalently described by $\mathbf{q}$ or $-\mathbf{q}$, it is necessary to ensure that the calculated quaternion at each time step maintains sign continuity with the quaternion at the previous time step, that is, no sign jumps occur discontinuously.

All simulation parameters remain the same as in the previous two simulations and no measurement noise is assumed in the vector measurements. The resulting plots are shown in Fig. 5.7. The system responses in Fig. 5.7 using the QUEST algorithm to estimate the quaternion are virtually identical to the system responses in Fig. 5.1. As such, the angular velocity observer developed here is practically viable for spacecraft implementation where both the controller and observer would utilize an estimated quaternion.

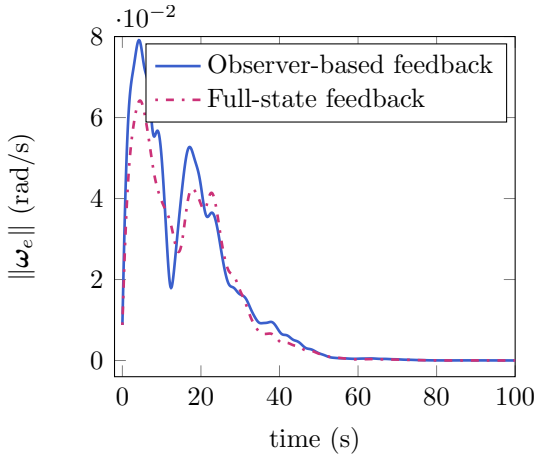

(a) Angular velocity tracking error norm

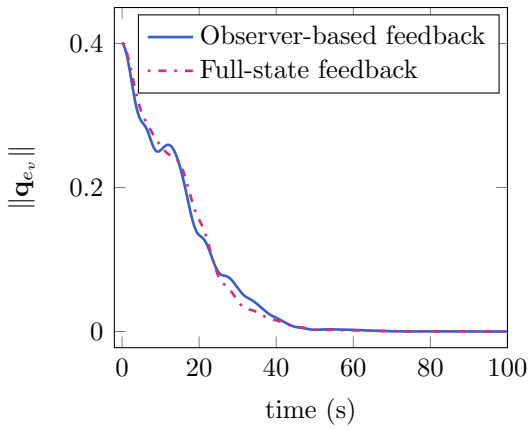

(b) Quaternion tracking error norm

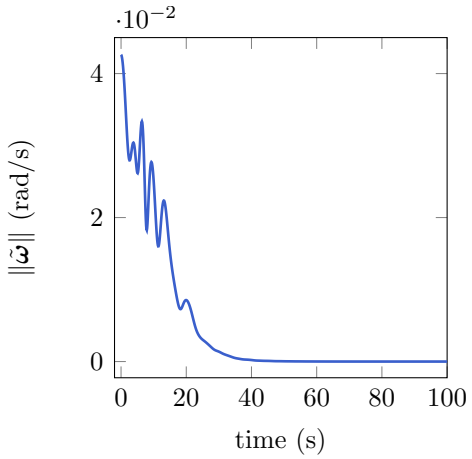

(c) Angular velocity estimation error norm

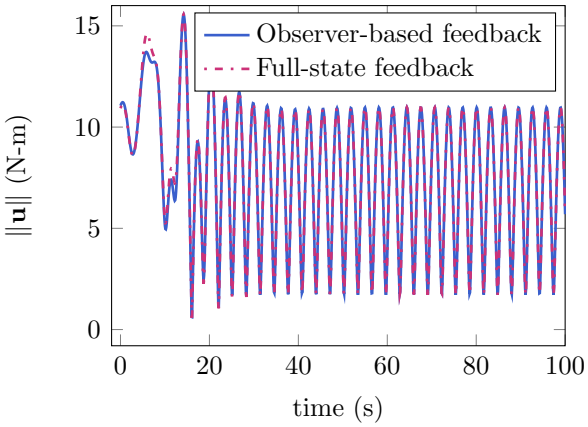

(d) Control torque norm

Figure 5.7: Attitude tracking control simulation for observer and controller driven by estimates of $\mathbf{q}$ generated by QUEST algorithm (no sensor noise). System response is identical to that in Figs. 5.1-5.2 where the quaternion is assumed to be directly available.

5.4.4 Inertia Matrix Uncertainty

In the final set of simulations, the convergence properties of the observer are evaluated for an imprecisely determined inertia matrix $\mathbf{J}$. As shown in Sec. 5.2.2, the observer is constructed using perfect knowledge of the inertia matrix. Hence, it is important to investigate, through numerical simulations, how robust the observer is in the face of parameter uncertainty. A zero-torque ($\mathbf{u}(t) = 0 \; \forall \; t \geq 0$) setting is prescribed in order to isolate only the behavior of the observer in the presence of inertia uncertainty. The true inertia matrix parameters are perturbed in a manner such that the perturbed inertia matrix $\mathbf{J}_{\text{pert}}$ takes on the form $\mathbf{J}_{\text{pert}} = \mathbf{J} + \Delta\mathbf{J}$ where $\Delta\mathbf{J} \in \mathbb{R}^{3\times 3}$ with $\Delta\mathbf{J} = \Delta\mathbf{J}^{\text{T}}$. In particular, the observer performance is investigated when subject to the following uncertainty:

$$\Delta\mathbf{J}_1 = \begin{bmatrix} 1 & 1 & 1.5 \\ 1 & 1 & 1.5 \\ 1.5 & 1.5 & -1 \end{bmatrix}, \qquad \Delta\mathbf{J}_2 = \begin{bmatrix} -1 & -0.4 & 0.6 \\ -0.4 & -2 & -0.7 \\ 0.6 & -0.7 & -5 \end{bmatrix}, \tag{5.63}$$

where $\|\Delta\mathbf{J}_1\| \approx 0.1\|\mathbf{J}\|$ and $\|\Delta\mathbf{J}_2\| \approx 0.3\|\mathbf{J}\|$.

In Fig. 5.8, the convergence behavior of the observer using the perturbed inertia matrices is compared to the observer performance when the true inertia parameters are exactly determined. Both the transient and steady state behaviors of the state estimation errors are clearly affected by the quality and magnitude of the uncertainty in the inertia matrix. While $\Delta\mathbf{J}_1$ represents a larger magnitude of uncertainty, it also corresponds with an overall perturbed

inertia matrix with smaller principal moments of inertia than the true inertia matrix. While the state estimation errors resulting from the observer employing $\mathbf{J}$ perturbed by $\Delta\mathbf{J}_1$ may appear to initially converge faster than when the inertia matrix is exactly known, the estimation errors ultimately only converges to within a bounded residual set. When the inertia uncertainty is given by $\Delta\mathbf{J}_2$, the perturbed inertia matrix results in a slightly larger principal moments of inertia than the true inertia matrix. In this case, while the transient performance is similar to when there are no perturbations in $\mathbf{J}$, once again, the state estimation errors only converge to a bounded residual set.

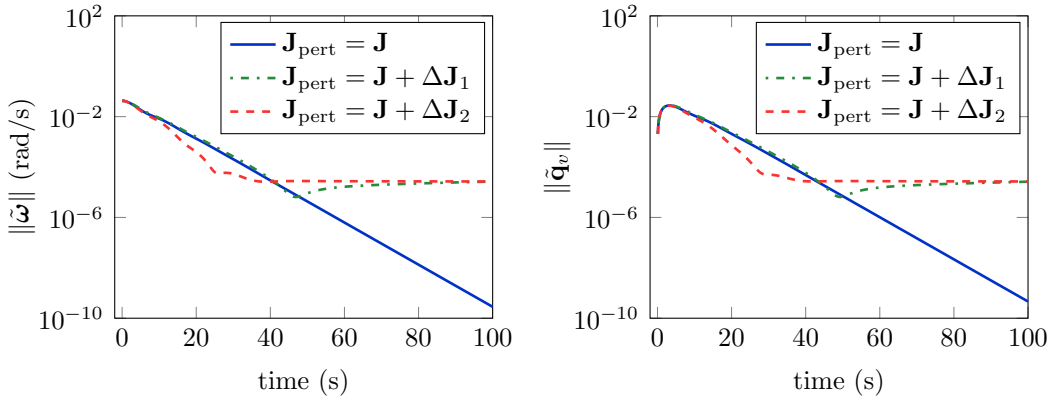

(a) Angular velocity estimation error norm

(b) Quaternion estimation error norm

Figure 5.8: Convergence properties of state estimation errors from the observer when inertia matrix parameters are uncertain.

5.5 Conclusions

In this chapter, the problem of angular velocity observer design is addressed for rigid body attitude tracking control in the absence of angular velocity mea-

surements. A novel smooth angular velocity observer is presented that ensures asymptotic convergence of estimation error states independently of the control design. Unlike existing methods that employ a switching scheme, the proposed observer ensures asymptotic convergence through a smooth structure. When combined with a separately designed PD attitude tracking control law, the novel observer scheme ensures global asymptotically stability of the closed-loop system. Accordingly, a separation property is established for the rigid-body attitude tracking problem with a smooth angular velocity observer construct, the first such result to the best of the author's knowledge. The distinguishing feature of this rich technical result lies in the use of a partial Lyapunov strictification process by which a non-strict Lyapunov function is converted into a strict Lyapunov function whose time derivatives contain nonpositive terms in all estimation error states. Closed-loop stability and convergence are proved by following a sequential logic approach, and the effectiveness of the combined observer-controller implementation is illustrated through numerical simulation studies.

Chapter 6

Conclusions

6.1 Summary

Attitude control is a technically rich and extensively studied subject in controls literature dating back several decades. A wide range of control solutions (linear, nonlinear, adaptive, observer-based, etc.) exist for various problem formulations. In the field of aerospace engineering, precise control of a spacecraft's orientation is often crucial to mission success, especially for those carrying out Earth-based observations, surveillance, or rendezvous applications. In this dissertation, the investigation of attitude control is undertaken to address three important aspects of the problem, mainly, adaptive control for time varying inertia matrix components, gyro-free attitude control design using unit vector measurements, and observer control design for attitude control in the absence of angular velocity measurements.

Adaptive control has been the focus of extensive research efforts over

the past many years as a powerful method to deliver precise attitude control for a spacecraft with arbitrarily large inertia matrix uncertainties. While several elegant solutions exist for controlling systems with constant uncertain parameters, research in adaptive attitude control of time-varying parameters is fairly limited. The work presented in Chapter 3, attempts to deal with these limitations by formulating an adaptive control law that compensates for time-varying parameters with known variation but unknown additive and multiplicative uncertainty.

The novel adaptive control solution proposed in Chapter 3 directly accounts for two types of inertia matrix variations: the first is formulated as a function of the control input itself in order to model fuel mass-loss, while the second is modeled as a function of time for the case when the variation occurs due to displacing mass (as in the case of a deploying solar array). In both cases, the uncertainty in the inertia matrix is directly handled by the adaptive control approach. When the inertia matrix is a function of the control input, the input coupling in the rigid body dynamics could lead to the control becoming unbounded if the parameter estimates approach zero. To circumvent this issue, using prior knowledge on the overall bounds of the uncertain parameters, a projection mechanism scheme is implemented in conjunction with some mild initial condition restrictions to keep the parameter estimates within a bounded convex set and away from the singularity regime, thereby ensuring a smooth and bounded control input for all time. Detailed derivations of the control law are provided along with a thorough analysis for the associated

stability and error convergence properties. In addition, numerical simulations are presented to highlight the performance benefits when compared with an adaptive control scheme that does not account for inertia variations.

The work in Chapter 4 is motivated by the fact that existing "velocity-free" attitude stabilization control laws require explicit feedback of the spacecraft attitude. However, since no sensor can directly measure the orientation of a vehicle, these control laws rely on an observer or estimator that reconstructs the attitude from unit vector measurements. While numerical algorithms based on Wahba's problem may be used for attitude determination, these algorithms treat the problem in the framework of static optimization and are, as such, not as robust or efficient as Kalman-filter type sequential-estimation techniques. However, filter algorithms require the use of angular velocity information in conjunction with unit-vector measurements. Further, while several nonlinear observers have been proposed that provide explicit convergence guarantees, these observers once again rely on angular velocity feedback. Thus, in the absence of angular velocity, the use of these estimation/observer schemes is not feasible.

Motivated by this shortcoming, Chapter 4 presents a novel attitude stabilization control law that is truly "velocity-free" in that it neither relies on angular velocity information directly through control feedback or indirectly through use in an estimation/observer algorithm that provides the attitude vector. Rather, the control law guarantees asymptotic convergence of the attitude and angular velocity by directly employing vector measurements for

feedback. Furthermore, the result presented herein is rooted in the classical passivity framework and does not utilize any observer-like scheme to satisfy the control result. Lyapunov-based stability analysis is used to prove asymptotic stabilization of the spacecraft to the desired orientation with zero angular velocity and all closed-loop signals remaining bounded. In addition, numerical simulation studies indicate that the novel gyro-free attitude control is robust to measurement errors to within a residual set.

In Chapter 5, a novel angular velocity observer is developed for attitude tracking control applications. The problem is motivated by the fact that gyro-failures or unreliability may lead to the angular velocity information being unavailable for use in typical PD like control laws. Unlike existing results that employ a switching structure for the observer to guarantee convergence to the true angular velocity, the new result presented herein is smooth and does not rely on switched or hybrid schemes. This important result stems from the use of a novel Lyapunov strictification process which plays a crucial role in formulating a strict Lyapunov function which contains negative terms in both the attitude and angular velocity estimation states. The proposed observer ensures asymptotic convergence of the estimated states to the true angular velocity independently of the control design. The observer is readily combined with an existing PD control law while still retaining asymptotic convergence properties of both the attitude tracking error and estimation error states. Thus, a separation property is established for the attitude tracking control problem when the smooth angular velocity observer is combined with

a PD control law. Lyapunov-based stability analysis is provided to prove all asserted claims in the chapter, while numerical simulation studies show that the algorithm is robust to noisy measurements and can be implemented using a QUEST-type attitude determination algorithm to reconstruct the quaternion from vector measurements.

6.2 Statement of Contributions

The following original contributions have been made in this dissertation to the field of attitude tracking control for spacecraft applications:

1. A novel adaptive attitude control scheme is proposed to directly compensate for spacecraft inertia changes arising from fuel mass-loss due to fast propulsive maneuvers and mass displacement commonly associated with deployable spacecraft components. Existing work in this area has previously only dealt with unknown constant inertia matrix components. In the work presented in this dissertation, spacecraft inertia matrix parameters are assumed to have known variable components with arbitrarily large multiplicative and additive uncertainties. The novel control law tackles inertia variations that occur as either pure functions of the control input, or functions of time and/or the state. The proposed control scheme has practical advantages over typical adaptive attitude tracking control since spacecraft often encounter non-trivial variations in inertia during flight [71, 72].

2. In the setting of complete absence of rate measurements either due to gyro-failure or unavailability, a novel stabilizing controller is proposed that utilizes vector measurements obtained from inertial sensors directly for feedback, without relying on the estimated attitude vector or angular velocity feedback. The control law is formulated in the classical passive systems framework, and does not rely on observers of any kind. Although many classical results for angular velocity-free control laws are available in existing literature, they are typically formulated using some kind of attitude parameterization. As such, these control laws must be integrated with an attitude estimation scheme that can provide the attitude of the vehicle using a combination of gyro-rate and vector measurements. Thus, regardless of the approach, most existing control laws have either an explicit or implicit requirement for angular velocity measurements. From this standpoint, a true "velocity-free" attitude control law has been developed in this dissertation, since both the direct and indirect requirement of angular velocity is completely eliminated. The distinguishing feature of this methodology is that, unlike existing results, the velocity-free control law is founded on the classical passive systems theory [63, 65].

3. A novel nonlinear switching-free angular velocity observer has been developed for attitude tracking control. The salient feature of this observer is that unlike existing methodologies that implement a switching scheme to obtain estimation error convergence, the presented observer is smooth

and ensures $\mathcal{C}^\infty$ continuity of estimation states. The observer guarantees asymptotic convergence of the estimation errors independently of the control design.

4. A separation property has been established for the combined implementation of the novel smooth observer developed in this dissertation with a separately designed PD attitude tracking control law. This result is the first of its kind for a smooth (switching-free) observer construction. [4, 70].

6.3 Recommendations for Future Research

Several avenues of future research have been identified to further the advancement of the research presented in this dissertation. A few important research directions are outlined below.

1. In Chapter 3, adaptive tracking control is presented for time-varying inertia matrix. A simplified model is provided to represent the variations that occur as a result of fuel-loss. An important area for further work would be to better model these variations based on the hardware components being used onboard.

2. The adaptive control in Chapter 3 is based on the certainty-equivalence (CE) principle. A worthwile direction for future research would be to derive the control law in a noncertainty equivalent framework [55, 56], which has been shown to be deliver overall performance which is superior

to CE adaptive control. The performance gains in non-CE adaptive control is a direct consequence of a stable attractive manifold design on the parameter adaptation process which leads to two important features: 1) parameter estimation stops whenever the estimates coincide with their true values, and 2) the closed-loop adaptive control system recovers the same performance as a deterministic (ideal) control law without parameter uncertainty.

3. The gyro-free attitude control law presented in Chapter 4 only handles the attitude stabilization question. Some technical limitations that prevent the extension of this control law to the full tracking case have been discussed in the chapter. A natural direction for this research would be to further explore the full tracking case through a different Lyapunov function construction or a modified control law.

4. Another useful line of future research for the gyro-free attitude stabilization problem would be to determine an effective way of selecting the matrices $\mathbf{A}$, $\mathbf{B}$, and $\mathbf{P}$ which is in some sense optimal for this particular problem. At present, these matrices are determined through a tedious trial and error process. An effective mechanization of this process would be very useful in consistently determining matrix quantities that yield fast convergence performance.

5. The observer presented in Chapter 5 has been developed under the assumption that the attitude vector is already available for use in the ob-

server and control design. A very important area of future research could focus on the development of an angular velocity observer that employs vector measurements directly rather than using the quaternion. Thus, this problem would run parallel to the problem of attitude tracking using vector measurement feedback. The main complication that may arise in this approach is that the mapping from the angular velocity estimation frame to the body frame would not be readily available, which is currently a critical piece of information that is used to compensate for the nonlinear gyroscopic angular velocity term in the rigid body dynamics and prove global asymptotic convergence. One way to circumvent this issue may be to estimate the quaternion alongside the angular velocity, although this brings up the circular issue that quaternion observers also typically rely on angular velocity information.

6. A final recommendation on the problem of angular velocity estimation is to investigate an adaptive angular velocity observer that does not require perfect knowledge of $\mathbf{J}$. Currently, the model-dependent observer presented in Chapter 5 experiences performance degradation when faced with inertia matrix uncertainty. Thus, a very useful line of research would be to explicitly account for inertia matrix uncertainties through parameter adaptation. Of course, this matter is complicated by the fact that adaptation typically relies on precise knowledge of the spacecraft angular velocity, and poses a significant challenge in simultaneously resolving these inherently coupled problems.

Appendix A

List of Publications

A.1 Relevant Journal Publications

1. D. Thakur and M. R. Akella. Gyro Free Rigid Body Attitude Stabilization Using Only Vector Measurements. *AIAA Journal of Guidance, Control, and Dynamics*. Article in review.

2. M. R. Akella, D. Thakur, and F. Mazenc. Partial Lyapunov Strictification: Smooth Angular Velocity Observers for Attitude Tracking Control. *AIAA Journal of Guidance, Control, and Dynamics*. Article in review.

3. D. Thakur, S. Srikant, and M. R. Akella. Adaptive Attitude-Tracking Control of Spacecraft with Uncertain Time-Varying Inertia Parameters. *AIAA Journal of Guidance, Control, and Dynamics*. Article in review.

A.2 Relevant Conference Publications

1. D. Thakur, F. Mazenc, and M. R. Akella. Partial Lyapunov Strictification: Smooth Angular Velocity Observers for Attitude Tracking Control. In *AIAA Space and Astronautics Forum and Exposition*, San Diego, CA, August 2014. Paper No. AIAA-2014-4420.

2. D. Thakur and M. R. Akella. Gyro Free Rigid Body Attitude Stabilization Using Only Vector Measurements on $SO(3)$. In *Proceedings of the 24th AAS/AIAA Space Flight Mechanics Meeting*, Santa Fe, NM, January 2014. Paper No. AAS 14-300.

3. D. Thakur, S. Srikant, and M. R. Akella. Adaptive Attitude-Tracking Control of Spacecraft with Uncertain Time-Varying Inertia Parameters. In *Proceedings of the 2013 AAS/AIAA Astrodynamics Specialist Conference*, Hilton Head, SC, August 2013. Paper No. AAS 13-838.

A.3 Other Publications

1. D. Thakur, S. Hernandez, and M. R. Akella. Spacecraft Swarm Finite-Thrust Cooperative Control Protocol for Common Orbit Convergence. In *24th AAS/AIAA Space Flight Mechanics Meeting*, Santa Fe, NM, January 2014. Paper No. AAS14-380.

2. D. Thakur, S. Hernandez, and M. R. Akella. Spacecraft Swarm Finite-Thrust Cooperative Control Protocol for Common Orbit Convergence.

AIAA Journal of Guidance, Control, and Dynamics. Article in review.

3. D. Thakur and M. R. Akella. Coordinated Control of Autonomous Vehicles in Three-Dimensional Rotating Formations. In *Proceedings of the 2013 AAS/AIAA Astrodynamics Specialist Conference*, Hilton Head, SC, August 2013. Paper No. AAS 13-918.

4. D. Thakur and B. G. Marchand. Hybrid Optimal Control for HIV Multi-Drug Therapies: A Finite Set Control Transcription Approach. *Mathematical Biosciences and Engineering*, 9:899 – 914, 2012.

5. D. Thakur and B. G. Marchand. Tracking Control of Nanosatellites with Uncertain Time Varying Parameters. In *Proceedings of the 2011 AAS/AIAA Astrodynamics Specialist Conference*, Girdwood, AK, August 2011. Paper No. AAS 11-592.

Bibliography

[1] J. Ahmed and D. S. Bernstein. Globally Convergent Adaptive Control of Spacecraft Angular Velocity Without Inertia Modeling. *American Control Conference*, 3(1):1540–1544, 1999.

[2] M. R. Akella, D. Seo, and R. Zanetti. Attracting Manifolds for Attitude Estimation in Flatland and Otherlands. *The Journal of the Astronautical Sciences*, 54(3-4):635–655, 2006.

[3] M. R. Akella and K. Subbarao. A Novel Parameter Projection Mechanism for Smooth and Stable Adaptive Control. *Systems & control letters*, 54(1):43–51, 2005.

[4] M. R. Akella, D. Thakur, and F. Mazenc. Partial Lyapunov Strictification: Smooth Angular Velocity Observers for Attitude Tracking Control. *AIAA Journal of Guidance, Control, and Dynamics*. Article in review.

[5] A. M. Annaswamy and K. S. Narendra. Adaptive Control of Simple Time Varying Systems. In *Proceedings of the 28th IEEE Conference on Decision and Control*, pages 1014–1018 vol.2, 1989.

[6] P. J. Antsaklis and A. N. Michel. *Linear Systems*, chapter 4. Birkhäuser, 2006.

[7] A. Astolfi and R. Ortega. Immersion and Invariance: A New Tool for Stabilization and Adaptive Control of Nonlinear Systems. *IEEE Trans. on Automatic Control*, 48(2):590–606, 2003.

[8] R. Bakker and A. Annaswamy. Stability and robustness properties of a simple adaptive controller. *Automatic Control, IEEE Transactions on*, 41(9):1352–1358, 1996.

[9] I. Y. Bar-Itzhack. REQUEST-A Recursive QUEST Algorithm for Sequential Attitude Determination. *Journal of Guidance, Control, and Dynamics*, 19(5):1034–1038, 1996.

[10] S. P. Bhat and D. S. Bernstein. A Topological Obstruction to Continuous Global Stabilization of Rotational Motion and the Unwinding Phenomenon. *Systems & Control Letters*, 39(1):63–70, 2000.

[11] F. Bullo and R. M. Murray. Proportional derivative (PD) control on the Euclidean group. In *European Control Conference*, pages 1091–1097, Rome, Italy, June 1995.

[12] F. Caccavale and L. Villani. Output Feedback Control for Attitude Tracking. *Systems and Control Letters*, 38:91–98, 1999.

[13] Y. C. Chang. An Adaptive $\mathcal{H}_\infty$ Tracking Control for a Class of Nonlinear

Multiple-Input-Multiple-Output (MIMO) Systems. *IEEE Transactions on Automatic Control*, 46:1432–1437, 2001.

[14] N. A. Chaturvedi, A. K. Sanyal, and N. H. McClamroch. Rigid-body attitude control. *Control Systems, IEEE*, 31(3):30–51, 2011.

[15] A. Chunodkar and M. Akella. Switching Angular Velocity Observer for Rigid-Body Attitude Stabilization and Tracking Control. *Journal of Guidance, Control, and Dynamics*, 37(3):869–878, 2014.

[16] B. T. Costic, D. M. Dawson, M. S. de Queiroz, and V. Kapila. Quaternion-Based Adaptive Attitude Tracking Controller Without Velocity Measurements. *Journal of Guidance, Control, and Dynamics*, 24(6):1214–1222, 2001.

[17] J. L. Crassidis, F. L. Markley, and Y. Cheng. Survey of Nonlinear Attitude Estimation Methods. *Journal of Guidance, Control, and Dynamics*, 30(1):12–28, 2007.

[18] C. A. Desoer and M. Vidyasagar. *Feedback Systems: Input-Output Properties*, chapter 6. SIAM, 2009.

[19] J. R. Forbes. Passivity-Based Attitude Control on the Special Orthogonal Group of Rigid-Body Rotations. *Journal of Guidance, Control, and Dynamics*, 36(6):1596–1605, 2013.

[20] S. S. Ge and J. Wang. Robust Adaptive Tracking for Time-Varying

Uncertain Nonlinear Systems With Unknown Control Coefficients. *IEEE Transactions on Automatic Control*, 48(8):1463–1469, 2003.

[21] G. C. Goodwin and D. Q. Mayne. A parameter estimation perspective of continuous time model reference adaptive control. *Automatica*, 23(1):57–70, 1987.

[22] T. Hamel and R. Mahony. Attitude estimation on $so(3)$ based on direct inertial measurements. In *Proceedings of the 2006 IEEE International Conference on Robotics and Automation*, pages 2170–2175. IEEE, 2006.

[23] P. A. Ioannou and E. B. Kosmatopoulos. *Adaptive Control*. Wiley Online Library, 2006.

[24] P. A. Ioannou and J. Sun. *Robust Adaptive Control*. Courier Dover Publications, 2012.

[25] S. Joshi, A. Kelkar, and J.-Y. Wen. Robust Attitude Stabilization of Spacecraft Using Nonlinear Quaternion Feedback. *Automatic Control, IEEE Transactions on*, 40(10):1800–1803, 1995.

[26] S. P. Kárason and A. M. Annaswamy. Adaptive Control in the Presence of Input Constraints. *IEEE Transactions on Automatic Control*, 39(11):2325–2330, 1994.

[27] H. K. Khalil. Adaptive output feedback control of nonlinear systems represented by input-output models. *Automatic Control, IEEE Transactions on*, 41(2):177–188, 1996.

[28] H. K. Khalil. *Nonlinear Systems*, chapter 3. Prentice-Hall, 1996.

[29] M. Krstic and P. Tsiotras. Inverse Optimal Stabilization of a Rigid Spacecraft. *Automatic Control, IEEE Transactions on*, 44(5):1042–1049, 1999.

[30] E. J. Lefferts, F. L. Markley, and M. D. Shuster. Kalman Filtering for Spacecraft Attitude Estimation. *Journal of Guidance, Control, and Dynamics*, 5(5):417–429, 1982.

[31] F. Lizarralde and J. T. Wen. Attitude Control Without Angular Velocity Measurement: A Passivity Approach. *Automatic Control, IEEE Transactions on*, 41(3):468–472, 1996.

[32] R. Mahony, T. Hamel, and J.-M. Pflimlin. Nonlinear complementary filters on the special orthogonal group. *Automatic Control, IEEE Transactions on*, 53(5):1203–1218, 2008.

[33] M. Malisoff and F. Mazenc. Further Constructions of Strict Lyapunov Functions for Time-Varying Systems. In *American Control Conference, 2005. Proceedings of the 2005*, pages 1889–1894. IEEE, 2005.

[34] M. Malisoff and F. Mazenc. *Constructions of Strict Lyapunov Functions*. Springer Communications and Control Engineering Series, 2009.

[35] F. L. Markley. Attitude Determination Using Vector Observations: A Fast Optimal Matrix Algorithm. *Journal of the Astronautical Sciences*, 41(2):261–280, 1993.

[36] F. L. Markley and D. Mortari. Quaternion attitude estimation using vector observations. *Journal of the Astronautical Sciences*, 48(2):359–380, 2000.

[37] F. Mazenc. Strict Lyapunov Functions for Time-Varying Systems. *Automatica*, 39(2):349–353, 2003.

[38] F. Mazenc, M. Malisoff, and O. Bernard. A Simplified Design for Strict Lyapunov Functions Under Matrosov Conditions. *IEEE Transactions on Automatic Control*, 54(1):177–183, 2009.

[39] F. Mazenc and D. Nesic. Lyapunov Functions for Time-Varying Systems Satisfying Generalized Conditions of Matrosov Theorem. *Mathematics of Control, Signals, and Systems*, 19(2):151–182, 2007.

[40] T. Mercker and M. Akella. Rigid-Body Attitude Tracking with Vector Measurements and Unknown Gyro Bias. *Journal of guidance, control, and dynamics*, 34(5):1474–1484, 2011.

[41] R. H. Middleton and G. C. Goodwin. Adaptive Control of Time-Varying Linear Systems. *IEEE Transactions on Automatic Control*, 33(2):150–155, 1988.

[42] D. Mortari. ESOQ: A closed-form solution to the Wahba problem. *Journal of the Astronautical Sciences*, 45(2):195–204, 1997.

[43] K. S. Narendra. Parameter adaptive control-the end? or the beginning?

In *Decision and Control, 1994., Proceedings of the 33rd IEEE Conference on*, volume 3, pages 2117–2125. IEEE, 1994.

[44] S. Nicosia and P. Tomei. Nonlinear Observer and Output Feedback Attitude Control of Spacecraft. *IEEE Transactions on Aerospace and Electronic Systems*, 28(4):970–977, 1992.

[45] J. B. Pomet and L. Praly. Adaptive nonlinear regulation: Estimation from the Lyapunov equation. *Automatic Control, IEEE Transactions on*, 37(6):729–740, 1992.

[46] P. Pounds, T. Hamel, and R. Mahony. Attitude Control of Rigid Body Dynamics from Biased IMU Measurements. In *Decision and Control, 2007 46th IEEE Conference on*, pages 4620–4625. IEEE, 2007.

[47] M. R Akella. Rigid Body Attitude Tracking Without Angular Velocity Feedback. *Systems & Control Letters*, 42(4):321–326, 2001.

[48] W. J. Rugh. *Linear System Theory*, chapter 15. Prentice-Hall, Inc., 1996.

[49] S. Salcudean. A Globally Convergent Angular Velocity Observer for Rigid Body Motion. *IEEE Transactions on Automatic Control*, 36(12):1493–1497, 1991.

[50] A. Sanyal, A. Fosbury, N. Chaturvedi, and D. Bernstein. Inertia-Free Spacecraft Attitude Tracking with Disturbance Rejection and Almost Global Stabilization. *Journal of guidance, control, and dynamics*, 32(4):1167–1178, 2009.

[51] S. Sastry and M. Bodson. *Adaptive Control: Stability, Convergence, and Robustness*, chapter 1. Prentice-Hall, 1989.

[52] S. Sastry and M. Bodson. *Adaptive Control: Stability, Convergence, and Robustness*, chapter 3. PrenticeHall, Upper Saddle River, NJ, 1989.

[53] H. Schaub and J. Junkins. *Analytical Mechanics of Space Systems*, chapter 3. AIAA Education Series, 2003.

[54] R. Schlanbusch, E. I. Grøtli, A. Loria, and P. J. Nicklasson. Hybrid Attitude Tracking of Rigid Bodies Without Angular Velocity Measurement. *Systems & Control Letters*, 61(4):595–601, 2012.

[55] D. Seo and M. R. Akella. High-Performance Spacecraft Adaptive Attitude-Tracking Control Through Attracting-Manifold Design. *Journal of Guidance, Control, and Dynamics*, 31(4):884–891, 2008.

[56] D. Seo and M. R. Akella. Non-Certainty Equivalent Adaptive Control for Robot Manipulator Systems. *Systems & Control Letters*, 58(4):304–308, 2009.

[57] M. D. Shuster. A simple Kalman filter and smoother for spacecraft attitude. *Journal of the Astronautical Sciences*, 37(1):89–106, 1989.

[58] M. D. Shuster. A Survey of Attitude Representation. *The Journal of Astronautical Sciences*, 41(4):439–517, 1993.

[59] M. D. Shuster and S. D. Oh. Three-axis attitude determination from vector observations. *Journal of Guidance, Control, and Dynamics*, 4(1):70–77, 1981.

[60] J. J. E. Slotine and W. Li. *Applied Nonlinear Control*, chapter 7. Prentice-Hall, 1991.

[61] A. Tayebi. Unit Quaternion-Based Output Feedback for the Attitude Tracking Problem. *Automatic Control, IEEE Transactions on*, 53(6):1516–1520, 2008.

[62] A. Tayebi, A. Roberts, and A. Benallegue. Inertial vector measurements based velocity-free attitude stabilization. *IEEE Transactions on Automatic Control*, 58(11), 2013.

[63] D. Thakur and M. R. Akella. Gyro Free Rigid Body Attitude Stabilization Using Only Vector Measurements. *AIAA Journal of Guidance, Control, and Dynamics*. Article in review.

[64] D. Thakur and M. R. Akella. Coordinated Control of Autonomous Vehicles in Three-Dimensional Rotating Formations. In *Proceedings of the 2013 AAS/AIAA Astrodynamics Specialist Conference*, Hilton Head, SC, August 2013. Paper No. AAS 13-918.

[65] D. Thakur and M. R. Akella. Gyro Free Rigid Body Attitude Stabilization Using Only Vector Measurements on $SO(3)$. In *Proceedings of the*

24th AAS/AIAA Space Flight Mechanics Meeting, Santa Fe, NM, January 2014. Paper No. AAS 14-300.

[66] D. Thakur, S. Hernandez, and M. R. Akella. Spacecraft Swarm Finite-Thrust Cooperative Control Protocol for Common Orbit Convergence. *AIAA Journal of Guidance, Control, and Dynamics*. Article in review.

[67] D. Thakur, S. Hernandez, and M. R. Akella. Spacecraft Swarm Finite-Thrust Cooperative Control Protocol for Common Orbit Convergence. In *24th AAS/AIAA Space Flight Mechanics Meeting*, Santa Fe, NM, January 2014. Paper No. AAS14-380.

[68] D. Thakur and B. G. Marchand. Tracking Control of Nanosatellites with Uncertain Time Varying Parameters. In *Proceedings of the 2011 AAS/AIAA Astrodynamics Specialist Conference*, Girdwood, AK, August 2011. Paper No. AAS 11-592.

[69] D. Thakur and B. G. Marchand. Hybrid Optimal Control for HIV Multi-Drug Therapies: A Finite Set Control Transcription Approach. *Mathematical Biosciences and Engineering*, 9:899 – 914, 2012.

[70] D. Thakur, F. Mazenc, and M. R. Akella. Partial Lyapunov Strictification: Smooth Angular Velocity Observers for Attitude Tracking Control. In *AIAA Space and Astronautics Forum and Exposition*, San Diego, CA, August 2014. Paper No. AIAA-2014-4420.

[71] D. Thakur, S. Srikant, and M. R. Akella. Adaptive Attitude-Tracking

Control of Spacecraft with Uncertain Time-Varying Inertia Parameters. *AIAA Journal of Guidance, Control, and Dynamics*. Article in review.

[72] D. Thakur, S. Srikant, and M. R. Akella. Adaptive Attitude-Tracking Control of Spacecraft with Uncertain Time-Varying Inertia Parameters. In *Proceedings of the 2013 AAS/AIAA Astrodynamics Specialist Conference*, Hilton Head, SC, August 2013. Paper No. AAS 13-838.

[73] J. Thienel and R. M. Sanner. A coupled nonlinear spacecraft attitude controller and observer with an unknown constant gyro bias and gyro noise. *Automatic Control, IEEE Transactions on*, 48(11):2011–2015, 2003.

[74] P. Tsiotras. Further Passivity Results for the Attitude Control Problem. *Automatic Control, IEEE Transactions on*, 43(11):1597–1600, 1998.

[75] G. Wahba. A Least Squares Estimate of Satellite Attitude. *SIAM review*, 7(3):409–409, 1965.

[76] A. Weiss, I. Kolmanovsky, and D. Bernstein. Inertia-Free Attitude Control of Spacecraft with Unknown Time-Varying Mass Distribution. In *62nd International Astronautical Congress*, pages IAC–11–C1.5.9, Cape Town, SA, 2011.

[77] J. T. Wen and K. Kreutz-Delgado. The Attitude Control Problem. *IEEE Trans. on Automatic Control*, 36(10):1148–1162, 1991.

[78] B. Wie. *Space Vehicle Dynamics and Control*, chapter 7. AIAA Education Series, 1998.

[79] B. Wie and P. M. Barba. Quaternion Feedback for Spacecraft Large Angle Maneuvers. *Journal of Guidance and Control*, 8(3):360–365, 1985.

[80] B. Wie, H. Weiss, and A. Arapostathis. Quaternion Feedback Regulator for Spacecraft Eigenaxis Rotations. *Journal of Guidance, Control, and Dynamics*, 12(3):375–380, 1989.

[81] J. Xu. A New Periodic Adaptive Control Approach for Time-Varying Parameters With Known Periodicity. *IEEE Transactions on Automatic Control*, 48(8):579–583, 2003.

[82] H. Yoon and P. Tsiotras. Adaptive Spacecraft Attitude Tracking Control with Actuator Uncertainties. *Journal of the Astronautical Sciences*, 56(2):251–268, 2008.

[83] Y. Zhang and P. Ioannou. Adaptive Control of Linear Time Varying Systems. In *Proceedings of the 35th IEEE Conference on Decision and Control*, pages 837–842, 1996.

Vita

Divya Thakur received her undergraduate degree in Aerospace Engineering at The University of Texas at Austin in 2006. She continued on to the graduate aerospace program at UT to obtain her Master's in 2009, and now her PhD in 2014. During her time as a graduate student, Divya has been the recipient of the Zonta International Amelia Earhart Fellowship, UT Continuing Doctoral Scholarship, UT College of Engineering Graduate Fellowship, as well as the American Astronautical Society John V. Breakwell Student Travel Award. She has also served as a teaching assistant for several undergraduate courses. At the completion of her PhD, Divya intends to pursue a postdoctoral research opportunity at the Air Force Research Laboratory's Space Vehicles Directorate in Albuquerque, NM.

Permanent Address: divya.thakur@utexas.edu

This dissertation was typeset with LaTeX 2_ε[1] by the author.

[1] LaTeX 2_ε is an extension of LaTeX. LaTeX is a collection of macros for TeX. TeX is a trademark of the American Mathematical Society.